ABSTRACT

Title of Dissertation: AN INTERSECTING NETWORK OF REGULATORS IS REQUIRED FOR RNA SILENCING AND NUCLEAR INTEGRITY IN *C. ELEGANS*

Daphne Rebecca Knudsen-Palmer, Doctor of Philosophy, 2024

Dissertation directed by: Associate Professor, Antony M. Jose, Department of Cell Biology and Molecular Genetics

Regulation of gene expression is required for an organism to develop, maintain homeostasis, and respond to environmental stimuli. While each cell in a multicellular organism contains the same genetic information, the epigenetic control of the expression of genes at different times is crucial for processes such as cell differentiation, division, and for allowing for cells to carry out different functions from one another. One type of such epigenetic regulation is mediated by small non-coding RNAs. Introduction of double-stranded RNA (dsRNA) and subsequent production of small interfering RNAs can result in sequence-specific mRNA silencing, creating the potential for highly specific therapeutics and pesticides. However, some targets are more easily silenced than others, and the mechanisms of silencing are not fully understood. Here we investigate regulators of small RNA-mediated silencing in the nematode *C. elegans* and find that they function in an intersecting network, allowing the potential for regulators to contribute to the silencing of any target. Quantitative modeling suggests that the production and turnover rates of a target at steady-state can affect the ease with which a target can be knocked down, and experimentally we found that changing the *cis*-regulatory sequences of a target can make it more susceptible to silencing. We found restricted production of RNA silencing intermediates, allowing for the recovery of a target

in response to dsRNA, which we observed experimentally in non-dividing cells. In addition to roles in response to dsRNA, we report that disruption of small RNA-based regulation can result in germline nuclear defects. In the absence of the intrinsically disordered and perinuclear granule-forming protein MUT-16, some of the nuclei in the syncytial germline appear enlarged, suggesting that small RNA-based regulation may be playing an active role in maintaining nuclear size. Taken together, these findings suggest that (1) regulators of small RNA silencing can contribute to the silencing of all targets as part of an intersecting network, as opposed to operating in specialized pathways and (2) small RNA-based regulation is required for nuclear integrity, providing a paradigm for studying control of nuclear size, where enlarged nuclei can be compared with wildtype nuclei in a shared syncytium. We speculate that these findings will improve understanding of RNA silencing across species and provide insight into understanding how nuclear size is controlled, a fundamental ability of all eukaryotes.

AN INTERSECTING NETWORK OF REGULATORS IS REQUIRED FOR RNA SILENCING AND NUCLEAR INTEGRITY IN *C. ELEGANS*

by

Daphne Rebecca Knudsen-Palmer

Dissertation submitted to the Faculty of the Graduate School of the
University of Maryland, College Park in partial fulfillment
of the requirements for the degree of
Doctor of Philosophy
2024

Advisory Committee:
Associate Professor Antony M. Jose, Chair
Professor Norma Andrews
Professor Kan Cao
Professor Eric Haag
Professor Leslie Pick

© Copyright by
Daphne Rebecca Knudsen-Palmer
2024

Dedication

This dissertation is dedicated to my parents,

who gave me everything,

so that I could give something.

Acknowledgments

The lessons I have learned from my time in graduate school are not limited to techniques, literature reviews, and data analysis; I have grown to approach problems entirely differently, think critically, work rigorously, and truly appreciate both the beauty and the complexity of biology. This journey would not have been nearly as fruitful without the help, advice, and inspiration of several people.

I am grateful to Dr. Antony Jose for his patience, time, and wisdom. From the time I rotated in the Jose lab I was blown away by Antony′s willingness to go above and beyond to mentor his students. It is obvious to me that I would not have learned as much nor accomplished as much in my research with any other mentor. I am grateful he saw potential in me and I will always be thankful for the countless inspirational whiteboard discussions we had at turning points in my work. I very much respect the care Antony took to make sure I was well-trained on many facets: not just designing and conducting experiments, but speaking, writing, and carefully considering each piece of data, from our own hands and from others. For all my future endeavors, I aim to maintain the level of critical thinking and rigor that Antony uses to approach his science and I aim to inspire others as he has inspired me.

Several Jose lab alumni have inspired me from the time I even rotated in the lab. I would like to thank Dr. Pravrutha Raman, Dr. Sindhuja Shugarts Devanapally, and Dr. Snusha Ravikumar for showing me what I could become as a scientist in the Jose lab, and I would like to thank Dr. Nathan Shugarts Devanapally for his guidance during my mid-PhD challenges. I thank Laura De Ravin for learning alongside me, and teaching me how to teach my work. I thank the current members of the Jose lab for their help and feedback.

Throughout the ups and downs of my research (and the state of the world), a few people supported me in ways that no one else could. I thank my parents for believing in me, listening to my failures and my successes, and showing me that I could accomplish anything I set my mind to. I thank my three siblings for inspiring me; not only has it been a joy to see all they have accomplished alongside the time I was in graduate school, but I cherished our game nights and memes that helped me take much-needed breaks. I thank my husband for encouraging me and seeing my accomplishments, as a scientist or otherwise, even when I felt stuck and could not see them myself. I will always be grateful for the support, respect, and inspiration I received from all my family.

I thank my dissertation committee, Dr. Eric Haag, Dr. Norma Andrews, Dr. Leslie Pick, and Dr. Kan Cao for devoting time to offer constructive feedback on my work. I also thank Dr. Zhongchi Liu for her feedback on my manuscript and my work until her retirement. I am very grateful for countless discussions with other faculty members at UMD and the feedback I have received over the years from members of the Baltimore Worm Club. I would like to thank Amy Beaven from the UMD Imaging Core for help with the confocal microscope and for being a truly exceptional resource, as well as Tim Maugel for help with the transmission electron microscopy.

Table of Contents

Dedication……ii
Acknowledgments……iii
List of Tables……viii
List of Figures……ix
Chapter 1: General Introduction……1
1.1. Preface……1
1.2. Regulation of gene expression by non-coding RNAs……1
1.3. Practical applications for small interfering RNAs……2
1.3.1. siRNA-based therapeutics……3
1.3.2. siRNA-based pesticides……3
1.4. Small RNA-based regulation of endogenous genes……4
1.4.1. Pre- and post-transcriptional repression by small RNAs……4
1.4.2. RNA granules as perinuclear hubs of RNA regulation……5
1.5. *Caenorhabditis elegans* as a model system for understanding both imported and endogenously triggered RNA regulation……5
Chapter 2: Target-specific requirements for RNA interference can arise through restricted RNA amplification despite the lack of specialized pathways ……9
2.1. Preface……9
2.2. Introduction……9
2.3. Materials and methods……11
2.3.1. Methods summary……11
2.3.2. Strains and oligonucleotides……12
2.3.3. Genetic screen……13
2.3.4. Whole genome sequencing……13
2.3.5. Modeling and simulation……14
2.3.6. Genome editing……15
2.3.7. Sequence and structure alignments……19
2.3.8. Feeding RNAi……19
2.3.9. RNA extraction and PCR with reverse transcription (RT-PCR)……20
2.3.10. Microscopy……21
2.3.11. Rationale for inferences……21
2.4. Results……22
2.4.1. Two genes with different thresholds for silencing reveal an intersecting network of regulators that mediate RNA interference……22
2.4.2. The genetic requirement for NRDE-3, but not for MUT-16 and/or RDE-10, can be by bypassed by enhancing dsRNA processing……31
2.4.3. Quantitative modeling of RNA interference and mRNA production provides rationales for a variety of target-specific outcomes……35
2.4.4. Changing *cis*-regulatory elements of a gene impacts its requirements for silencing by dsRNA……44
2.4.5. Gene expression can recover after knockdown despite the presence of amplification mechanisms……47
2.4.6. Sequences in target mRNA that match the dsRNA trigger are hot zones of pUG RNA production……49
2.5. Discussion……51

2.5.1. Universal and gene-specific requirements for RNAi……....51
2.5.2. How are 2º siRNAs made?.....52
2.5.3. Trade-offs in RNA interference……57
Chapter 3: Disruption of small RNA-based regulation results in nuclear morphology defects in the germline……...71
3.1. Preface……..71
3.2. Introduction……...71
3.3. Materials and methods……..72
3.3.1. Strains and oligonucleotides……..72
3.3.2. Germline dissections and DAPI staining……...73
3.3.3. Microscopy……73
3.3.4. Genome editing……..74
3.3.5. RNA extraction and transcriptomics……..75
3.3.5.1. For poly-A RNA-seq (Figure 3-4)……76
3.3.5.2. For total RNA-seq (Figure 3-5)……76
3.4. Results……...77
3.4.1. Loss of MUT-16 results in some germline nuclei that are enlarged……..77
3.4.2. The loss of MUT-16 and RDE-10 suggest defects in the nuclear envelope……..82
3.4.3. Genes that are redundantly affected by MUT-16 and RDE-10 suggest candidates for explaining defects in nuclear integrity……87
3.4.4. The loss of RDE-10 does not appear to affect nuclear size……...93
3.5. Discussion……....93
3.5.1. Small RNAs and phase separation……94
3.5.2. "The Karyoplasmic Ratio"……95
Chapter 4: General Discussion……...99
4.1. Toward the ideal drug……..99
4.2. Non-infinite amplification of siRNAs……100
4.3. Is the control of nuclear size an active or a passive process?.....102
Chapter 5: Future Directions……....104
5.1. Preface……104
5.2. Introduction……104
5.3. Materials and methods……104
5.3.1. Strains……..104
5.3.2. Feeding RNAi……..105
5.3.3. Microscopy……..106
5.4. Results……106
5.5. Discussion……...110

Appendix A: Exploration of an *hrde-1(-)* missense mutant……112
A.1.Preface……112
A.2. Introduction……112
A.3. Materials and methods……...113
A.3.1. Strains and oligonucleotides……113
A.3.2. P0 and F1 feeding RNAi……..114
A.3.3. Making heterozygous mutants for feeding RNAi……....114
A.3.4. CRISPR Cas9-based genome editing……..115

A.3.5. Sequence Alignments……..116
A.3.6. Protein domain identification and Pymol……116
A.4. Results……...116
A.4.1. Sequence alignment of protein-coding Argonautes suggests that a glycine in the L1 domain is highly conserved……116
A.4.2. Mutation within a conserved residue does not disrupt *bli-1* silencing capability……119
A.5. Discussion……121
Appendix B: Ectopic expression of a germline gene in the intestine……..123
B.1. Preface……123
B.2. Introduction……123
B.3. Materials and methods……123
B.3.1. Strains and oligonucleotides……123
B.3.2. Heat shock……....125
B.3.3. Microscopy……..125
B.3.4. Creation of *rrf-1(-);T* strains……125
B.4. Results……126
B.5. Discussion……...127

Bibliography……...…….128

List of Tables

Table 2-1: Strains used in Chapter 2……58
Table 2-2: Oligonucleotides used (5′ to 3′) in Chapter 2……60
Table 2-3: Statistics for comparisons in Chapter 2……..61

Table 3-1: Strains used in Chapter 3……95
Table 3-2: Oligonucleotides used (5′ to 3′) in Chapter 3……96

Table 5-1: Strains used in Chapter 5……..104

Table A-1: Strains used in Appendix A……..112
Table A-2: Oligonucleotides used (5′ to 3′) in Appendix A……...112

Table B-1: Strains used in Appendix B……...123
Table B-2: Oligonucleotides used (5′ to 3′) in Appendix B……123

List of Figures

Figure 1-1: Exogenous and endogenous pathways of small RNA-based gene regulation……..…6

Figure 2-1: RNA interference of two somatic targets show stark differences in their requirements for MUT-16 and RDE-10……..…..……23
Figure 2-2: A forward-genetic screen identifies a mutation that is expected to disrupt the Maelstrom domain of RDE-10…….…..…26
Figure 2-3: Gene-specific requirements and complex redundancy can arise from a single RNA regulatory network……..…28
Figure 2-4: Support for an intersecting regulatory network……..30
Figure 2-5: Gene-specific requirements for regulators of RNA silencing can be bypassed in two ways……...32
Figure 2-6: Overexpressing RDE-4 in the hypodermis…….34
Figure 2-7: An equilibrium model for RNAi…….36
Figure 2-8: A quantitative model allows exploration of parameters for RNAi in *C. elegans*…...38
Figure 2-9: Impact of model parameters on the time to knockdown (τ_{kd}) and the duration of knockdown (t_{kd})……..42
Figure 2-10: *Cis*-regulatory regions are not sufficient to confer genetic requirements for silencing in response to dsRNA…….44
Figure 2-11: Replacing the *unc-22* 3′ *cis*-regulatory sequence with that of *bli-1* results in twitching defects without the addition of dsRNA……..45
Figure 2-12: F1 only *bli-1* RNAi yields similar graded requirements for MUT-16, RDE-10, and NRDE-3 for silencing…….46
Figure 2-13: Animals recover from a pulse of RNAi and production of pUG RNAs is restricted despite continuous exposure to dsRNA…….48
Figure 2-14: Graphical summary of Chapter 2……..51
Figure 2-15: The predicted structure of the Maelstrom domain of RDE-10 is similar to that of the 3′-5′ exonuclease ERI-1……..54

Figure 3-1: Disruption of small RNA-based regulation results in germline defects……..78
Figure 3-2: Newly generated *mut-16(-)* mutants show some enlarged nuclei…….81
Figure 3-3: Disruption of small RNA amplification in *mut-16(-) rde-10(-)* double mutants shows deformed nuclear envelopes and deformed nucleoli……...83
Figure 3-4: The loss of MUT-16 disrupts thousands of genes……86
Figure 3-5: Total RNA sequencing reveals genes that are regulated by both MUT-16 and RDE-10……88
Figure 3-6: A nearly 60kb deletion on Chromosome II is present in *mut-16(jam148) rde-10(jam196)* double mutants……90
Figure 3-7: The loss of RDE-10 does not result in enlarged nuclei……92

Figure 4-1: Amplification of siRNAs with respect to a target transcript…….101

Figure 5-1: Exploring roles for RDE-10 in the germline…….108
Figure 5-2: Structural speculations for RDE-10 and RDE-11……..110

Figure A-1: Protein-coding Argonautes share a conserved glycine within the Linker 1 domain……..118
Figure A-2: Disruption of the conserved glycine has the potential to disrupt folding of the L1 domain……..120
Figure A-3: Animals lacking HRDE-1 do not show a defect in *bli-1* silencing……..121
Figure A-4: Sanger sequencing of AMJ1097……..122

Figure B-1: Loss of HRDE-1 at high temperatures leads to misexpression of a germline gene in the soma……...126

Chapter 1: General Introduction

1.1 Preface

This introduction was influenced by a number of key reviews (cited within the text) in addition to discussions with advisor Antony Jose and members of the Jose Lab.

1.2 Regulation of gene expression by non-coding RNAs

Regulation of gene expression is a process that must be accurately controlled in order for a cell to carry out any function, from maintaining homeostasis, to differentiating, to dividing. Many factors are involved in this control: the organization of chromatin, availability of transcription factors, splicing, non-coding RNAs, and many more. Among non-coding RNAs, they can be divided into 2 major groups: long non-coding RNAs (lncRNAs reviewed in (1)), and small RNAs, which include microRNAs (miRNAs, reviewed in (2)), PIWI-interacting RNAs (piRNAs, reviewed in (3)), and small interfering RNAs (siRNAs, reviewed in (4)).

Long non-coding RNAs (lncRNAs) are characterized as non-coding RNAs that are greater than 200 nucleotides in length (5–8). While previously thought to be created by low RNA polymerase fidelity (9), lncRNAs have since been shown to play roles in development (10) and cell differentiation (11). In humans, the Hox transcript antisense RNA (*HOTAIR*) has been shown to induce chromatin condensation (12), and defects in *HOTAIR* regulation have been linked to a variety of cancers (13–16), demonstrating the importance of gene regulation that is controlled by lncRNAs.

In contrast to lncRNAs, small RNAs (micro, pi, and small interfering) tend to be ~20-35 nucleotides in length, depending on the type of RNA and the species in which it is found, are antisense to target mRNAs, and are bound by an Argonaute protein (reviewed in (17)). microRNAs

were first discovered in the nematode *C. elegans* where they were shown to be required for proper development of the animal (18, 19), and have been shown to negatively regulate a variety target mRNAs by binding to sites within a target's 3′ untranslated region (20, 21). piRNAs particularly function within the germline of an organism, acting to prevent transposons from being expressed (22–27). Small interfering RNAs have the potential to match any sequence, and gene silencing can be induced by introducing double-stranded RNA that is homologous to the target, in a process called RNA interference (28). siRNAs can bind targets directly and recognition by an siRNA can induce chromatin modifications (see Chapter 1.4.1).

Taken together, these examples highlight the diversity of non-coding RNAs and emphasize the importance they play within a cell and throughout development.

1.3 Practical applications for small interfering RNAs

RNA interference (RNAi) was first defined in the nematode *C. elegans* and describes the process by which double-stranded RNA (dsRNA) can cause sequence-specific silencing (28). Although not conserved across all eukaryotes, RNAi likely evolved as an antiviral mechanism (reviewed in (29)), and RNAi machinery can be found in some species of yeast (30), plants (31–34), insects (35, 36), and mammals, including humans (37). The potential to create drugs using RNAi is immense, since in theory, the sequence of the target mRNA is all that is needed to create a dsRNA trigger. This approach also allows for highly specific treatments that are unlikely to cause off-target affects, as opposed to, for example, a chemotherapeutic drug that targets all dividing cells. RNAi-based applications face two challenges: 1. Some targets are easier to silence than others, and the reasons for this remain unclear (see Chapter 2) and 2. Transport of the dsRNA to the correct tissue, uptake into cells, and eventual exit out of endosomes is difficult to achieve (see

Discussion point 4.1). Despite these challenges, a number of applications have been developed and are used in both medicine (reviewed in (38, 39)) and in agriculture (reviewed in (40)).

1.3.1 siRNA-based therapeutics

Since 2018 (and as of this writing), six dsRNA drugs have been approved by the FDA to treat a variety of diseases: patisiran (41) and vutrisiran (42) for hereditary transthyretin amyloidosis, givosiran to help prevent acute porphyria attacks (43), inclisiran to combat hypercholesterolemia (44), and lumasiran (45) and nedosiran (46) for primary hyperoxaluria type 1. These drugs are used to target mRNAs in the liver, which is among the easier organs to target. Determining the proper dosage for such drugs can be difficult due to the limitations of delivery, leaving much to be explored within this area of therapeutics. Despite these challenges, these six drugs have already demonstrated the ability to treat disease using RNA interference.

1.3.2 siRNA-based pesticides

Historically, pesticides that are effective at killing a large range of invasive species are very harmful to the environment and the surrounding ecosystem. As an extreme example, DDT (dichlorodiphenyltrichloroethane) was wildly effective at killing insects, drastically reducing malaria in the United States in a matter of years (47–49), however, the nerve impulse-affecting agent was banned from use because of its long half-life (50) and negative effects on surrounding wildlife (51). As with human therapeutics, RNAi provides the potential to create pesticides that are highly specific, reducing the impact on other species within an ecosystem while still being able to protect crops. Indeed, genetically-modified corn seeds that produce dsRNA targeting an essential gene in rootworms has been an effective solution to combat this specific pest (52–54).

Non-GMO approaches are promising as well; dsRNA that is encapsulated in lipid nanoparticles can be sprayed onto tobacco leaves to target viruses carried by aphids (55). Both of these applications are able to target the pests without having much of an effect on the surrounding ecosystem. As with human therapeutics, the choice of which gene to target is imperative for making an effective pesticide, and the understanding of RNAi machinery in many invasive insects remains to be better characterized in order to ensure effective dosages and/or reduce the chances of resistance.

1.4 Small RNA-based regulation of endogenous genes

1.4.1 Pre- and post-transcriptional repression by small RNAs

As mentioned above (Chapter 1.2), lncRNAs such as HOTAIR have the ability to induce chromatin compaction, resulting in transcriptional repression of many genes simultaneously (12), but small RNAs have also been shown to play roles in the control of chromatin. Small RNAs in *Arabidopsis thaliana* and other plants can direct DNA methylation (reviewed in (56, 57)), and small RNAs in *Tetrahymena* can guide chromatin condensation and even DNA deletion at specific loci (58). In *C. elegans,* siRNAs are sufficient to direct chromatin condensation, in part by recruiting the HP1-like (heterochromatin protein 1) protein HPL-2 and histone methyltransferases (SET-25, MET-2, SET-32) (reviewed in (59)).

In addition to repression at the transcriptional level, small RNAs can control expression of a gene by blocking or otherwise degrading mRNAs before they are translated. As previously mentioned, microRNAs can repress translation by binding to the 3′ untranslated region of a target (18–21). piRNAs and siRNAs can bind within the coding region of a target mRNA, which can lead to downstream degradation, and thus silencing (60). Notably, not all siRNA-based recognition

leads to mRNA silencing; some siRNAs have been thought to contribute positively to the expression of some targets (60). These examples of roles for pre- and post-transcriptional regulation demonstrate the versatility of small RNAs in controlling mRNA expression.

1.4.2 RNA granules as perinuclear hubs of RNA regulation

While many cellular organelles are contained by a membrane (e.g. mitochondria) membrane-less compartments are capable of forming in a process called liquid-liquid phase separation (61–63). One type of these compartments is called a germ granule, and as the name suggests, can be found in the germ line of some animals. Referred to as "Nuage," meaning "cloud," in mice and *Drosophila,* these compartments are found adjacent to the nucleus in germ cells and involved in small RNA-mediated gene regulation, especially regulation that is triggered by piRNAs (64–68). These granules do not have to be homogenous; indeed, in *C. elegans,* up to four distinct perinuclear granules have been defined: P granules (61, 69, 70), Z granules (71, 72), SIMR foci (73), and *Mutator* foci (74, 75). Much like oil in water, these condensates separate from the surrounding cytosol based on their composition, and require the presence of both intrinsically disordered proteins and RNAs (75–77). More recently, sub compartments of P granules have been observed (78), suggesting that these phase-separated granules can spatially facilitate small RNA-mediated regulation in a highly specific manner.

1.5* Caenorhabditis elegans *as a model system for understanding regulation triggered by both imported and endogenously expressed RNA.

Since the discovery of RNA interference in *C. elegans* (28), machinery involved in small RNA-based regulation has been very well characterized (reviewed in (79, 80)). All RNA silencing

that occurs by the addition of dsRNA from an outside source (through injection of dsRNA into the animal (28), feeding animals *E. coli* that express dsRNA matching a target gene in the worm (81), or secreted from transgenes that express dsRNA in neurons (82, 83)) requires the transmembrane importer SID-1 (84, 85). Thus, RNA-based regulation that requires SID-1 and downstream factors including the dsRNA-binding protein RDE-4 (86) and the primary Argonaute RDE-1 (87, 88) has often been referred to as "Exogenous RNAi." More recently, SID-1 has been implicated in the regulation of endogenous targets, suggesting that there may be endogenously generated dsRNA (89). Therefore, a more accurate description for dsRNA-triggered silencing may be "Imported dsRNA-based regulation" or "Imported RNAi" (see Figure 1-1A).

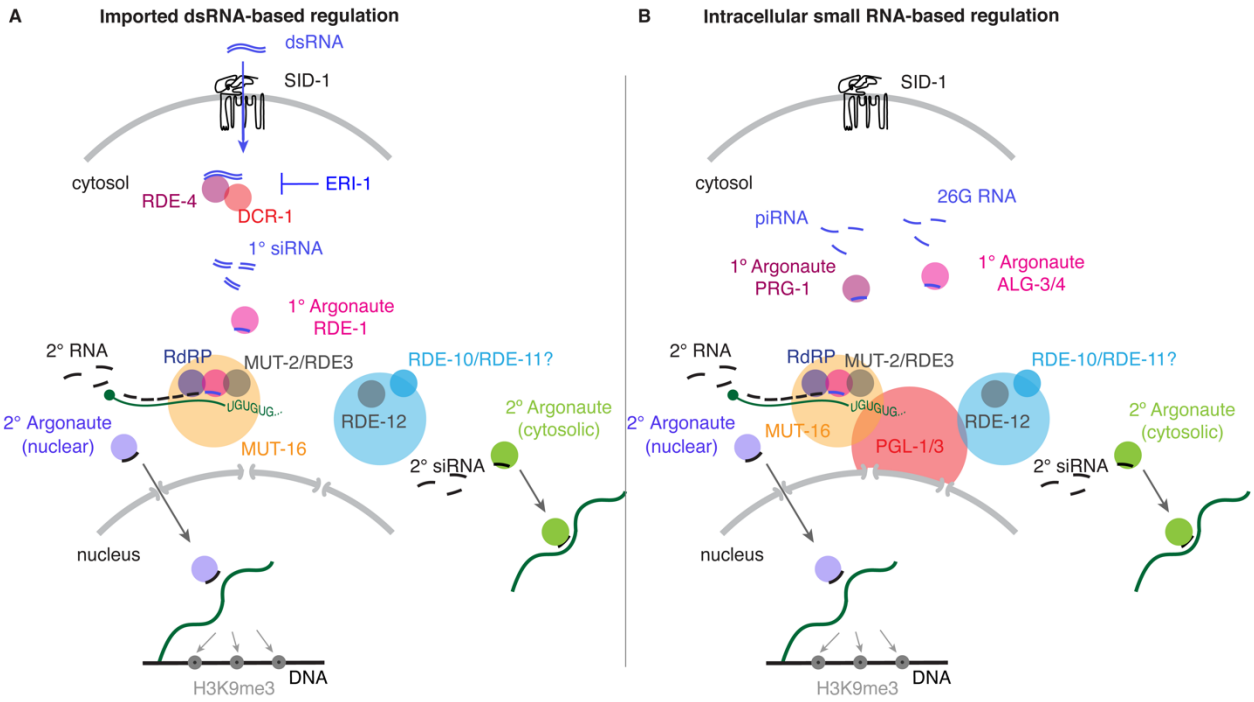


Figure 1-1. Simplified depiction of small RNA-processing in *C. elegans*. (A) Imported dsRNA-based regulation. The transmembrane protein SID-1 (black) is required for dsRNA (dark blue) entry into a cell. RDE-4 (dark pink) binds dsRNA and recruits DCR-1 (red) which cleaves the trigger into smaller dsRNA molecules. After cleavage, the 1º Argonaute RDE-1 (pink) cleaves one strand of this smaller dsRNA and binds to the other (1º siRNA), and this complex can recognize a target mRNA (dark green) and initiate cleavage. The intrinsically disordered protein MUT-16 (orange) is required to recruit factors such as MUT-2/RDE-3 (gray), which adds poly-UG repeats

to the cleaved 3′ end of the target. An RNA-dependent RNA polymerase (RdRP, purple) uses the pUG-tailed mRNA as a template to produce 2º siRNAs. The Maelstrom domain protein RDE-10 forms a complex with RDE-11 and is required for amplification. The subcellular localization and biochemical roles for these proteins are unclear, but RDE-10/11 could associate with the DEAD-box helicase RDE-12 (see Chapter 5 for more). Amplified 2º siRNAs bind a 2º Argonaute, and these complexes can bind target transcripts in the cytosol (light green) or in the nucleus (lavender). Nuclear siRNA-regulation can recruit downstream histone modifiers to guide chromatin condensation. (B) Small-RNA based regulation resulting from endogenous piRNA or 26G RNA triggers. Mature piRNAs bind to the 1º Argonaute PRG-1 (dark pink), and mature 26G RNAs can bind the 1º Argonautes ALG-3/4 (pink) or ERGO-1 (not pictured). Many germline targets are regulated by intracellularly expressed RNA, and germline small RNA-mediated regulation can occur in perinuclear granules, for example P granules which require PGL-1 (red). Downstream target recognition and 2º amplification occurs using the components involved in these processes when triggered by dsRNA.

Similarly, RNA-based regulation that occurs in SID-1-independent ways has often been referred to as "Endogenous RNAi." Given that some endogenous genes are dependent on SID-1 (89), small RNA-mediated regulation that is triggered by piRNAs (90) or 26G RNAs (91–93) could be more appropriately called "Intracellular small RNA-based regulation" (see Figure 1-1B).

After recognition of a target mRNA by a 1º siRNA-1º Argonaute complex, regardless of the source of the trigger, target mRNAs are cleaved, and poly-UG (pUG) repeats are added to the 3′ end (94–96). These pUG repeats have the potential to form quadruplexes (97), and these tails have been hypothesized to stabilize targets for amplification. RNA-dependent RNA polymerases (RdRPs) such as EGO-1 and RRF-1 use the stabilized mRNA as a template to produce 2º siRNAs (98–100). MUT-16, RDE-10, and associated proteins are required for proper amplification of 2º siRNAs (74, 101–104). After amplification, 2º siRNAs are bound to a 2º Argonaute and can cause sequence-specific silencing (105–107).

In addition to mechanistic differences between sources of RNA triggers (imported vs. intracellular), RNA silencing can function differently in different tissues, especially in the germline versus the soma. Factors involved in the amplification of small RNAs (MUT-16, PGL-

1/3, etc.) form phase-separated granules in the germline (70, 74, 104), and while they are expressed in the soma, they are not detectable as granules. The nuclear Argonaute NRDE-3 is often thought to function in the soma (106) while HRDE-1 is thought to function in the germline (108) based on fluorescent reporters. However, it is possible that these 2º Argonautes are not definitely restricted to either the germline or the soma, just as germ granule components can play roles in the soma (see Appendix B for potential somatic roles for HRDE-1).

Despite the extensive discoveries made regarding RNA silencing in *C. elegans* in the past few decades, there remain mechanistic details that are unclear. *C. elegans* contains 20 protein-coding Argonautes (105, 107), while humans have 8 (109), and *Drosophila* only 5 (110). The abundance of Argonaute paralogs raises the question of whether specific Argonautes have specific classes of targets, but given that aside from the bias for a 5′G on the siRNA (90, 111), it seems unlikely that targets would require specific Argonautes for silencing. Additionally, some genes are more easily knocked down, and the reasons for this are unclear. In this dissertation, we investigate the relationship between regulators of small RNA-mediated regulation and their targets, providing considerations for practical uses of small RNAs and enhancing our understanding of the complex but fundamental process of regulation of gene expression.

Chapter 2: Target-specific requirements for RNA interference can arise through restricted RNA amplification despite the lack of specialized pathways.

2.1 Preface: A large part of this work was initially published as a preprint on *bioRxiv* (112) and has since been updated after going through the review process. Figure 2-12 was added as a supplement to the work previously completed. Pravrutha Raman generated the data in Figures 2-5D, 2-5E, 2-6 and part of 2-5B. Laura de Ravin generated the data in Figure 2-1C. Pravrutha Raman and Farida Ettefa performed the genetic screen (described in 2.3.3) and Antony Jose analyzed the whole genome sequence data of the mutants from this screen (described in 2.3.4). All other data was generated by Daphne Knudsen-Palmer.

2.2 Introduction:

Double-stranded RNA (dsRNA) can trigger the conserved mechanism of RNA interference (RNAi) to degrade mRNA of matching sequence (28), and thus silence gene expression, in many organisms. This conservation has made dsRNA-based drugs useful in crops (113), insects (114), and humans (115). While a dsRNA-based drug can be designed using just the mRNA sequence of any target gene, the intracellular effectiveness of the drug and the ease with which an organism could escape the drug by developing resistance are difficult to predict. Predicting both efficacy and susceptibility to resistance for each target could inform the selection of a suitable target from two or more equivalent candidates. Extensive characterization of RNAi in the nematode *C. elegans* (reviewed in ref. (79)) makes it a suitable system to examine how differences between target genes and reliance on specific regulators contribute to efficacy and resistance.

A skeletal pathway that is required for gene silencing in response to the addition of dsRNA has been worked out in *C. elegans* (Figure 2-1A). Long dsRNA is imported through the transmembrane protein SID-1 (84, 85), after which it is bound by the dsRNA-binding protein RDE-4 (86), which recruits the endonuclease DCR-1 (116) to cleave the long dsRNA into smaller dsRNAs (117). The primary Argonaute protein RDE-1 (87, 88) cleaves one strand of the smaller dsRNA (118) and associates with the other, making it a 1º short interfering RNA (siRNA) that can guide the recognition of target mRNAs of matching sequence (siRNAs; processing, pink). After recognition by RDE-1-bound siRNAs, the target mRNAs are cleaved and the more 5′ of the two fragments are stabilized through the addition of 3′ UG-dinucleotide repeats (95) by the nucleotidyltransferase RDE-3 (94) to form pUG RNAs (96), which act as templates for the amplification of 2º siRNAs (100) by RNA-dependent RNA polymerases. This amplification of silencing signals through the production of 2º siRNAs is facilitated by the intrinsically disordered protein MUT-16 (74, 101) the Maelstrom domain-containing protein RDE-10 (102, 103), and their interactors (74, 102–104). These 2º siRNAs are bound by one of several Argonautes (105), resulting in the eventual degradation of target mRNAs in the cytoplasm, which requires a cytoplasmic Argonaute, and/or co-transcriptional silencing of the target gene in the nucleus, which requires a nuclear Argonaute (e.g., NRDE-3 (106) in somatic cells). Although it is difficult to compare the silencing of two different genes by controlling all relevant variables, past studies have highlighted gene-specific differences in the efficacy of RNAi under different conditions (e.g., when RNAi is enhanced through the loss of the exonuclease ERI-1 (119), when nuclear silencing is blocked in somatic cells through loss of NRDE-3 (120), or when different concentrations of dsRNA are used (121)). Understanding the sources of such differences and the underlying

mechanisms will improve our ability to design efficacious dsRNA drugs that are difficult to evade through the development of resistance.

Here we analyze the requirements for silencing two exemplar genes and use quantitative modeling to advance a parsimonious view of RNAi in somatic cells. We show that MUT-16, RDE-10, and NRDE-3 are each required for the silencing of *bli-1,* but any two of these proteins are sufficient for *unc-22* silencing. These differences can be explained by differences in the thresholds for silencing the two genes using an intersecting network of regulators but not by parallel pathways of regulation after primary mRNA recognition. The requirement for NRDE-3 but not for MUT-16 or RDE-10 can be bypassed by enhancing the processing of dsRNA, suggesting that loss of NRDE-3 has the least impact on the efficiency of silencing. A dynamic model of RNA changes during silencing by dsRNA reveals several criteria for efficient RNA silencing. Insights from modeling led us to discover the influence of *cis*-regulatory regions on the requirements for RNAi, the recovery of animals from RNAi within non-dividing cells, and a dearth of pUG RNA production by 2º siRNAs.

2.3 Materials and methods

2.3.1 Methods summary

All strains (Table 2-1) were grown at 20ºC on Nematode Growth Medium (NGM) plates seeded with OP50 *E. coli* (122). Strains with mutations were generated through a genetic screen after mutagenesis using N-ethyl-N-nitrosourea (ENU), using standard genetic crosses (122), or using Cas9-mediated genome editing (123–125). Mutations induced upon ENU exposure were identified using whole genome sequencing (Illumina) followed by analyses of the resultant fastq files. Simulations of the RNAi response were used to identify the domain and range of values

consistent with experimental data (Figure 2-3) and to explore parameters that support silencing (equilibrium model (Figure 2-7) and dynamic model (Figs. 4 and 2-9)). Feeding RNAi experiments were performed by exposing worms to bacteria that express dsRNA (81, 126) either continuously or for a brief period (Figure 2-13A). Multiple sequence alignment (Figure 2-7) was performed using Clustal Omega (127) and manually annotated using Illustrator (Adobe). Comparisons of protein structures were performed using AlphaFold predictions (128, 129), pair-wise alignment on Protein Data Bank (130), and the PyMOL Molecular Graphics System (v. 2.4.1 Schrödinger, LLC). Levels of *rde-4* mRNA (Figure 2-6) and pUG RNA (Figure 2-13C) were measured using reverse-transcription followed by polymerase chain reaction (RT-PCR). Transgenic strains that express *rde-1(+)* and *rde-4(+)* in specific tissues were generated using Mos1-mediated single copy insertion (MosSCI) (131). Oligonucleotides used are in Table 2-2. Exact p-values and additional details for each experiment are in Table 2-3. All code used (R, Python, and Shell) is available at https://github.com/AntonyJose-Lab/Knudsen_et_al_2023.

2.3.2 Strains and oligonucleotides used

All strains (listed in Table 2-1) were cultured on Nematode Growth Medium (NGM) plates seeded with 100 µl of OP50 *E. coli* at 20ºC and strains made through mating were generated using standard methods (122). Oligonucleotides used are in Table 2-2. Strains generated using Mos1-mediated Single Copy Insertion (MosSCI, ref. (131)) of *rde-4* or *rde-1* rescues in the germline (as in ref. (132)) or of *rde-4* rescues in the hypodermis (120) were used in this study.

2.3.3 Genetic screen

This screen was performed by mutagenizing a strain (AMJ174) with the transgene *T* (*oxSi487[mex-5p::mCherry::H2B::tbb-2 3'UTR::gpd-2 operon::GFP::H2B::cye-1 3'UTR + unc-119(+)]*, (133)) silenced for >200 generations after introducing a mutation in *lin-2(jam30)* (sgRNA (P1), primers (P2, P3, P4) using Cas9-mediated genome editing of AMJ844 (*iT; dpy-2(e8)*, (133)) while correcting the *dpy-2(e8)* mutation to wild type (creating *dpy-2(jam29)*; sgRNA (P5), primers (P6, P7, P8)). The *lin-2* mutation limits brood size (134) and facilitates screening. Near-starved animals (P0) of all life stages were mutagenized using 1mM N-Ethyl-N-Nitrosourea (ENU, Toronto Research Chemicals) for 4-6 hours. Mutagenized animals were washed four times with wash buffer (0.01% Triton X-100 in M9) and 2-3 adult animals were placed on NG plates seeded with OP50. Over the next 3 weeks, F1, F2, and F3 progeny were screened to isolate mutants that show mCherry fluorescence. These animals were singled out (up to 7 animals from each P0 plate) and tested for the persistence of expression in descendants. Of the 15 fertile mutants isolated using this primary screen, five with mutations in *mut-16* were analyzed in this study.

2.3.4 Whole genome sequencing

Libraries were prepared using TruSeq DNA Library Prep kits (Illumina) and samples were sequenced at Omega Biosciences. The fastq files obtained after Illumina sequencing (1x PE 150 b, Omega Biosciences) were analyzed to identify candidate mutations responsible for the observed defects in the sequenced strains. For each strain, sequences were trimmed using cutadapt (v. 3.5), mapped to the *C. elegans* genome (WBcel235/ce11) using bowtie2 (v. 2.4.2), sorted using samtools (v. 1.11), and the resulting .bam file was analyzed to call variants using snpEff (v. 5.0e). The variants classified as ′HIGH′ or ′MODERATE′ in the .ann.vcf file for each strain that were

not shared by any two or more strains were culled as new mutations caused by mutagenesis in each strain. These new mutations in each strain were compared with those of all other strains (′in silico complementation′) using a custom script to identify sets of strains with different mutations in the same genes. Specific details for each step are provided within the scripts ′1_fastq_to_sorted_bam.sh′, ′2_sorted_bam_to_mutated_genes.sh′, ′3_in_silico_complementation.sh′ available at GitHub (https://github.com/AntonyJose-Lab/Knudsen_et_al_2023). Raw fastq files for the strains analyzed in this study (AMJ1023, AMJ1025, AMJ1035, AMJ1042, and AMJ1091) have been submitted to SRA (PRJNA928750).

2.3.5 Modeling and simulation

The RNAi response was explored using three models of increasing complexity: (1) a single-network model of protein factors with branching pathways for RNA amplification and subsequent gene silencing (Figure 2-3); (2) an equilibrium model for the dependence of mRNA and pre-mRNA on small RNAs and other RNA intermediates (Figure 2-7); and (3) a dynamic model using ordinary differential equations for the dependence of mRNA and pre-mRNA on small RNAs and other RNA intermediates (2-8 and 2-9). Simulations of single network and exploration of equilibrium model were conducted in R (v. 3.6.3). Simulations of the dynamic model were conducted in Python (v. 3.8.5) and in R (v. 4.1.0).

Intersecting network: Random numbers from 0 to 2 were selected for each of the assigned variables (Nm, Nr, *Om*, *Or*) and parameter sets that satisfy experimental constraints were plotted. Specific details are provided within the script ′2022_6_13_RNAi_in_Celegans_linear_modified.R′ available at GitHub (https://github.com/AntonyJose-Lab/Knudsen_et_al_2023).

Equilibrium model: This model for RNAi interference assumes that all reactions have reached equilibrium. Additional assumptions include (1) 1º siRNAs, then pUG RNAs, then 2º siRNAs are made sequentially, (2) no 3º siRNAs are produced for these somatic targets (supported by ref. (135)), (3) there is no recycling of full-length mRNA or full-length pre-mRNA after small RNA binding, i.e., multiple rounds of binding by different small RNAs to the same intact mRNA or pre-mRNA molecules is not allowed and (4) there are no other mechanisms for the turnover of the RNA species considered in the timescale considered. Specific details are provided within the script ′2022_2_9_RNAi_network_thresholds_simpler.R′ available at GitHub (https://github.com/AntonyJose-Lab/Knudsen_et_al_2023).

Dynamic model: A series of differential equations were used to describe the rate of change for dsRNA, 1º siRNAs, mRNAs, pre-mRNAs, pUG RNAs, and 2º siRNAs, and numerically simulated using the 4th Order Runge-Kutta method. Specific details are provided within the scripts ′2022_6_29_Celegans_RNAi_ODEs_RK4_method_d6.py′ and ′2022_7_14_RNAiDynamics_ODEs_Parameter_Analysis.R′ available at GitHub (https://github.com/AntonyJose-Lab/Knudsen_et_al_2023).

2.3.6 Genome editing

The gonads of adult *C. elegans* were injected with nuclear-localized Cas9 (PNA Bio) preincubated at 37°C for 10 min with a hybridized crRNA/tracrRNA (Integrated DNA Technologies), as well as an oligonucleotide or PCR-amplified homology repair template. Plates with successfully edited F1 animals were identified by screening the Dpy or Rol animals obtained when using *dpy-10* editing as a co-CRISPR (123, 124) or for Rol animals when using the pRF4 plasmid as a co-injection marker (125).

To introduce a premature stop codon in *mut-16:* Injection of a crRNA with the target sequence (P9) (Integrated DNA Technologies), tracrRNA, Cas9, a *mut-16(-)* homology repair template (P10) mimicking the mutation in *mut-16(jam139),* predicted amino acid change Y294*, and *dpy-10* crRNA (P11) and *dpy-10(-)* homology repair template (P12) into N2 or AMJ1489 and subsequent screening were performed as described above. Genotyping for *mut-16(jam148, jam240, jam265, jam266, jam267, or jam268)* was performed using duplex PCR (P13, P14) followed by restriction digestion with BstBI. The nonsense mutations in different strains (AMJ1397, AMJ1611, AMJ1672, AMJ1673, AMJ1674, and AMJ1675) were verified by Sanger sequencing.

To make the *mut-16(-) rde-10(-)* double mutant: Injection of a crRNA with the target sequence (P15) (Integrated DNA Technologies), tracrRNA, Cas9, a *rde-10(-)* homology repair template (P16) mimicking the mutation in *rde-10(jam248)*, and *dpy-10* crRNA (P11) and *dpy-10(-)* homology repair template (P12) into AMJ1397 (*mut-16(jam148))* and subsequent screening were performed as described above. Genotyping for *rde-10(-)* was performed using duplex PCR (P17, P18) followed by restriction digestion with EcoRV. A strain with a mutation in *rde-10* that results in a 115-bp frameshift followed by an early stop codon was designated as AMJ1470.

To introduce the mutation in *rde-10* that will encode RDE-10(Ser228Phe): Injection of a crRNA with the target sequence (P15) (Integrated DNA Technologies), tracrRNA, Cas9, a *rde-10(-)* homology repair template (P16) mimicking the mutation in *rde-10(jam248)* (Figure 2-2), and pRF4 into N2 and subsequent screening were performed as described above. Genotyping for the mutation was performed using duplex PCR (P17, P18) followed by restriction digestion with EcoRV. A strain with the missense mutation verified by Sanger sequencing was designated as AMJ1489.

To introduce a premature stop codon in *rde-10*: Injection of a crRNA with the target sequence listed as (P19) (Integrated DNA Technologies), tracrRNA, Cas9, a *rde-10(-)* homology repair template (P20) (predicted amino acid change Q73*) and pRF4 into N2 and subsequent screening were performed as described above, Genotyping for *rde-10(-)* was performed using duplex PCR (P21, P22) and restriction digestion with DpnII to isolate the mutant from N2. A strain with a 2-bp deletion near Q73 that results in a frameshift and an early stop codon was designated as AMJ1614.

To introduce a premature stop codon in *nrde-3*: Injection of a crRNA with the target sequence (P23) (Integrated DNA Technologies), tracrRNA, Cas9, a *nrde-3(-)* homology repair template (P24), mimicking *nrde-3(gg066)* (25), and pRF4 into N2 and subsequent screening were performed as described above. Genotyping for *nrde-3(jam205)* was performed using duplex PCR (P25, P26) followed by restriction digestion with AclI. A strain with the nonsense mutation verified by Sanger sequencing was designated as AMJ1510.

To introduce a premature stop codon in *eri-1:* Injection of a crRNA with the target sequence (P27) (Integrated DNA Technologies), tracrRNA, Cas9, an *eri-1(-)* homology repair template (P28), predicted to encode ERI-1(E225*) after the edit, and pRF4 into AMJ1611 or N2 and subsequent screening were performed as described above. Genotyping for *eri-1(jam260, jam261, jam262, jam263, or jam264)* was performed using duplex PCR (P29, P30) followed by restriction digestion with DpnII. Additionally, when *eri-1(mg366)* was crossed with other mutants, duplex PCR with P31 and P32 was used for genotyping.

To create a transgene with the *bli-1* promoter: Injection of two crRNAs with the target sequences (P33, P34) (Integrated DNA Technologies), tracrRNA, Cas9, a homology repair template that was amplified using sequences (P35, P36) (Phusion High-Fidelity DNA Polymerase,

New England BioLabs), which amplifies the promoter region of *bli-1,* and pRF4 into AMJ1195 [*mex-5p::gfp::cye-1 3′ utr*] (40) and subsequent screening were performed as described above. Genotyping for *bli-1p::gfp* was performed using triplex PCR (P37, P38, P39). Additional genotyping after crosses was done using triplex PCR with sequences (P40, P41, P42). The resulting strain (AMJ1709) resulted in successful integration of ~75% of the *bli-1* promoter upstream of the *mex-5* promoter, and showed GFP expression within the hypodermis (most notable in the head region, see Figure 2-10C) and in the germline (data not shown).

To mutate the 3′*cis*-regulatory regions of *bli-1*: Injection of two crRNAs with the target sequences (P43, P44) (Integrated DNA Technologies), tracrRNA, Cas9, a homology repair template that was amplified using sequences (P45, P46) (Phusion High-Fidelity DNA Polymerase, New England BioLabs), which amplifies the 3′utr + 50bp of *unc-22,* and pRF4 into N2 and subsequent screening were performed as described above. Genotyping for the altered *bli-1* gene was performed using triplex PCR (P47, P48, P49). A strain with partial (~65%) integration of the *unc-22 3'cis* region, a repeat of the first 183 bp of the *unc-22 3'cis* region, and the endogenous *bli-1 3'cis* region was designated as AMJ1754 and a strain with complete integration was designated as AMJ1755.

To mutate the 3′ *cis*-regulatory regions of *unc-22*: Injection of two crRNAs with the target sequences (P50, P51) (Integrated DNA Technologies), tracrRNA, Cas9, a homology repair template that was amplified using sequences (P52, P53) (Phusion High-Fidelity DNA Polymerase, New England BioLabs), which amplifies the 3′utr + 50bp of *bli-1,* and pRF4 into N2 and subsequent screening were performed as described above. Genotyping for the altered *unc-22* gene was performed using triplex PCR (P47, P48, P54). Strains with mutated *unc-22* 3′ *cis* region were isolated and designated as AMJ1730 and AMJ1731.

2.3.7 Sequence and structure alignments

Sequences of *C. elegans* proteins were obtained from WormBase; sequences of proteins from all other species were obtained from UniProt. Alignments were created using Clustal Omega (EMBL-EBI) with default settings.

PyMOL (v. 2.4.1) was used to modify and annotate PDB files. The RDE-10 (UniProt: Q9N3S2) PDB file is based on predictions from AlphaFold. Protein domains were colored based on homology to domains as found in the EMBL-EBI Pfam database (Maelstrom: PF13017). The protein structure alignment was done using the Pairwise Structure Alignment from Protein Data Bank with rigid parameters (RMSD Cutoff 3; AFP Distance Cutoff: 1600; Fragment length: 8). The exonuclease domain of ERI-1 (UniProt:O444606) and of MUT-7 (UniProt:P34607) were compared with the Maelstrom domain of RDE-10.

2.3.8 Feeding RNAi.

Control RNAi by feeding *E. coli* containing the empty dsRNA-expression vector (L4440), which can generate a short dsRNA derived from the multiple cloning site but does not produce dsRNA against any *C. elegans* gene, was done in parallel with all RNAi assays.

P0 and F1 feeding: Bacteria expressing dsRNA was cultured in LB media with 100 µg/µl carbenicillin overnight at 37ºC at 250 rpm. 100 µl of cultured bacteria was then seeded onto RNAi plates [NG agar plate supplemented with 1 mM isopropyl β-D-1-thiogalactopyranoside (IPTG) (Omega) and 25 µg/ml carbenicillin (MP Biochemicals)]. Adult animals were passaged onto seeded RNAi plates and removed after 24hr. Progeny were scored for silencing by bacteria expressing dsRNA targeting *unc-22* (defect evident as twitching within ~3 min. in 3 mM levamisole) or *bli-1* (defect evident as blisters along the body).

P0 pulse feeding: L4 and young adult animals were placed on seeded RNAi plates for 1hr after which they were transferred to an OP50 plate for 1hr, and then transferred to a new OP50 plate once again to minimize the residual RNAi food carryover. Animals were left on OP50 plates and scored every 24hr for 8 subsequent days with transfer to new OP50 plates every two days to prevent overcrowding.

F1 only feeding: A single L4 or young adult (1 day older than L4) animal (P0) was placed on an RNAi plate seeded with 5µl of OP50 and allowed to lay eggs. After 1 day, when most of the OP50 was eaten, the P0 animal was removed, leaving the F1 progeny. 100µl of an overnight culture of RNAi food (*E. coli* which express dsRNA against a target gene) was added to the plate. Two or three days later, the F1 animals were scored for gene silencing by measuring gene-specific defects.

2.3.9 RNA extraction and PCR with reverse transcription (RT-PCR)

Total RNA was extracted using TRIzol (Fisher Scientific) from pellets of mixed-stage animals collected from non-starved but crowded plates in biological triplicate for each strain after exposure to either *unc-22* RNAi or the L4440 vector. The aqueous phase was then washed with an equal amount of chloroform and precipitated overnight at -20°C with 10 µg glycogen (Invitrogen) and 1 ml of isopropanol. RNA pellets were washed twice with 70% ethanol and resuspended in 25 µl of nuclease free water.

RT-PCRs for pUG RNAs (Figure 2-13C) were done as described earlier (96). Briefly, cDNA was created from isolated RNA using Superscript III Reverse Transcriptase (ThermoFisher) and a universal primer (P55) that contains nine AC repeats and two adapter sequences. The cDNA was used as a template for a Phusion (NEB) PCR with the first set of primers (adapter 1 P56; *gsa-1* P57; 0kb P58; 1kb P59). The amplicon was diluted 1:20 and used as template for the nested

Phusion PCR with the second set of primers (adapter 2 P60; *gsa-1* P61; 0kb P62; 1kb P63). The final PCR product (20 µl) was loaded on a 1% agarose gel and imaged. An annealing temperature of 60ºC was used for *gsa-1* and 57ºC was used for all other primer sets.

For semi-quantitative RT-PCR (Figure 2-6), RNA from each strain was isolated from 50 L4-staged animals as described earlier (136). Primer P64 was used to reverse transcribe the sense strand of *rde-4* and P65 was used to reverse transcribe the sense strand of *tbb-2*. The resulting cDNA was used as a template for PCR (30 cycles for both *rde-4* and *tbb-2*) using Taq polymerase and gene-specific primers (P66, P67 for *rde-4* and P68, P69 for *tbb-2*). Intensities of the bands were quantified using Image J (NIH). The relative intensity of the *rde-4* band normalized to that of the *tbb-2* band was set as 1.0 in wild type. The relative normalized intensity of the *rde-4* band in WM49 (*rde-4(ne301)*) was subtracted from that in AMJ611 to report the levels of *rde-4(+)* mRNA (0.3 relative to wild type).

2.3.10 Microscopy

Following *gfp* RNAi (Figs. 5C, 5D), F1 adult animals were mounted in 10 µl of 3 mM levamisole on a 2% agar pad and imaged under a coverslip using a Nikon AZ100 microscope and Prime BSI Express sCMOS camera. A C-HGFI Intensilight Hg Illuminator was used to excite GFP (filter cube: 450 to 490 nm excitation, 495 dichroic, and 500 to 550 nm emission). Representative images for GFP expression were adjusted to identical levels in Fiji (NIH) for presentation.

2.3.11 Rational for inferences

Prior knowledge: Gene-specific requirements for RNA silencing could reflect specialization along pathways, as is supposed for multiple endogenous small RNA pathways in *C.*

elegans. Reasons that impact the efficiency of silencing a gene are obscure because of a lack of a quantitative model for RNAi that incorporates recently discovered RNA intermediates.

Evidence supporting key conclusions: Three different proteins, MUT-16, RDE-10, and NRDE-3, play a role in RNAi such that each is singly required for silencing *bli-1* but any two are sufficient for silencing *unc-22*. Simulations support the parsimonious hypothesis that this difference in requirements can be explained by quantitative contributions from regulators within an intersecting network for silencing both genes but not by parallel pathways downstream of mRNA recognition. Consistently, the requirement for NRDE-3 for silencing *bli-1* is bypassed by enhancing the processing of dsRNA through the loss of ERI-1 or the overexpression of RDE-4.
A quantitative model for RNAi of any gene at steady state reveals several ways that differences in genetic requirements could arise for silencing different genes. Experimental tests that confirm predictions of the quantitative models include changes in the requirement for NRDE-3 for silencing caused by altering *cis*-regulatory regions of the gene targeted by dsRNA; recovery from silencing in non-dividing cells after exposure to a pulse of *unc-22* dsRNA, which supports the turnover of all key RNA intermediates (1º siRNAs, 2º siRNAs, and pUG RNAs) through mechanisms that are currently unknown; and the dearth of pUG RNA generation by 2º siRNAs, consistent with a lack of 3º siRNAs.

2.4 Results

2.4.1 Two genes with different thresholds for silencing reveal an intersecting network of regulators that mediate RNA interference.

To identify regulators of RNA interference (RNAi), we performed a primary screen for mutants that disrupt the maintenance of mating-induced silencing of a transgene followed by a secondary screen for mutants that are also defective in the silencing of endogenous genes by ingested dsRNA (Figure 2-2A).

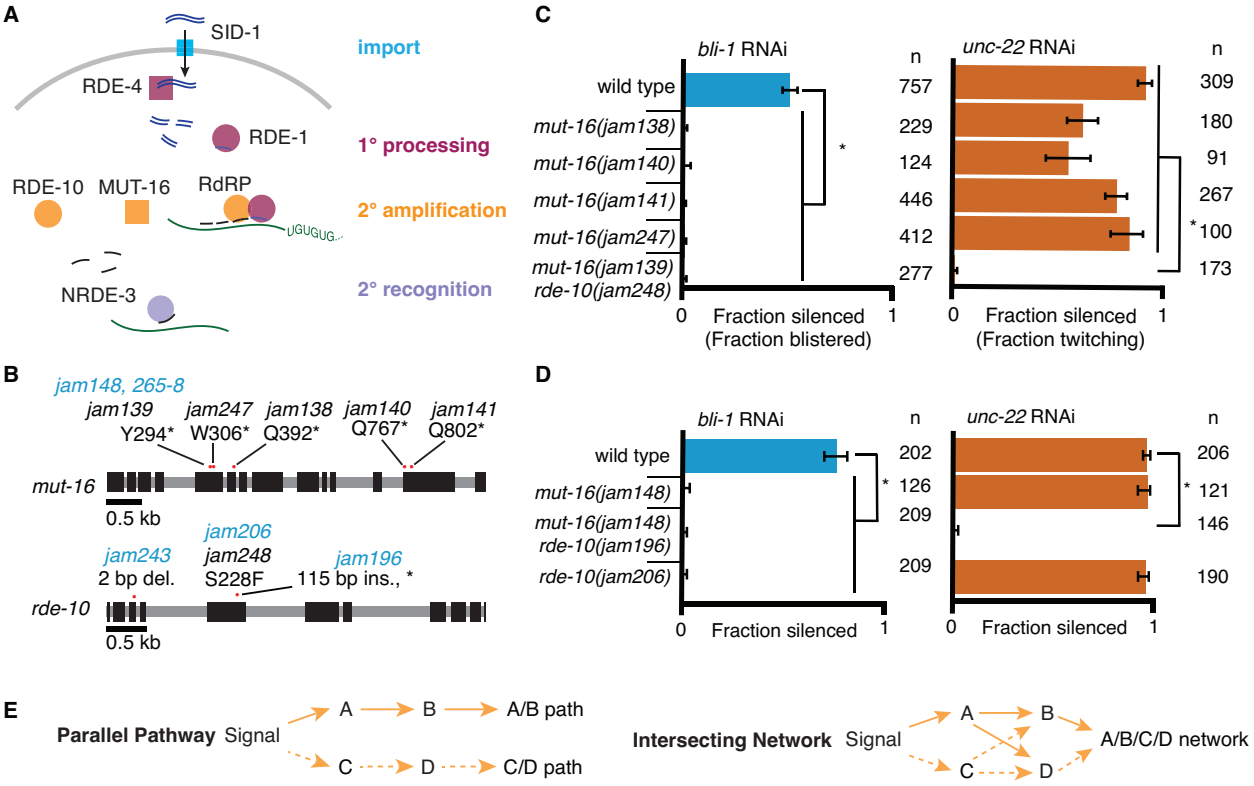


Figure 2-1. RNA interference of two somatic targets show stark differences in their requirements for MUT-16 and RDE-10. (A) Overview of RNA interference in somatic cells. Double-stranded RNA (dsRNA, blue) enters the cell through the importer SID-1 (import, teal), after which it is processed by the dsRNA-binding protein RDE-4 and the endonuclease Dicer into 1° short interfering RNAs (siRNAs) that are bound by the primary Argonaute RDE-1 (1° processing, pink). mRNA transcripts (green) recognized by these 1° siRNAs are modified after cleavage by the 3′ addition of UG repeats (pUG RNA) and act as templates for the amplification of 2° siRNAs aided by the intrinsically disordered protein MUT-16, the Maelstrom-domain containing protein RDE-10, and RNA-dependent RNA polymerases (2° amplification, orange). These 2° siRNAs can bind secondary Argonaute(s) (e.g., NRDE-3), which can then recognize additional complementary targets (2° recognition) and cause gene silencing. See text for details. (B) Gene schematics depicting the mutant alleles found in a genetic screen (black) and/or created using genome editing (blue). Black boxes indicate exons and red dots indicate locations of mutations. Allele names (e.g., *jam139*) and expected amino acid change in the corresponding proteins (e.g., mutation of a tyrosine codon to a stop codon, Y294*) are indicated. See Figure 2-2 for details of genetic screen. (C and D) Response to *bli-1* or *unc-22* RNAi in different mutants.

For each mutant, the fraction of animals that showed *bli-1* silencing or *unc-22* silencing (fraction silenced) and the numbers of animals scored (n) are shown. Asterisks indicate $p < 0.05$ for each comparison (brackets) using Wilson′s estimates with continuity correction and error bars represent 95% confidence interval. (C) Of five isolates with a mutation in *mut-16*, four (*jam138*, *jam140*, *jam141*, and *jam247*) failed to silence *bli-1* (blue) but retained *unc-22* silencing (orange). The other mutant failed to silence both genes and additionally had a mutation in *rde-10* (*mut-16(jam139) rde-10(jam248)*). (D) Mutants created using genome editing recapitulated the selective silencing of *unc-22* in *mut-16(-)* single mutants (*mut-16(jam148)*) and the failure to silence both genes in *mut-16(-) rde-10(-)* double mutants (*mut-16(jam148) rde-10(jam206)*). Using genome editing to recreate the *jam248* mutation, which is expected to make a mutant protein (RDE-10(S228F)) that disrupts the Maelstrom domain (see Figure 2-2), resulted in animals (*rde-10(jam196)*) that showed *unc-22* silencing but not *bli-1* silencing. (E) Selective requirement for a regulator could reflect two underlying mechanisms of RNA silencing: (1) Two parallel pathways (left, A/B path vs C/D path) that are differentially used for different target genes; or (2) One intersecting network (right, A/B/C/D network) with quantitative contributions by all regulators along with different thresholds for each target gene.

Mating males with a transgene that expresses fluorescent proteins to hermaphrodites that lack the transgene can initiate silencing in progeny that lasts in descendants for hundreds of generations (133), providing a stable strain that can be mutagenized to look for mutations that result in the recovery of expression from the fluorescent transgene. Of the 15 fertile mutants that showed re-expression, whole-genome sequencing followed by in silico complementation (see Materials and Methods), revealed five mutants that had premature stop codons in *mut-16* (Figure 2-1B), a known regulator of RNAi that is required for the production of secondary siRNAs (74, 101, 104). MUT-16 is required for the silencing of all tested somatic targets except the muscle gene *unc-22* (74), which showed residual silencing (′+++′ vs ′+′ but not ′-′ in (101)) and is considered a sensitive target for RNAi (28). While all five putative *mut-16* mutants failed to silence the hypodermal gene *bli-1* (Figure 2-1C, *left*), only four of the five showed *unc-22* silencing (Figure 2-1C, *right*).

Upon further analysis of the mutant that failed to silence *unc-22*, we found that this mutant also contained a missense mutation in RDE-10, another known regulator of RNAi that is required

for the production of secondary siRNAs (102, 103). This missense mutation (Ser228Phe) is expected to disrupt the Maelstrom domain of RDE-10 (Figure 2-2C), and thus could result in a loss of RDE-10 function. To eliminate possible confounding effects of multiple mutations in strains isolated from a genetic screen, we used Cas9-mediated genome editing to introduce mutations in *mut-16* (null) and/or *rde-10* (null or a missense mutation that encodes Ser228Phe) in a wild-type background (Figure 2-1B). While the newly created *mut-16(null)* mutants showed *unc-22* silencing as expected, *mut-16(null) rde-10(null)* (Figure 2-1D, *right,* Figure 2-4B) double mutants failed to silence *unc-22*. Since *unc-22* is a particularly sensitive target for RNAi (28), this lack of *unc-22* silencing in the absence of two regulators with roles in the amplification of 2º siRNAs suggests that 1º siRNA production and RDE-1-mediated recognition of the mRNA is likely not sufficient to cause silencing of most genes. These observations suggest that MUT-16 and RDE-10 are redundantly or additively required for silencing *unc-22* and that the Maelstrom domain of RDE-10 is required for this function. Since the primary Argonaute RDE-1 is required for the silencing of all somatic targets (Figure 2-1A; (87, 88)), including *unc-22*, we propose that MUT-16 and RDE-10 act in parallel downstream of RDE-1 to promote the amplification of 2º siRNA. This branching of the RNAi pathway downstream of RDE-1 could result in strictly parallel pathways where MUT-16 and RDE-10 are used to silence different sets of genes (Figure 2-1E, *left*) or in an intersecting network where both regulators contribute to the silencing of all genes (Figure 2-1E, *right*).

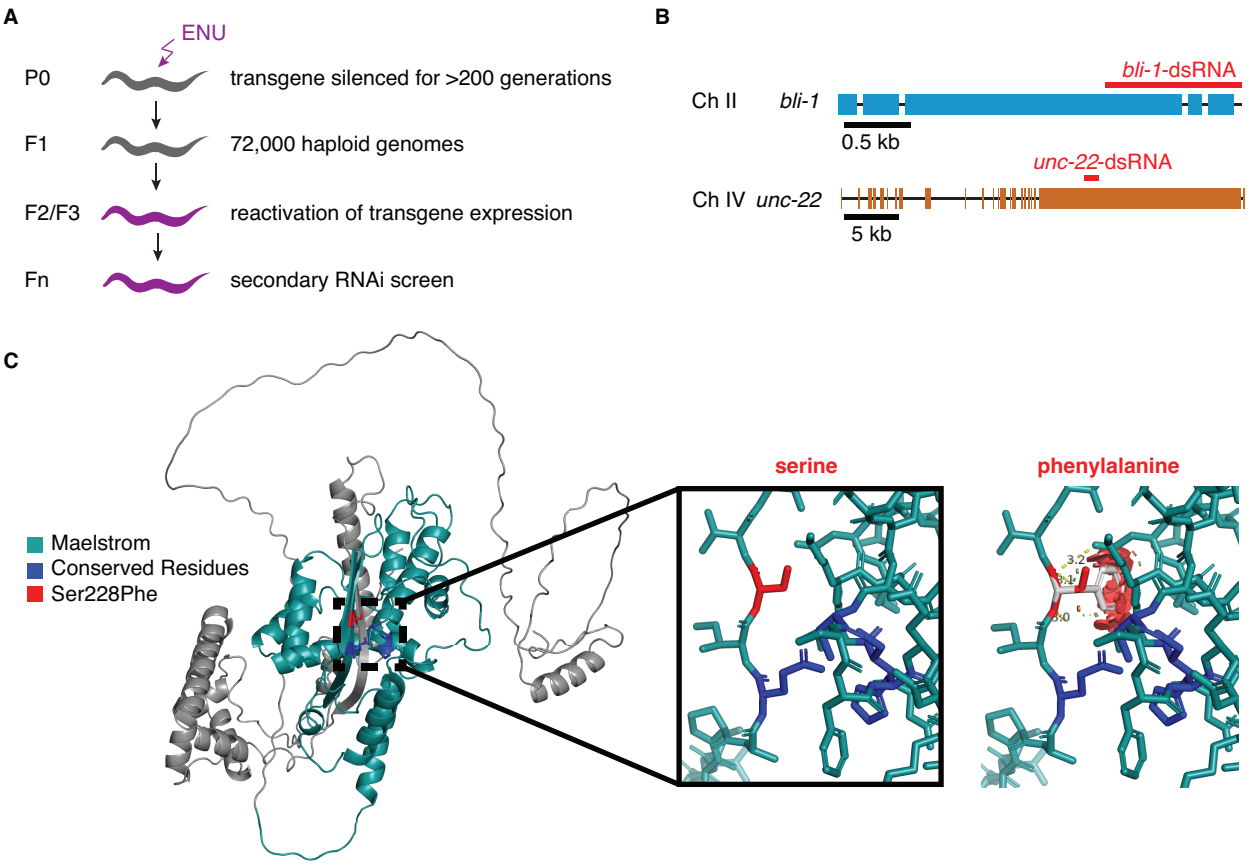


Figure 2-2. A forward-genetic screen identifies a mutation that is expected to disrupt the Maelstrom domain of RDE-10. (A) Schematic depicting the screen. Males containing a transgene (*mex-5p::mCherry::h2b::tbb-2 3'utr::gpd-2 operon::gfp::h2b::cye-1 3'utr)* were mated to wild-type hermaphrodites, and progeny that showed silencing of the transgene were isolated. Animals that had been thus silenced for over 200 generations were mutagenized with N-ethyl-N-nitrosourea (ENU). Homozygous mutants that showed a re-activation of the transgene expression were isolated, and then subjected to a secondary feeding RNAi screen where the ability to silence two targets (*bli-1* and *unc-22*) was tested. (B) Schematics depicting the genes that were targeted by feeding RNAi. Black boxes, indicating exons, and regions that share homology with the dsRNA (blue, *bli-1;* orange, *unc-22*) are shown. (C) Predicted structure of RDE-10 showing the expected steric hinderance caused by the Ser228Phe mutation isolated in the screen. (*left*) The structure predicted by AlphaFold (128, 129) contains a Maelstrom domain (teal; Pfam: PF13017). Ser228 (red) and the conserved ECHC motif that can bind zinc (dark blue) are highlighted. (*middle* and *right*) Closeup of residue 228, showing the wild-type Ser (*middle*) and one orientation of Phe (*right*), which highlights the expected steric hinderance (red).

Additional observations suggest differences in the requirements for silencing *bli-1* and *unc-22*. Animals that lack MUT-16 (Figure 2-1D), RDE-10 (Figure 2-1D) or the nuclear Argonaute

NRDE-3 (120) fail to silence *bli-1* but not *unc-22.* However, *rde-10(-); nrde-3(-)* double mutants fail to silence *unc-22* (102). Therefore, if there were strictly parallel pathways downstream of MUT-16 and RDE-10, then NRDE-3 would be expected to function downstream of MUT-16 but parallel to RDE-10. To test this possibility, we generated *nrde-3(-)* mutants using genome editing (Figure 2A) and compared silencing in single mutants and double mutant combinations using the newly generated mutants lacking MUT-16, RDE-10, or NRDE-3. As expected, all single mutants failed to silence *bli-1* but silenced *unc-22*. Surprisingly, all double mutants failed to silence both *bli-1* and *unc-22* (Figure 2-1D and 2-3B). This requirement for any two of MUT-16, RDE-10, or NRDE-3 suggests that the RNAi pathway cannot be strictly parallel downstream of RDE-1 (see Figure 2-4A).

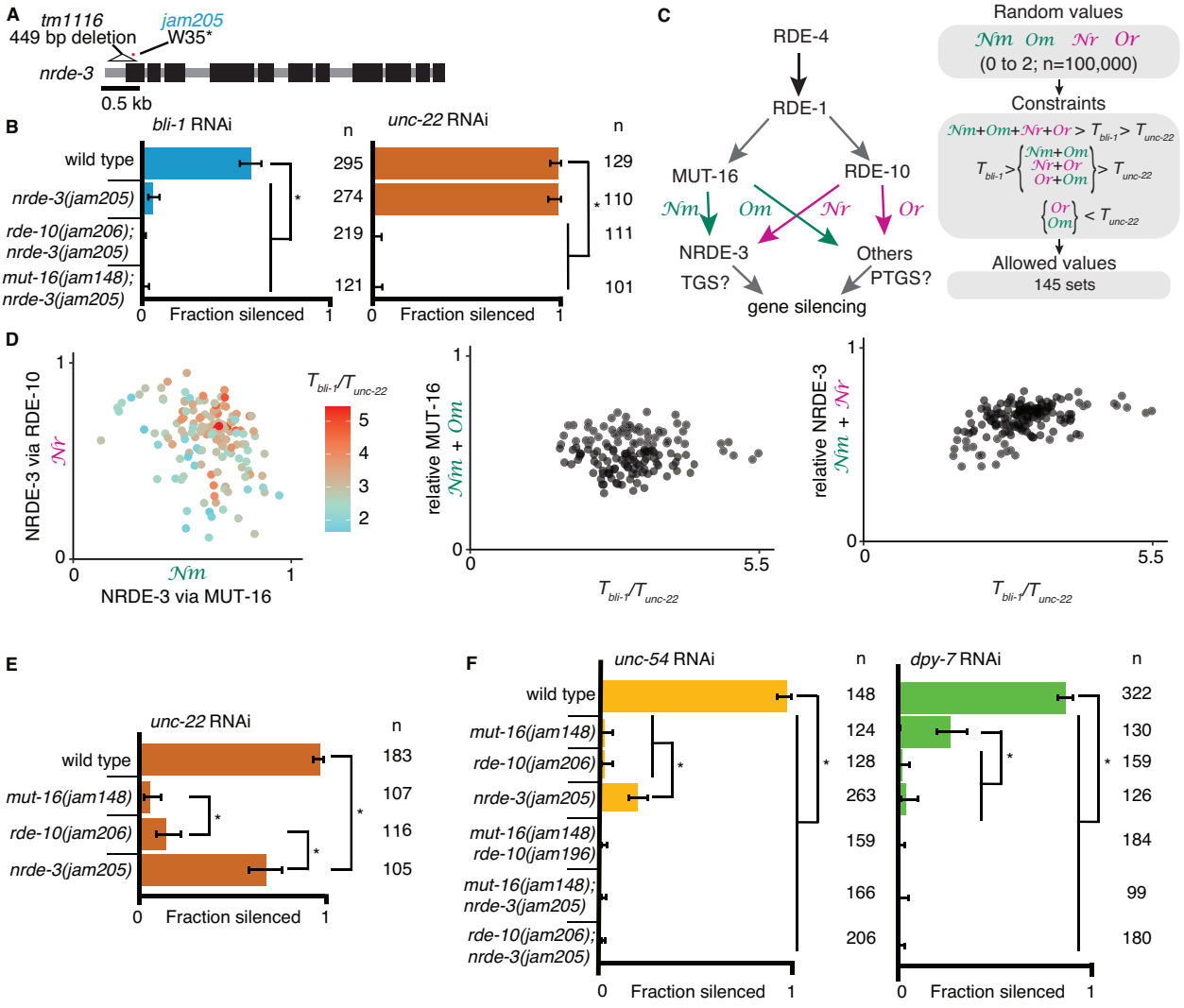


Figure 2-3. Gene-specific requirements and complex redundancy can arise from a single RNA regulatory network. (A) Schematic (as in Figure 2-1) depicting *nrde-3* alleles. (B) Feeding RNAi of *bli-1* and *unc-22.* Fractions silenced, numbers scored, comparisons, asterisks, and error bars are as in Fig. 1. Single mutants lacking NRDE-3 (*nrde-3(jam205)*) fail to silence *bli-1* but not *unc-22*. Double mutants fail to silence both targets. (C and D) Mutual constraints among parameters required for a single RNA regulatory network to support experimental results. (C, left) Model for a single network of interactors that regulate all RNAi targets in somatic cells. All targets require import (SID-1) and processing (RDE-4 and RDE-1) of dsRNA. Branching after 1° siRNA processing results in four distinct paths (Nm, Nr, *Om*, *Or*) that together contribute to gene silencing, which could occur through co-transcriptional gene silencing (TGS) and/or post-transcriptional gene silencing (PTGS) mechanisms. (C, *right*) Representation of simulation workflow. First, random values between 0 and 2 were drawn for each of the four variables (Nm, Nr, *Om*, *Or*). Second, constraints were added based on the experimental results in Figure 2-3B and Figure 2-1D. Third, allowed values that satisfied all experimental conditions were culled. Of 100,000 sets of random values simulated (0 to 2 for Nm, Nr, *Om*, *Or* and 0 to 100 for the ratio of thresholds $T_{bli\text{-}1}/T_{unc\text{-}22}$), 145 were consistent with all observed responses to RNAi. These allowed numbers reveal the domain of parameter values that support the observed range of gene silencing

outcomes using feeding RNAi. (D, *left*) The contribution of NRDE-3 via MUT-16 (Nm) versus that via RDE-10 (Nr) for different ratios of thresholds for *bli-1* versus *unc-22* silencing ($T_{bli\text{-}1}/T_{unc\text{-}22}$) are shown. (D, *center* and *right*) The relative contributions to silencing that require MUT-16 (Nm + *Om,* D, *center*) or NRDE-3 (Nm + Nr*,* D, *right*) do not frequently take extreme values and both support a low value for the ratio of thresholds ($T_{bli\text{-}1}/T_{unc\text{-}22}$ < ~5.5 despite allowed values of up to 100). (E) Feeding RNAi of *unc-22* assayed as in Fig. 1, but using aged plates, resulting in weaker RNAi. Animals that lack MUT-16 (*mut-16(jam148)*) have the most severe defect, followed by animals lacking RDE-10 (*rde-10(jam206)*), which is followed by animals lacking NRDE-3 (*nrde-3(jam205)*). (F) Feeding RNAi of *unc-54* or *dpy-7.* Fractions silenced, numbers scored, comparisons, asterisks, and error bars are as in Fig. 1. Silencing of *unc-54* showed a partial dependency on NRDE-3, while silencing of *dpy-7* showed a partial dependency on MUT-16, suggesting that the quantitative requirement for a regulator can differ depending on the target.

The stark differences in the extents of silencing *bli-1* (~0%) versus *unc-22* (~100%) (Figure 2-1D and 2-3B) in animals lacking MUT-16, RDE-10, or NRDE-3 suggest that there could be target-specific pathways for silencing, or more parsimoniously, that each regulator contributes to the silencing of both targets as part of an intersecting network, through transcriptional gene silencing (TGS) and/or post-transcriptional gene silencing (PTGS) (Figure 2-3C), with *unc-22* being more sensitive to silencing than *bli-1*. For such an intersecting network with quantitative contributions by multiple regulators of RNAi to explain the silencing of somatic targets, including targets like *unc-22* and *bli-1* that show dramatic differences, it should be possible to identify values for the relative contributions of each regulatory path (Nm = from MUT-16 to NRDE-3, Nr = from RDE-10 to NRDE-3, *Om* = from MUT-16 to other Argonautes, and *Or* = from RDE-10 to other Argonautes in Figure 2-3C, *left*) and for gene-specific thresholds ($T_{bli\text{-}1}$ = level of BLI-1 function below which a defect is detectable, and $T_{unc\text{-}22}$ = level of UNC-22 function below which a defect is detectable) that are consistent with all experimental data (′constraints′ in Figure 2-3C, *right*). Of the 100,000 sets of parameters simulated, 145 sets satisfied all experimental constraints (Figure 2-3D). These allowed parameter sets were obtained despite the conservative assumption that the levels of mRNA knockdown for detecting observable defects for *bli-1* and *unc-22* are similar.

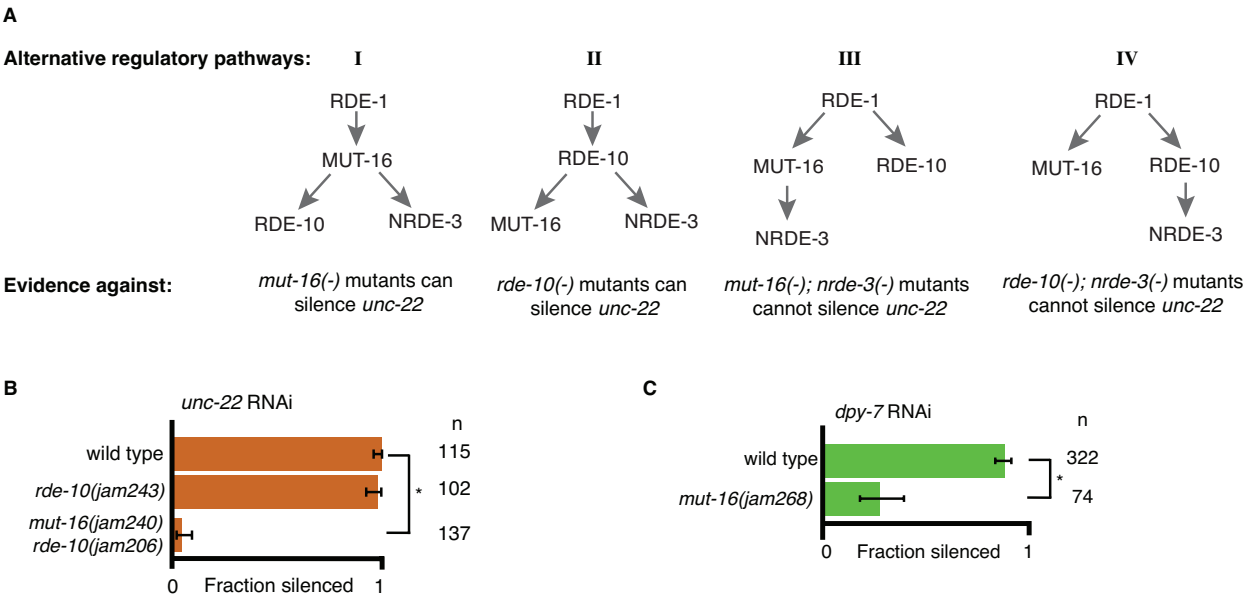


Figure 2-4. Support for an intersecting regulatory network. (A) Alternative regulatory pathways excluded by data. Four plausible alternative models of the one presented in Figure 2-3C along with the experimental evidence from Figs. 2-1 and 2-2 are shown. (B and C) Feeding RNAi of *unc-22* or *dpy-7.* Fractions silenced, numbers scored, comparisons, asterisks and error bars are as in Fig. 2-1. (B) An allele of *rde-10* that results in a premature stop codon (*jam243*) is still capable of silencing *unc-22* to near wild type levels. A newly created premature stop codon in *mut-16(-)* (*jam240*) created in the background of the RDE-10(Ser228Phe) mutant (*jam206*) fails to silence *unc-22,* supporting the findings in Fig. 2-1D. (C) An additional allele of *mut-16(-)* (*jam268*) shows about 25% silencing in response to *dpy-7* RNAi, supporting the findings in Fig. 2-3E.

Relaxing this assumption will lead to a larger number of allowed parameter sets. These valid parameter sets included cases with different relative contributions from RDE-10 and MUT-16 to NRDE-3-dependent silencing for a range of threshold differences for silencing *bli-1* versus *unc-22* (Figure 2-3D, left). Furthermore, extreme contributions of MUT-16 versus RDE-10 (Figure 2-3D, middle) or NRDE-3 versus other Argonautes (Figure 2-3D, right) were absent. Finally, only thresholds for *bli-1* silencing that are less than ~5.5x the threshold for *unc-22* silencing were supported despite the allowed range of up to 100x (Figure 2-3D). Consistent with different quantitative contributions to silencing by each regulator, reducing the availability of *unc-22* dsRNA revealed a graded silencing response: *mut-16(-)* < *rde-10(-)* < *nrde-3(-)* (Figure 2-3E;

~5% silencing in *mut-16(jam148)* ~15% in *rde-10(jam206)* and ~70% in *nrde-3(jam205)*). Consistent with the possibility of differential contributions from each regulator for different targets (Figure 2-3D), while partial silencing is observable in the absence of NRDE-3 but not MUT-16 or RDE-10 when the muscle gene *unc-54* is targeted (Figure 2-3F, *left*), partial silencing is observed in the absence of MUT-16 but not NRDE-3 or RDE-10 when the hypodermal gene *dpy-7* is targeted (Figure 2-3F, *right*).

Taken together, our results are consistent with a single network for RNAi targeting somatic genes where intersecting regulatory pathways downstream of mRNA recognition provide quantitative contributions to silencing.

2.4.2 The genetic requirement for NRDE-3, but not for MUT-16 and/or RDE-10, can be bypassed by enhancing dsRNA processing.

The production of pUG RNAs and 2º siRNAs requires the participation of mRNA (Figure 2-1A), making the contributions of some steps during RNAi gene-specific. Therefore, genes could differ in their dependence on proteins required for steps downstream of dsRNA processing and 1º siRNA production. Such differential dependencies could in principle be overcome by increasing the amount of available processed dsRNA and/or 1º siRNA when alternative parallel paths are available (e.g., loss of NRDE-3, MUT-16, or RDE-10 in Figures 2-1 and 2-2) but not when no alternative paths are available (e.g., loss of both MUT-16 and RDE-10 in Figure 2-1B) or when the increase in dsRNA processing is insufficient. To test these predictions, we increased dsRNA processing and examined silencing in animals lacking different regulators required for the silencing of *bli-1* and/or *unc-22*.

One approach for increasing dsRNA processing is the release of factors such as the endouclease DCR-1 from competing endogenous pathways by removing the exonuclease ERI-1 (137).

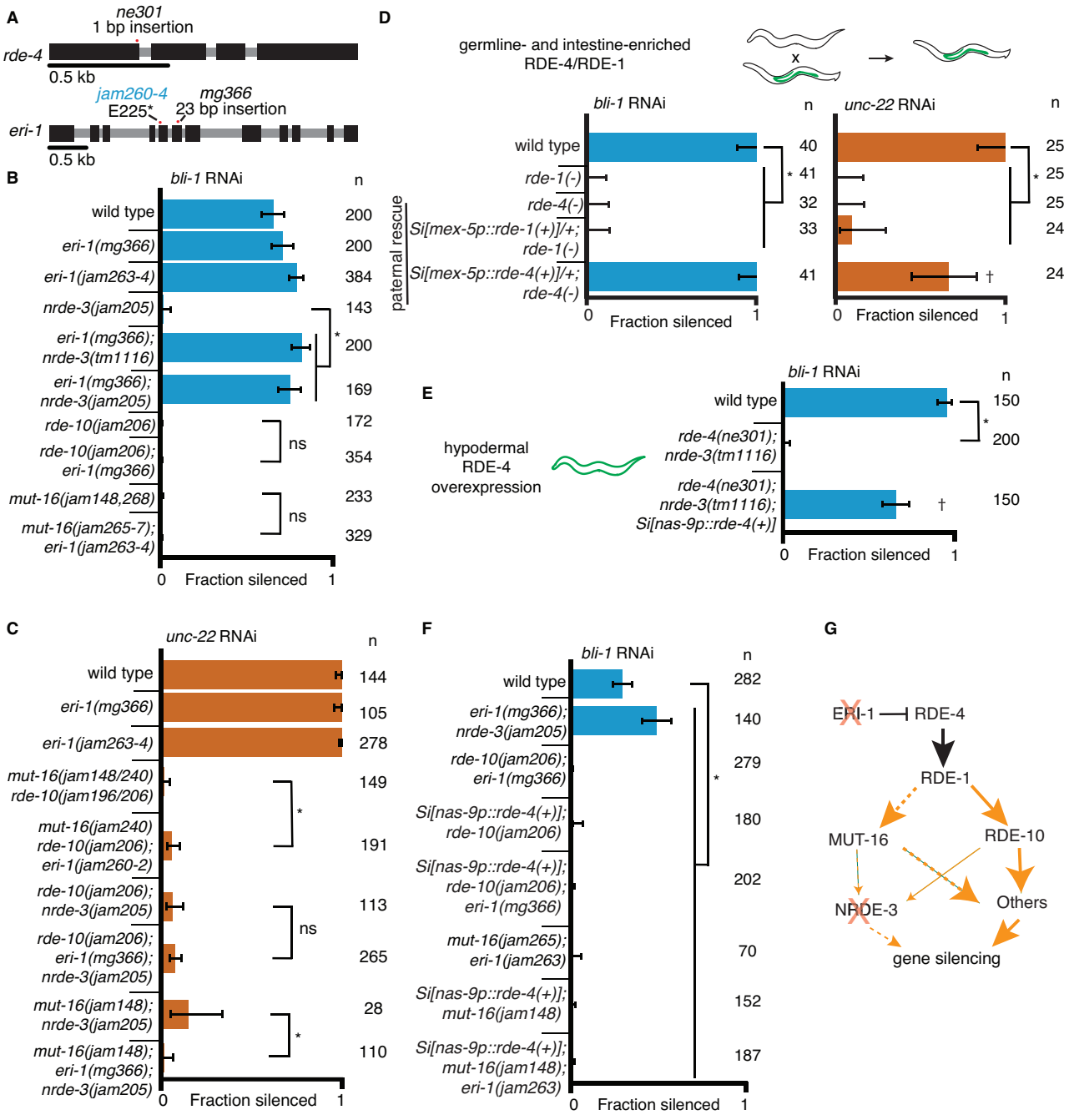


Figure 2-5. Gene-specific requirements for NRDE-3 can be bypassed in two ways. (A) Gene schematics (as in Figure 2-1) of *rde-4* and *eri-1*. (B and C) Loss of ERI-1 can bypass the NRDE-3 requirements for silencing *bli-1* but not the other requirements for silencing *bli-1* or *unc-22*.

Feeding RNAi targeting *bli-1* (B) or *unc-22* (C) with fractions silenced, numbers scored, comparisons, asterisks, and error bars as in Fig. 1. (B) Loss of ERI-1 (*mg366, jam263,* and *jam264* alleles) can compensate for the role of NRDE-3 (*tm1116* and *jam205* alleles) but not of RDE-10 (*jam206* allele) or MUT-16 (*jam148*, *jam265*, *jam266*, *jam267*, and *jam268* alleles) in *bli-1* silencing. See Table 2-3 for additional information. (C) Silencing of *unc-22* is not restored by loss of ERI-1 (*mg366*, *jam260*, *jam261*, and *jam262* alleles) in mutants that also lack any two of *mut-16* (*jam148* and *jam240* alleles), *rde-10* (*jam196* and *jam206* alleles), or *nrde-3* (*jam205* allele). See Table 2-3 for additional information. (D to E) Overexpression of RDE-4 in the hypodermis can bypass the requirement for NRDE-3 in *bli-1* silencing. (D) Minimal amounts of RDE-4 are sufficient for somatic silencing. (*top*) Schematic depicting generation of male progeny with paternal inheritance of a single-copy transgene (*Si[…]*) that expresses *rde-4(+)* or *rde-1(+)* under the control of the *mex-5* promoter (*mex-5p*) in the germline (green) of *rde-4(-)* or *rde-1(-)* animals, respectively (germline- and intestine-enriched RDE, based on rescue of RNAi in *rde-1(-)* animals (39)). (*bottom*) Male cross progeny with the transgene were scored after feeding only F1 animals, showing that unlike animals with germline- and intestine- enriched RDE-1, animals with similarly enriched RDE-4 can rescue both *unc-22* and *bli-1* silencing. Thus, small amounts of RDE-4 potentially mis-expressed in the hypodermis or a non-autonomous effect of RDE-4 from the germline or intestine is sufficient for silencing in the muscle and hypodermis. † indicates $p<0.05$ when compared to either wild type or the *rde-4(-)* mutant and other symbols are as in (B). (E) Silencing of *bli-1* is restored in *nrde-3(tm1116)*; *rde-4(ne301)* double mutants when *rde-4(+)* is overexpressed in the hypodermis (*Si[nas-9p::rde-4(+)]*). (F) Silencing of *bli-1* is not restored in animals lacking MUT-16 or RDE-10, despite the overexpression of RDE-4 in the hypodermis and/or the loss of ERI-1. (G) Summary depicting the bypass of NRDE-3 when ERI-1 is eliminated and/or RDE-4 is overexpressed. The increase in dsRNA processing increases the contributions of NRDE-3-independent paths to silencing.

In addition to the increased availability of DCR-1 when ERI-1 is removed, downstream factors involved in siRNA amplification (e.g. MUT-16, MUT-2/RDE-3, RDE-10/11, etc.) and 2º Argonautes (e.g. WAGOs) would be more available to contribute to silencing in response to ingested dsRNA. We used available *eri-1* mutants (Figure 2-5A, *mg366*) and mutants generated using Cas9-mediated genome editing (Figure 2-5A, *jam260* to *jam264*) to test if requirements for silencing *bli-1* and/or *unc-22* could be bypassed. Loss of ERI-1 enabled *bli-1* silencing in animals lacking NRDE-3, but not in animals lacking RDE-10 or MUT-16 (Figure 2-5B). Furthermore, loss of *eri-1* was not sufficient for the complete rescue of *unc-22* silencing in animals lacking any two of these three regulators (Figure 2-5C). An alternative approach for increasing dsRNA processing is the overexpression of the dsRNA-binding protein RDE-4, which recruits dsRNA for processing

by DCR-1 (86, 117). Minimal amounts of RDE-4 can support RNAi as evidenced by silencing in *rde-4(-)* adult progeny of *rde-4(+/-)* hermaphrodites (Figure S7E in ref. (132)) and in *rde-4(-)* animals with trace levels of ectopic expression from multicopy *rde-4(+)* transgenes (Figure 2 in (120)). We found that even hemizygous males expressing *rde-4(+)* from a single-copy transgene driving expression in the germline and the intestine under the control of the *mex-5* promoter (132) was sufficient for rescuing both *bli-1* and *unc-22* silencing (Figure 2-5D). Similar expression of *rde-1(+)*, however, was not sufficient for rescuing silencing in *rde-1(-)* animals (Figure 2-5D), suggesting that small amounts of RDE-4 but not RDE-1 are sufficient for RNAi. RDE-4 can be selectively overexpressed in the hypodermis using a single-copy transgene with a *nas-9* promoter (overexpression evident in Figure 2-6; and selectivity demonstrated in 2-8C in (120)). This hypodermal expression of *rde-4(+)* was sufficient to enable *bli-1* silencing in an otherwise *rde-4(-); nrde-3(-)* background (Figure 2-5E). Thus, either loss of ERI-1 or overexpression of RDE-4 can bypass the need for NRDE-3 for silencing *bli-1*, suggesting that the requirement for this regulator does not reflect a specific need for a particular regulator (NRDE-3) but reflects a larger amount of silencing signals required for reducing *bli-1* function sufficiently to cause a detectable defect.

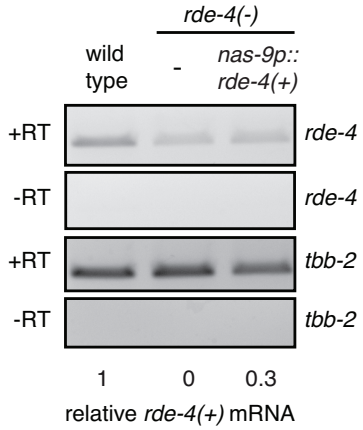


Figure 2-6. Overexpressing RDE-4 in the hypodermis. Semiquantitative RT-PCR of *rde-4* mRNA and *tbb-2* mRNA (control) in wild-type animals, *rde-4(-)* animals, or *rde-4(-)* animals expressing *rde-4(+)* in the hypodermis using a single-copy transgene (*Si(nas-9p)*). +RT and -RT indicate whether reverse transcriptase was used. The normalized mRNA abundance in *rde-4(-)* animals was subtracted from all lanes. With the observation in Fig. 3E and abundance of *rde-4* transcripts in the germline in wild-type animals (in situ data from NEXTDB), expression at ~30% of wild type is expected to be an overexpression in the hypodermis.

However, loss of ERI-1 and/or overexpression of RDE-4 could not compensate for the loss of RDE-10 or MUT-16 for *bli-1* silencing (Figure 2-5F), suggesting that these regulators make a

more substantial contribution to *bli-1* silencing than NRDE-3. These observations further support the idea that 1º siRNAs alone are not sufficient to cause silencing, consistent with the lack of *unc-22* silencing in *mut-16(-) rde-10(-)* double mutants (Figure 2-1B, 2-1D). One explanation for these results is that in *eri-1(-); nrde-3(-)* double mutants (Figure 2-5G), a different 2º Argonaute is able to compensate for the lack of NRDE-3, whereas in *mut-16(-); eri-1(-)* or *rde-10(-); eri-1(-)* double-mutants, the reduction of 2º siRNAs is too great to cause a detectable Bli-1 defect.

Taken together, these results suggest that gene-specific requirements for some proteins that function in RNAi do not reflect different pathways for silencing different genes, but rather a quantitative requirement for regulators acting as part of an intersecting RNA regulatory network.

2.4.3 Quantitative modeling of RNA interference and mRNA production provides rationales for a variety of target-specific outcomes.

The many protein regulators of RNAi drive changes in RNA metabolism, including the production of new RNA species (1º siRNA, 2º siRNA, and pUG RNA), that are associated with the targeted gene. Although these changes can be indicators of RNA silencing, the quantitative relationship between such RNA intermediates and the extent of gene silencing measured as a reduction in function of the targeted gene or its mRNA levels is unclear. A priori, reduction in the mRNA levels of a gene could depend on universal processing of imported dsRNA, production of secondary small RNAs with the participation of gene-specific mRNAs, and downregulation of pre-mRNA and mRNA influenced by pre-existing gene-specific RNA metabolism. To understand how these gene-specific factors could influence RNA silencing, we began by analyzing the impact of a few characteristics of a gene on mRNA (*m*) and pre-mRNA levels (*p*) after RNAi. We first used a sequential equilibrium model, where we assume each step must be completed before beginning

the next, e.g. dsRNAs are fully processed into 1º siRNAs, then 1º siRNAs can recognize transcripts to result in the production of pUG RNAs, and so on (Figure 2-7A).

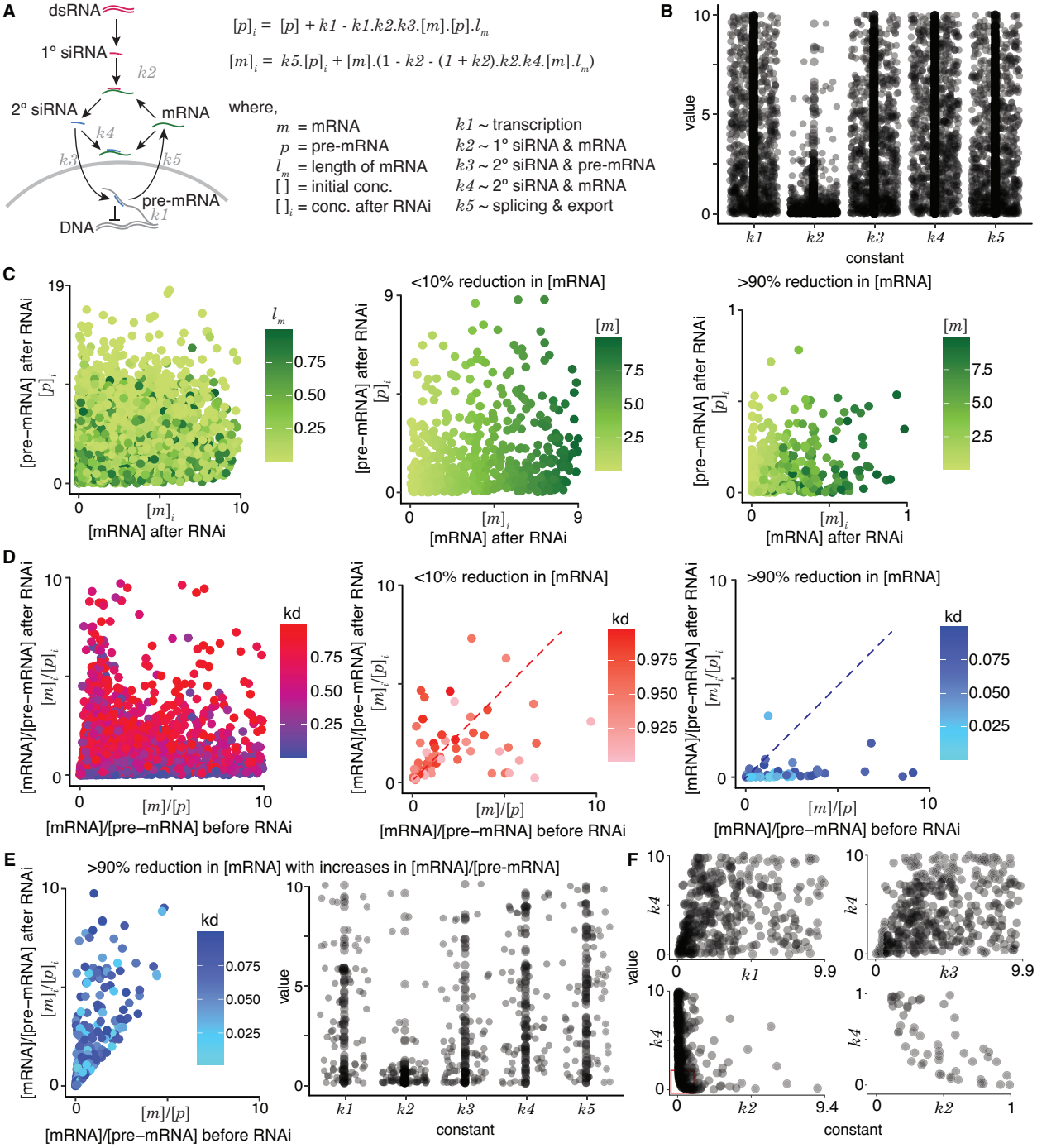


Figure 2-7. An equilibrium model for RNAi. (A) Model highlighting different RNA species and their interactions during RNA interference. *Left*, Schematic showing downstream events upon processing of intracellular dsRNA. *Right,* Equations for the pre-mRNA ($[p]_i$) and mRNA ($[m]_i$) concentrations after RNAi in terms of the concentrations before RNAi ($[p]$ and $[m]$) and the length

of the transcript (l_m). Rate constants for transcription (*k1*), binding constants for complex formation (1º siRNA-mRNA (*k2*), 2º siRNA-pre-mRNA (*k3*), and 2º siRNA-mRNA (*k4*)), and rate constants for splicing followed by export out of the nucleus (*k5*) were considered. (B) Distributions of allowed values for all constants that are consistent with knockdown. One million random sets of values from 1 to 10 were assigned for all constants and the 790 sets that supported knockdown ($[m]_i < [m]$) and residual presence of pre-mRNA and mRNA ($[m]_i > 0$ and $[p]_i > 0$) were selected and plotted. Most values of *k2* were small as expected to satisfy the $[m]_i > 0$ constraint because its square is subtracted in the equation for $[m]_i$. (C) RNAi can result in a variety of residual concentrations of pre-mRNA and mRNA. *Left*, Different ratios of residual mRNA and pre-mRNA ($[m]_i/[p]_i$) are possible for a given length of the target mRNA (l_m: 0 to 1). *Middle* and *Right*, Impact of $[m]$ on $[m]_i$ and $[p]_i$. *Middle*, When the knockdown is poor (<10%), the concentrations of mRNA after RNAi ($[m]_i$) remain close to concentrations before RNAi ($[m]$) as expected for all levels of residual pre-mRNA ($[p]_i$) as evidenced by the graded levels of $[m]_i$ that mirror the graded levels of $[m]$. *Right*, When the knockdown is strong (>90%), the low concentrations of mRNA after RNAi ($[m]_i$) can be associated with a range of values for $[p]_i$. (D) RNAi can alter the ratios of pre-mRNA and mRNA. *Left*, Changes in the ratios of mRNA to pre-mRNA upon RNAi ($[m]/[p]$ before to $[m]_i/[p]_i$ after) are possible for a variety of extents of knockdown (kd = $[m]_i/[m]$: 0 to 1). *Middle* and *Right*, Impact of kd on $[m]/[p]$ versus $[m]_i/[p]_i$. Increases and decreases in the ratios of mRNA to pre-mRNA (above versus below the dotted line) can occur in response to both poor (<10% with $0.9 < kd < 1.0$, *middle*) and good (>90% with $0.0 < kd < 0.1$, *right*) knockdown. While it appears that most cases of efficient knockdown are associated with a decrease in the ratio of mRNA to pre-mRNA (i.e., only one point above dotted line in *right*), increasing the numbers of parameter sets explored could reveal additional examples. (E) (left) Same as in (D, *right*) except only values that were to the left and above the dotted line. Instead of one million simulated values, one hundred million values were simulated to better examine the range of possible values in this group. (*center*) Same as in (B) but for the values culled in (E, *left*). (F) Constants (*k1* to *k5*) do not appear to show strong correlations with one another, except for *k2* and *k4*. The lack of values in the bottom left corner comparing *k2* to *k4* (bottom graphs) reflects the expectation that efficient silencing is not possible when both the primary and secondary binding constants are low.

We tested parameters that would result in varying levels of target RNA knockdown (790 of 1 million simulated parameters resulted in $[m]_i < [m]$, $[m]_i > 0$, and $[p]_i > 0$; Figure 2-7B). Under this simple model, we found that (1) RNAi can result in different residual concentrations of RNAs for different genes (Figure 2-7C); (2) for a given gene, silencing can alter the ratio of pre-mRNA to mRNA (Figure 2-7D and 2-7E); and (3) effective targeting of mRNA by primary or secondary small RNAs is required for strong silencing (Figure 2-7F). These observations hint at the influence of gene-specific factors on the functional outcome of RNAi and impel the exploration of a more detailed dynamic model.

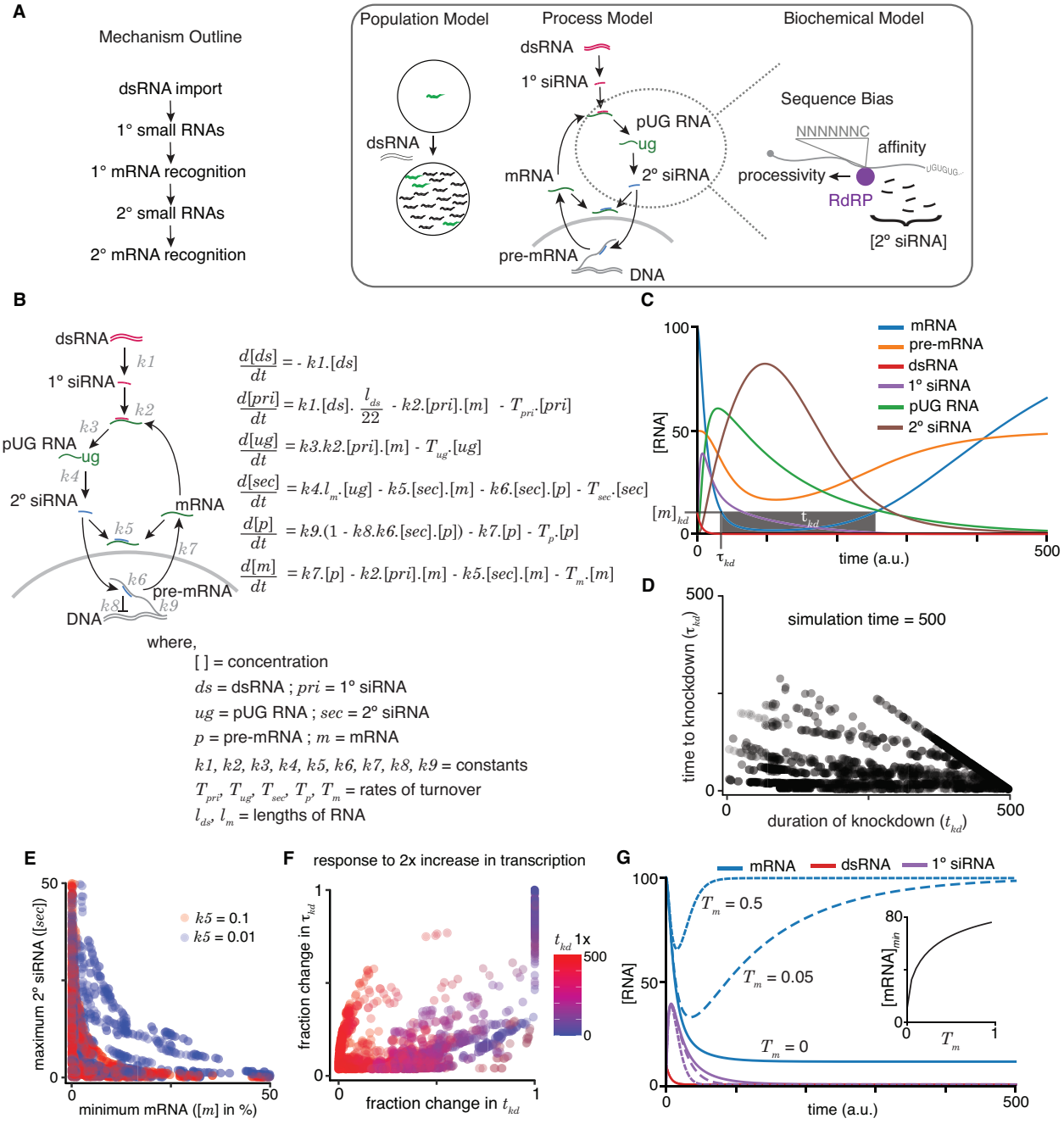


Figure 2-8. A quantitative model allows exploration of parameters for RNAi in *C. elegans*. (A) RNAi can be modeled to understand (from *left*) the responding populations of animals, the outline of mechanism, the process highlighting RNA species, the biochemical sub-steps (e.g., 2º siRNA production using pUG RNA, right). This study focuses on the overall RNA-mediated processes that accompany RNAi. (B) Schematic (*left*) and ordinary differential equations (*right*) describing the production and turnover of different RNA species. Rate constant for 1º siRNA processing from dsRNA (*k1*), binding constant for 1º siRNA binding target mRNA (*k2*), rate

constant for pUG RNA production (*k3*), rate constant for 2º siRNA production (*k4*), binding constant for 2º siRNAs binding mRNA (*k5*) or pre-mRNA (*k6*), rate constant for export and splicing of transcripts from the nucleus (*k7*), rate constant for repression of transcription (*k8*), and rate constant for new transcript production (*k9*). Other terms are described in the figure. (C) Relative changes in the concentrations of each RNA ([RNA] vs. time in a.u.; dsRNA, mRNA, pre-mRNA, pUG RNA, 1º siRNA, and 2º siRNA) for an example set of parameters (all turnover rates = 0.05, $k1 = 1$, $k2 = 0.01$, $k3 = 1$, $k4 = 0.05 * l_m = 0.5$, $k5 = 0.01$, $k6 = 0.01$, $k7 = 0.1$, $k8 = 0.05$, $k9 = 7.5$) are illustrated. A reduction to 10% of initial mRNA concentration is designated as the threshold for detecting a defect upon knockdown ($[m]_{kd}$), the time needed to reach the threshold (t_{kd}) and the time for which mRNA levels remain below the threshold (t_{kd}) are also indicated. (D) Relationship between the duration of knockdown and the time to knockdown (t_{kd} and t_{kd} are as in (C)). (E) Relationship between mRNA concentration and 2º siRNA accumulation. The minimum mRNA concentrations and maximum 2º siRNA concentrations reached for different transcripts with two different binding constants of 2º siRNAs binding to mRNA ($k5 = 0.1$, red and $k5 = 0.01$, blue) are plotted. Also see Fig. 2-9. (F) Impact of doubling transcription on transcripts with different knockdown parameters. Each transcript is colored based on its initial duration of knockdown (t_{kd}, blue to red gradient) before a 2-fold increase in the rate constant for transcription (*k9*) and the resultant fractional change in the duration of knockdown t_{kd} is plotted against that in the time to knockdown t_{kd}. (G) Genes with higher turnover are harder to knockdown. Response of mRNAs and their respective 1º siRNA with the same steady-state concentrations but with different rates of mRNA turnover (solid lines: $T_m = 0$, large dashes: $T_m = 0.05$, small dashes: $T_m = 0.5$) upon addition of 10 molecules of dsRNA are shown. (*inset*) Relationship of the minimum concentration of mRNA ($[\text{mRNA}]_{min}$) with its T_m in response to a fixed amount of dsRNA.

A qualitative outline of the molecular mechanism for RNAi in *C. elegans* has been deduced based on a variety of studies over the last two decades (mechanism outline; 2-8A, *left*), but the cellular, subcellular, and kinetic details of every step remain obscure. Quantitative modeling of RNAi - or indeed any process of interest - could be done at many scales (2-8A, *right*) based on the level of understanding sought and experimental data available for testing predictions. For example, the responses of different animals in a population to dsRNA exposure (population model; 2-8A, *right*) or the changes in key RNA species after entry of dsRNA into the cytosol (process model; 2-8A, *right*) could be modeled. At yet greater detail, one step such as the amplification of small RNAs using pUG RNA templates could be modeled by incorporating sequence bias, processivity of RdRP, etc. (biochemical model; 2-8A, *right*). Of these scales, we focused on the process model because early process models of RNAi (e.g., ref. (138)) were proposed before crucial discoveries on the biogenesis of 2º siRNAs without forming long dsRNA (100) and the stabilization of mRNA

templates as pUG RNAs (95, 96). Therefore, we incorporated these recent developments and modeled how the addition of dsRNA could disrupt the steady-state RNA metabolism of the targeted gene using ordinary differential equations (2-8B). The steady-state levels of pre-mRNA and mRNA - which depend on production, maturation, and turnover - could be altered upon the addition of matching dsRNA through the generation of new RNA species (1º siRNA, 2º siRNA, pUG RNA) that are also subject to turnover. To accommodate these known intermediates and interactions, we used six differential equations to describe the rate of change of key RNA species (dsRNA (*ds*), 1º siRNA (*pri*), pUG RNA (*ug*), 2º siRNA (*sec*), pre-mRNA (*p*), and mRNA (*m*)) with rate or binding constants for different processes (*k1* through *k9*), turnover rates for different RNAs (T_{pri}, T_{ug}, T_{sec}, T_p, T_m), and variables for the lengths of RNAs (l_{ds} - dsRNA; l_m - mRNA). For example, the rate of change over time for 1º siRNA is modeled as

$$k1.[ds].\frac{l_{ds}}{22} - k2.[pri].[m] - T_{pri}.[pri]$$

which includes the idea that 1º siRNAs are cleaved into 22nt sequences at a certain rate dependent on the dsRNA concentration ($k1.[ds].\frac{l_{ds}}{22}$), the amount of 1º siRNAs that can bind target transcripts ($k2.[pri].[m]$), and the turnover of the 1º siRNAs ($T_{pri}.[pri]$), which notably is dependent on the concentration of the 1º siRNAs.

To illustrate the relative dynamics of different RNA species upon the addition of dsRNA, we computed the concentrations of dsRNA, 1º siRNA, pUG RNA, 2º siRNA, pre-mRNA, and mRNA using the equations after assigning arbitrary values for the different constants (2-8B; see legend for parameter values). To account for the non-negative values of all RNA species within cells, we ensured that the values of incremental change *dx* for any species *x* was only added if $(x+dx) > 0$ and set to be 0 if $(x+dx) \leq 0$. This bounding of the rate equations allows for any approach to zero. As expected, the levels of dsRNA decrease (2-8B, red) as it is processed into 1º

siRNA (2-8B, purple), which eventually decays because of turnover. This transient accumulation of 1º siRNA is followed by that of pUG RNAs (2-8B, green) and of 2º siRNA (2-8B, brown). Silencing of the target is reflected in the lowered levels of mRNA (2-8B, blue) and pre-mRNA (2-8B, orange). However, these levels eventually recover upon turnover of the silencing intermediates (1º siRNA, pUG RNA, 2º siRNA). Although we assumed the turnover of 1º siRNA, 2º siRNA, and pUG RNA for the modeling, the experimental demonstration of recovery (either of individual RNA species or of the entire phenotype) from RNA silencing in non-dividing cells would be needed to support the existence of such turnover mechanisms for these different types of RNAs.

For any gene, the time to knockdown (t_{kd}) and the duration of knockdown (t_{kd}) could be used to evaluate the efficiency of RNAi (knockdown = 10% of initial mRNA concentration in 2-8B). The different RNA species made downstream of 1º RNA binding in *C. elegans* provide the opportunity for multiple parameters to differ between genes. Therefore, we varied each parameter and examined t_{kd} and t_{kd} as indicators of efficiency (Figure 2-9). Overall, t_{kd} and t_{kd} were uncorrelated (2-8C), with cases of rapid but transient knockdown, which would necessitate multiple dosing of dsRNA for sustained effects. While loss of function through the reduction of mRNA levels is often the intended goal of knockdown, RNA intermediates could serve as convenient and quantitative measures of molecular changes. For example, the abundant 2º siRNAs have been a widely used molecular indicator of silencing (e.g., ref. (111)). However, the maximal amount of 2º siRNAs that accumulate is not correlated with strong silencing as measured by the minimal amount of mRNA during knockdown (2-8D). Additionally, an increase in transcription generally resulted in poorer knockdown through changes in both t_{kd} and t_{kd} (2-8E), consistent with the obvious expectation that a gene with transcriptional upregulation during exposure to dsRNA will be more difficult to knockdown.

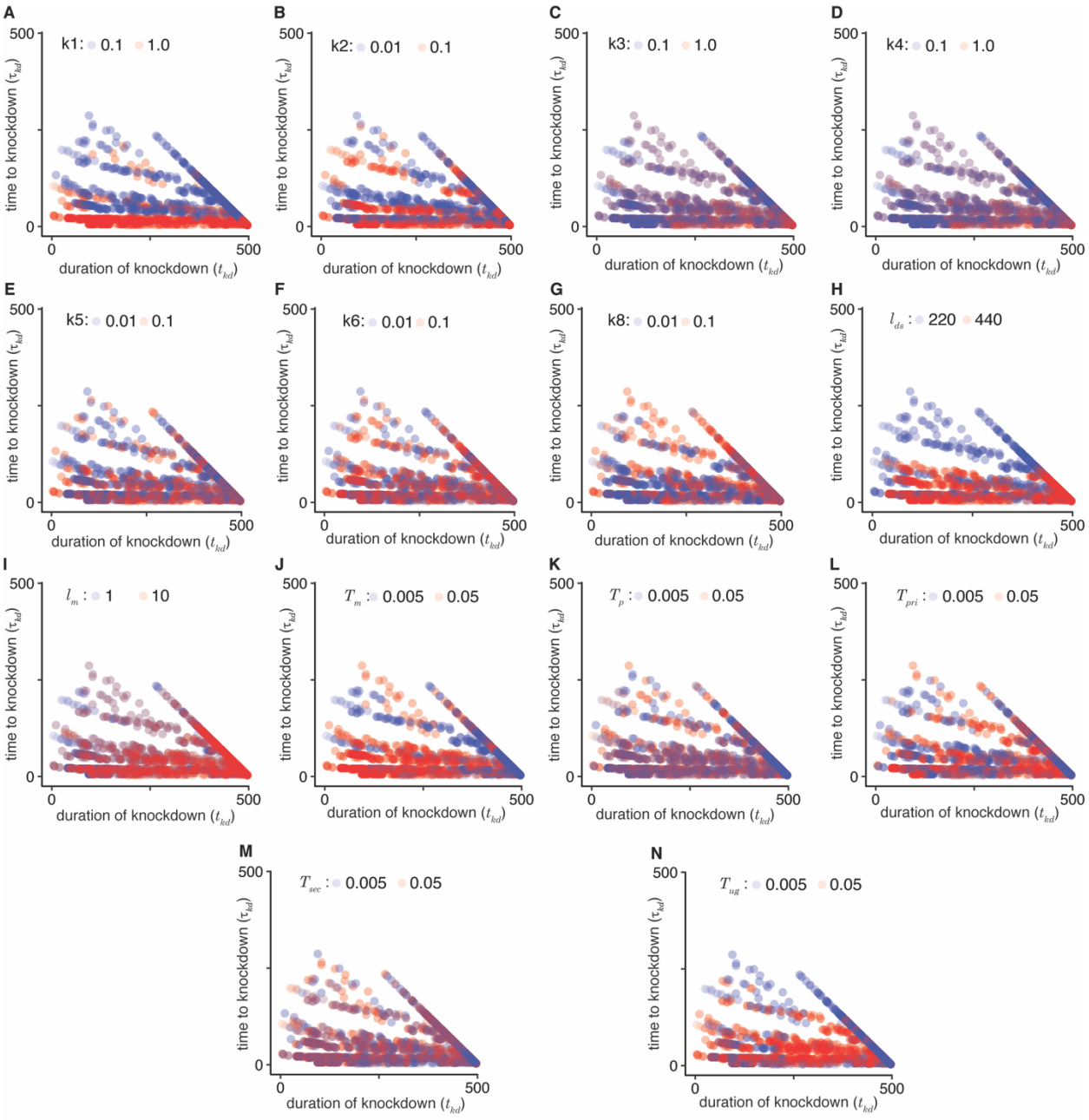


Figure 2-9. Impact of model parameters on the time to knockdown (t_{kd}) and the duration of knockdown (t_{kd}). A low (blue) and high (red) value was selected for each parameter and the t_{kd} and t_{kd} that result upon similarly varying all other parameters were plotted. Comparisons for 1º siRNA production ((A), *k1* = 0.1 vs. 1.0), recognition of transcripts and1º siRNAs ((B), *k2* = 0.01 vs. 0.1), pUG RNA production ((C), *k3* = 0.1 vs. 1.0), 2º siRNA production ((D), *k4* = 0.1 vs. 1.0), binding of transcripts and 2º siRNAs ((E), *k5* = 0.01 vs. 0.1), transcript maturation, i.e., splicing and export out of the nucleus ((F), *k6* = 0.01 vs. 0.1), downregulation of transcription ((G), *k8* = 0.01 vs. 0.1), length of dsRNA ((H), l_{ds} = 220 vs. 440), length of target mRNA ((I), l_m = 1 vs. 10),

mRNA turnover ((J), T_m = 0.005 vs. 0.05), pre-mRNA turnover ((K), T_p = 0.005 vs. 05), 1º siRNA turnover ((L), T_{pri} = 0.005 vs. 0.05), 2º siRNA turnover ((M), T_{sec} = 0.005 vs. 0.05), and pUG RNA turnover ((N), T_{ug} = 0.005 vs. 0.05) are shown.

Efficient silencing using dsRNA is possible in many organisms, including mammals, despite silencing relying on mostly post-transcriptional degradation of mRNA without the production of pUG RNA or 2º siRNA (139). To explore differences between genes that could impact the efficiency of RNA silencing universally in any system, we simulated knockdown through the post-transcriptional loss of mRNA alone by eliminating production of pUG RNAs, and thus downstream secondary small RNAs and transcriptional silencing (2-8B, *k3* = 0). When a fixed amount of dsRNA was exposed to different genes with the same amount of mRNA at steady state, genes with higher mRNA turnover rates showed less efficient knockdown (2-8F). This inverse relationship is expected because to maintain the same steady state levels, genes with higher mRNA turnover must also have higher mRNA production. As a result, for the same amount of added dsRNA and the same steady-state level of mRNA before exposure to dsRNA, the mRNA levels will recover faster for genes with higher production coupled with higher turnover.

In summary, varying a few gene-specific parameters clarified the diversity of outcomes that are possible in response to the same dose of dsRNA. Gene-specific differences make the time to knockdown and the duration of knockdown uncorrelated and reduce the utility of key intermediates of RNA silencing as predictors of knockdown efficiency. Increases in transcription during exposure to dsRNA and high turnover of mRNA coupled with high production at steady state reduce the efficiency of knockdown. While the predictions of the model include quantitative relationships that will require advances in the quantitative measurement of many steps during RNAi, the model also makes some qualitative predictions that can be immediately tested.

2.4.4 Changing *cis*-regulatory elements of a gene impacts its requirements for silencing by dsRNA.

A key realization from the exploration of the dynamic model for RNAi is that pre-existing RNA regulation of a gene impacts the response to dsRNA. However, the individual impacts of the many features of a gene that together set its RNA metabolism (e.g., promoter, 3′ *cis*-regulatory regions, introns, genomic location, etc.) are usually unknown. Nevertheless, as tests of this possibility, we altered target genes using Cas9-mediated genome editing and examined changes, if any, in the genetic requirement for NRDE-3 for silencing by ingested dsRNA.

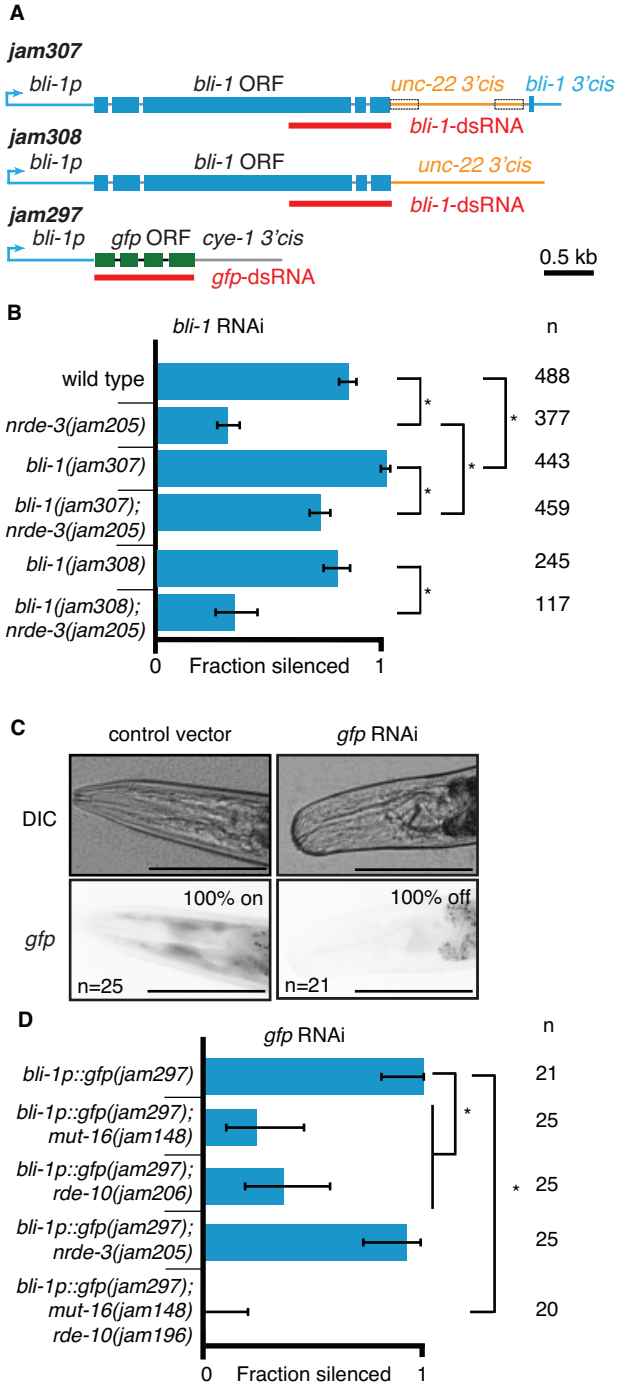


Figure 2-10. Changing *cis*-regulatory regions or open reading frames can alter the observed dependence on NRDE-3 for silencing by dsRNA. (A) Schematics (as in Fig. 1) of the hybrid genes created to test the role of 3′ and 5′ *cis*-regulatory sequences in the response to dsRNA (see Methods for details). (B) The need for NRDE-3 to cause silencing using *bli-1*-dsRNA is reduced when the 3′ *cis*-regulatory sequences of *bli-1* are replaced with that of *unc-22* (*bli-1(jam307)*). Fractions silenced, numbers scored, comparisons, asterisks, and error bars are as in Fig. 1 (C) Representative images (DIC, top; GFP fluorescence, bottom) of the head region of *bli-1p::gfp::cye-1 3'cis* animals either in response to a control vector (pL4440, *left*) or in response to *gfp*-dsRNA (*right*)). The presence or absence of *gfp* in the head region was used to score the fraction silenced in (D). Scale bar = 100µm. (D) Use of the *bli-1* promoter alone does not confer the genetic requirements for silencing *bli-1*. Silencing of GFP expressed from the *bli-1p::gfp::cye-1 3'cis* transgene (*bli-*

1p::gfp(jam297)) by *gfp*-dsRNA was measured in a wild-type background, in animals lacking NRDE-3 (*nrde-3(jam205)*), in animals lacking RDE-10 (*rde-10(jam206*)), in animals lacking MUT-16 (*mut-16(jam148)*), and in animals lacking both MUT-16 and RDE-10 (*mut-16(jam148) rde-10(jam196)*). Fractions silenced, numbers scored, comparisons, asterisks, and error bars are as in Figure 2-1.

First, we swapped the 3′ *cis*-regulatory regions of *bli-1* and *unc-22* (Figure 2-10A, 2-11A). Animals with the *unc-22 3'cis* sequence in place of the *bli-1 3'cis* (*bli-1p::bli-1::unc-22 3'cis*) showed a much reduced dependence on NRDE-3 (Figure 2-10B), Animals with the *bli-1 3'cis* sequence downstream of the coding sequence of *unc-22* (*unc-22p::unc-22::bli-1 3'cis*) showed substantial twitching even without *unc-22* RNAi (Figure 2-11B). Yet, we were able to discern an enhancement upon addition of *unc-22* dsRNA. This enhancement was absent in animals lacking NRDE-3. Together, these results provide evidence for prior regulation (potentially mediated via the 3′ UTR) impacting the genetic requirements for silencing.

Next, we used the *bli-1* 5′ *cis*-regulatory regions (promoter) and the cyclin E 3′ *cis*-regulatory regions to drive *gfp* expression in hypodermal cells (Figure 2-10A; *bli-1p::gfp::cye-1 3'cis*). Animals with this gene showed expression of GFP in the hypodermis, which is most easily visible in the head region and is detectably silenced by ingested *gfp*-dsRNA in a wild-type background (Figure 2-10C).

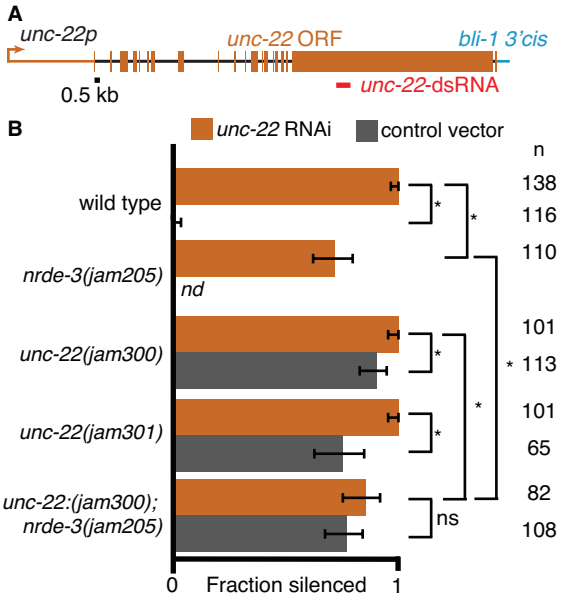


Figure 2-11. Replacing the *unc-22* 3′ *cis*-regulatory sequence with that of *bli-1* results in defects that show a NRDE-3-dependent enhancement when exposed to *unc-22*-dsRNA. (A) Schematic depicting the removal of the endogenous *unc-22 3′ cis*-regulatory region and the addition of the *bli-1 3′ cis*-regulatory region. (B) Silencing in response to *unc-22*-dsRNA (orange) or the control vector (grey). Fractions silenced, numbers scored, comparisons, asterisks and error bars are as in Figure 2-1. Disruption of the *unc-22 3′ cis*-regulatory region results in animals that show twitching in 3mM levamisole even without the

addition of *unc-22* dsRNA. Addition of *unc-22*-dsRNA resulted in significantly more animals with altered *cis*-regulatory regions (*unc-22(jam300), unc-22(jam301)*) showing twitching. This enhancement was not observed in animals that also lack NRDE-3 (*unc-22(jam300); nrde-3(jam205)*). Given the low effect size for NRDE-3 dependence, we do not interpret these results as conclusive, but rather present the data for completeness.

Similar silencing was detectable in animals lacking NRDE-3 (Figure 2-10D), but the silencing in animals lacking MUT-16 or RDE-10 was much weaker (Figure 2-10D). These observations are in contrast to the observed lack of detectable silencing of the wild-type *bli-1* gene in response to *bli-1*-dsRNA in animals lacking NRDE-3, MUT-16, or RDE-10 (Figure 2-1D and 2-3B), suggesting that the *bli-1* promoter is not sufficient to confer these requirements on all genes. An F1 only feed showed similar results (Figure 2-12) suggesting that these requirements are not dependent on dsRNA entering the embryo as occurs from a P0->F1 feed.

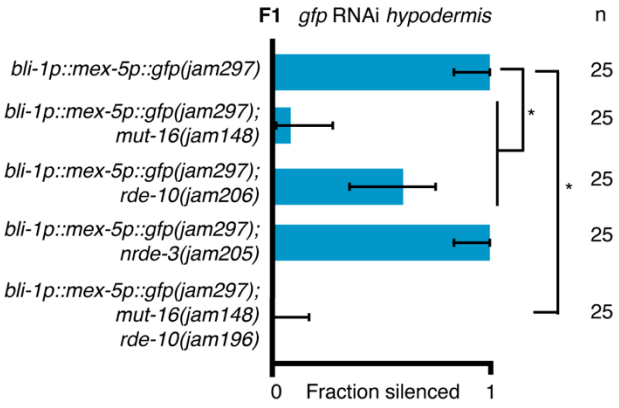


Figure 2-12: F1 only *bli-1p::gfp* RNAi yields similar graded requirements for MUT-16, RDE-10, and NRDE-3 for silencing. Feeding RNAi of *gfp* where only the F1 (not the parent) were exposed to dsRNA and the presence or absence of GFP expression was scored in the hypodermis. Fractions silenced, numbers scored, comparisons, asterisks and error bars are as in Figure 2-1. Animals that lack MUT-16 (*mut-16(jam148)*) showed the least silencing, followed by animals that lack RDE-10 (*rde-10(jam206)*), and then NRDE-3 (*nrde-3(jam205*)) which was comparable to wild type.

Together, these results reveal that two different genes expressed under the same promoter within the same tissue can have different requirements for silencing in response to dsRNA (*bli-1* vs *gfp* under the control of *bli-1p*). These initial attempts to change the requirements for the response to dsRNA by altering the pre-existing regulation of target genes encourage the exploration of additional factors predicted to differentially influence RNA silencing of different genes (Figure 2-8, Figure 2-9).

2.4.5 Gene expression can recover after knockdown despite the presence of amplification mechanisms.

The dynamic model (Figure 2-8) assumes that all key RNA intermediates (1º siRNA, 2º siRNA, and pUG RNA) are subject to turnover. If this assumption is true, animals should be able to recover from RNA silencing in non-dividing cells despite the production of abundant 2º siRNAs using RNA-dependent RNA polymerases. Experimental detection of the re-establishment of wild-type phenotype after a pulse of RNAi would provide evidence not only for the recovery of mRNA levels but also the subsequent production of functional protein. To test this possibility, we exposed wild-type animals to a 1-hr pulse of dsRNA matching the sensitive target *unc-22* and examined them for the Unc-22 defect every 24 hours (Figure 2-13A). With this limited exposure to dsRNA, we observed only ~80% silencing after the first 24 hours, which reached ~100% by day 3, suggesting that it takes a couple of days after exposure to small amounts of dsRNA to observe complete silencing. This delay could be driven by the time required for the buildup of RNA intermediates required for silencing (1º siRNA, 2º siRNA, and/or pUG RNA), for the turnover of UNC-22 protein, and/or for the dissipation of events downstream of the molecular role of UNC-22. Consistent with recovery, silencing was only observed in ~50% of the animals on day 5, which dropped to ~36% by the eighth day after RNAi. In contrast, animals that were continually fed *unc-22* RNAi showed ~100% silencing even at day 7 (Figure 2-13A), suggesting that the RNAi machinery remains functional in aging animals. Thus, these results support the turnover of all key RNA intermediates generated during RNAi – 1º siRNA, 2º siRNA, and pUG RNA, and highlights for the first time that a target gene can recover from RNAi even in non-dividing cells, meaning that dilution of RNAi intermediates cannot explain this recovery.

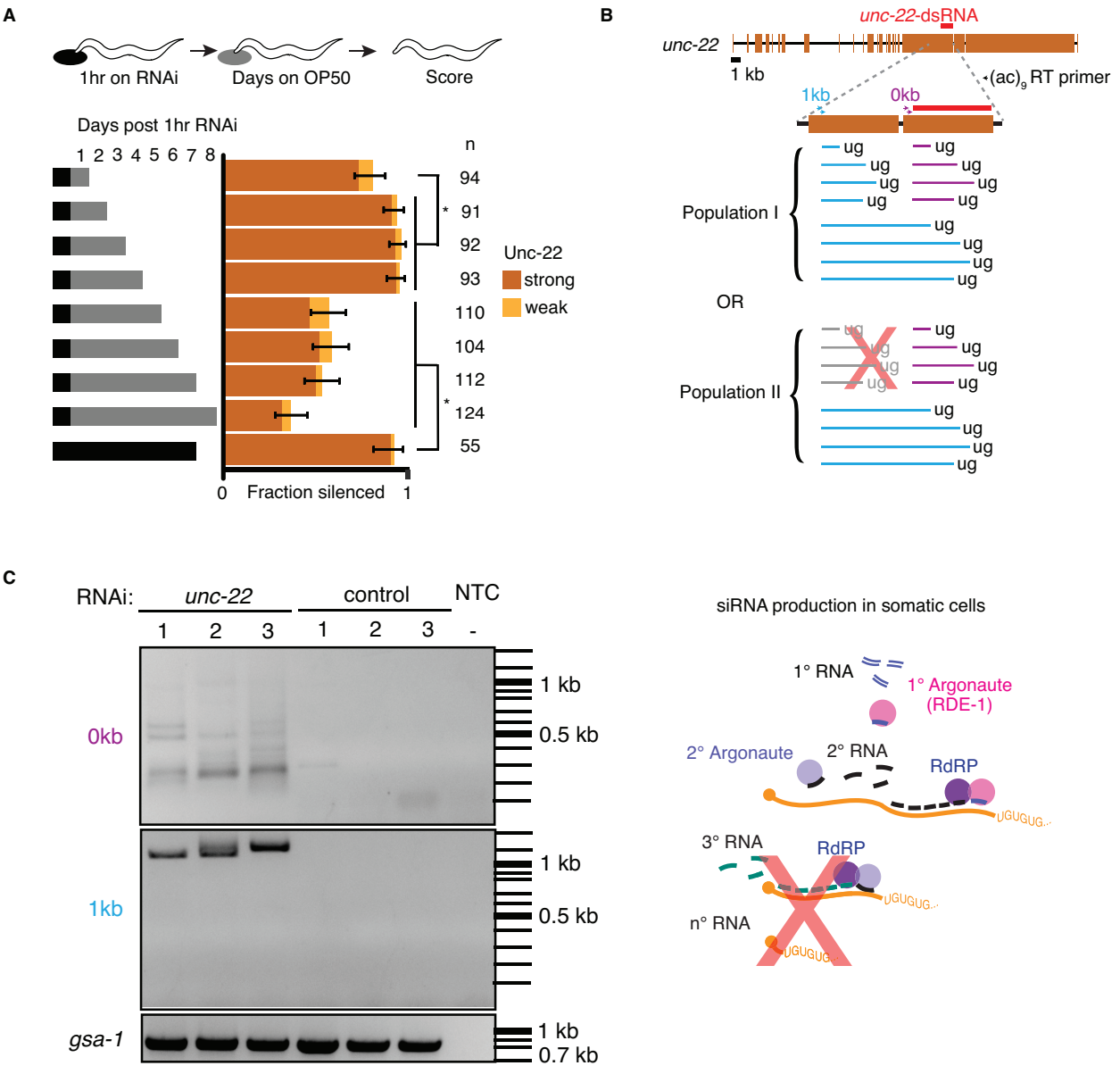


Figure 2-13. Animals recover from a pulse of RNAi and production of pUG RNAs is restricted despite continuous exposure to dsRNA. (A) Response to a pulse of feeding RNAi. (*top*) Schematic of assay. Animals were exposed to *unc-22* RNAi for one hour and then returned to OP50 plates. (*bottom*) A separate cohort of animals was scored for silencing after each subsequent 24hr period. Fractions silenced, numbers scored, comparisons, asterisks, and error bars are as in Fig. 1. A weak Unc-22 defect indicates animals that were nearly completely still except for a slight twitch of the head or of the tail. (B) pUG RNA production in response to continuous exposure to *unc-22* dsRNA. (*top*) Schematic depicting the PCR primers used for the RT-PCR to detect pUG RNAs. Two sets of primers (0kb, purple; 1kb, blue) positioned 5′ of the *unc-22*-dsRNA (orange), combined with an RT primer that contains nine CA repeats were used. (*bottom*) Populations of small RNAs that might be detected by pUG-PCR as above. Population I would suggest that amplified 2º siRNAs in addition to 1º siRNAs are capable of guiding target mRNA cleavage and poly-UG addition. Population II would suggest only 1º siRNAs can initiate pUG

RNA production. (C) (*left*) Distribution of DNA amplified from pUG RNAs. Lanes with PCR products amplified from total RNA of animals fed *unc-22* dsRNA (*unc-22*) or L4440 dsRNA (control) isolated from three biological replicates each (1-3), or a no-template control (NTC) with no added RNA (-) are shown. Different bands are detected for each primer set (0kb, top vs. 1kb, bottom). A gene with a poly-UG sequence encoded in the genome (*gsa-1*) serves as a loading control. (*right*) Schematic of siRNA production in somatic cells. Successive rounds of amplified small RNAs would map progressively closer to the 5′ end of the target transcript. Since we did not detect poly-UG addition upstream of the region homologous to the dsRNA trigger, it is unlikely that 3º siRNAs are being produced.

2.4.6 Sequences in mRNA that match the trigger dsRNA are hot zones of pUG RNA production.

Of the RNA intermediates generated during RNAi, pUG RNAs have been proposed to be used as stable templates to produce small RNAs (96). Sustained production of small RNAs could occur if the targeting of mRNA by 2º siRNA resulted in further pUG RNA production, subsequent 3º siRNA production, and so on, thereby providing a way for silencing to persist despite the turnover of all RNA species. However, the production of such 3º siRNA has been observed only when targeting a germline gene (140) and not when targeting a somatic gene (135). To examine whether such repeated rounds of pUG RNA production occur during RNAi of *unc-22*, we fed wild-type worms bacteria that express *unc-22* dsRNA or control dsRNA (L4440) and looked for the presence of pUG RNAs. These RNAs are detected as a heterogenous mixture using RT-PCR with a poly-CA 3′ primer and gene-specific 5′ primers. Consistent with the production of pUG RNAs upon targeting by 1º siRNAs, we detected pUG RNAs generated after cleavage within the *unc-22* mRNA sequence that matches the dsRNA (Figure 2-13B, 0kb 5′ primer). Since, 2º siRNAs are made with a 5′ bias on the mRNA template (100, 135) pUG RNAs generated in response to targeting by 2º siRNAs are expected to include mRNAs cleaved upstream of the sequence matching the dsRNA. Surprisingly, all pUG RNAs detected using a 5′ primer ~1kb upstream of the target sequence were larger than 1 kb (Figure 2-13B, 1kb 5′ primer), suggesting that there is a

dearth of pUG RNA formation through cleavage within 1 kb upstream of sequences targeted by dsRNA. Notably, this absence is despite the expected relative ease of amplifying shorter sequences when compared with amplifying longer sequences using the same primers. This lack of detectable pUG RNAs upstream suggests that, during RNAi in somatic cells, the addition of pUG tails is enriched within a zone on target mRNAs that share homology with the dsRNA trigger ("pUG zone"). This restricted production of pUG RNAs supports the idea that amplification is not perpetual and that mRNA levels can thus recover over time.

2.5 Discussion

Our results suggest that an intersecting network of regulators formed by the intrinsically disordered protein MUT-16, the Maelstrom-domain protein RDE-10, the nuclear Argonaute NRDE-3, and other Argonaute proteins can explain silencing of somatic targets by RNA interference despite stark differences in the genetic requirements for silencing different genes. The requirement for NRDE-3 can be overcome by enhanced dsRNA processing or by changing the *cis*-regulatory sequences of the target gene. However, the combined loss of both MUT-16 and RDE-10 eliminates all detectable silencing and this requirement cannot be overcome by enhancing dsRNA processing. Animals can recover from silencing in non-dividing cells, which supports the turnover of all key RNA intermediates (1º siRNA, 2º siRNA, and pUG RNA). Consistent with the ability to recover from silencing, unlimited rounds of siRNA amplification is curbed by restricting the cleavage and tailing of mRNAs for making pUG RNAs to ′pUG zones′ that match the dsRNA sequence.

2.5.1 Universal and gene-specific requirements for RNAi.

RNAi requires the entry of dsRNA into cells, the processing of dsRNA into small RNAs, recognition of target mRNA, generation of additional small RNAs, and downstream gene silencing mechanisms. The upstream processes of entry, processing, and recognition do not depend on the mRNA being targeted and are thus presumably universal. Consistently, the dsRNA importer SID-1, the endonuclease DCR-1, and the primary Argonaute RDE-1 are required for all RNAi. In contrast, since the mRNA is used as a template to generate the abundant secondary small RNAs in *C. elegans* (135) or additional dsRNAs in other systems (e.g., in plants ref. (141)), the silencing of different mRNAs could diverge through the selective recruitment of different collections of regulators. In support of this possibility, the two model genes we analyze in this study, *unc-22* and *bli-1*, show stark differences in the requirements of some RNAi factors for silencing (Figure 2-1).

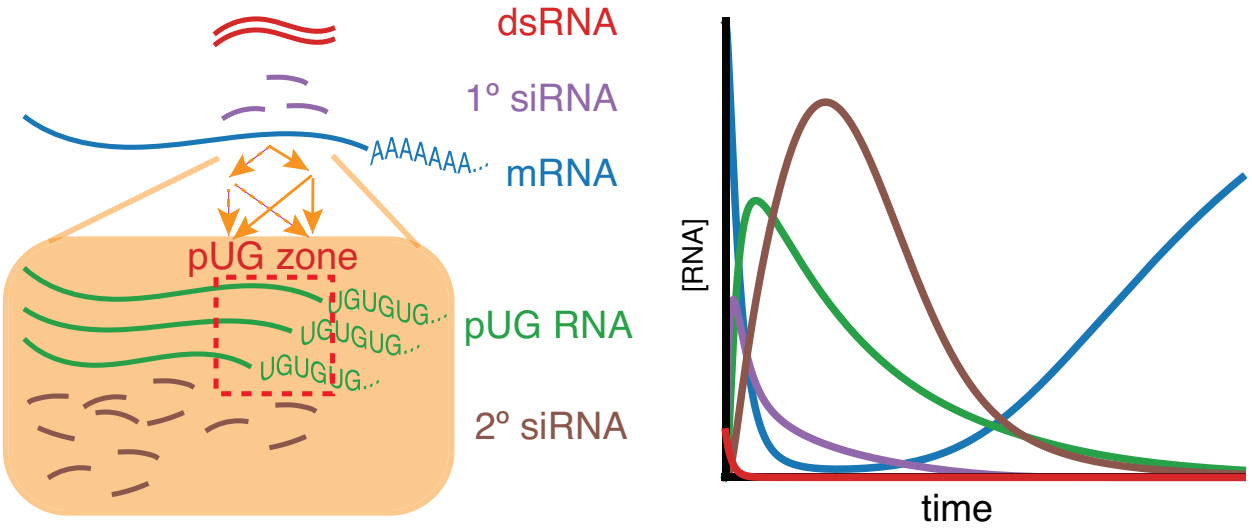


Figure 2-14. Graphical summary of Chapter 2. (*left*) Amplification of small RNAs occurs through an intersecting network of regulators (orange arrows) and in response to somatic RNAi, the addition of poly-UG repeats (green) is restricted to a 'pUG zone' (red) that is homologous to the dsRNA trigger. (*right*) In response to a pulse of dsRNA (red), levels of the target mRNA (blue) recover, suggesting that the RNA silencing intermediates (1° siRNAs, purple; pUG RNAs, green; 2° siRNAs, brown) undergo turnover.

While these differences could be attributed to their expression in different tissues, the ability to bypass some requirements (Figure 2-5) argues against this possibility. Specifically, if the

requirement for NRDE-3 for silencing *bli-1* (hypodermal gene) but not *unc-22* (muscle gene) is because of the lack of a parallel regulator in the hypodermis but not in the muscle, then enhancing dsRNA processing would be unable to bypass the NRDE-3 requirement (Figure 2-5). Neither the silencing of *dpy-7* nor the silencing of *bli-1p::gfp* requires NRDE-3 for silencing despite their expression in the hypodermis (Figure 2-3F, Figure 2-10D). Strikingly, changing the 3′*cis*-regulatory sequences of *bli-1* also made its silencing largely independent of NRDE-3 (Figure 2-10B), providing direct evidence for the prior regulation of a gene dictating the genetic requirements for silencing in response to dsRNA. The fact that any two of MUT-16, NRDE-3, and RDE-10 - three very structurally and functionally different proteins - are required for *unc-22* silencing suggests that each of these proteins could be contributing to silencing of any RNAi target. Despite this potential use of an intersecting network for silencing all somatic genes, different genes could critically depend on different regulators because of differences in their mRNA metabolism and/or subcellular localization (summarized as threshold differences in Figure 2-3). Intermediate steps that require the participation of mRNA such as the production of 2º siRNA could have complex dependencies, making RNA intermediates poor predictors of silencing efficiency (2-8D). For example, the subcellular localization of mRNA could increase or decrease its interaction with RdRPs and thus influence the levels of 2º siRNAs made. Future studies that address the dynamics and subcellular localization of target mRNA before RNAi and the subcellular localization of components of the RNAi machinery are required to test these hypotheses.

2.5.2 Production of 2º siRNAs.

Multiple small RNA species of defined lengths and 5′-nt bias have been detected in *C. elegans*. Of these, 22G RNAs (2º siRNAs) are the most abundant and arise from amplification

downstream of exposure to dsRNA and in multiple endogenous small RNA pathways (111). Our results suggest that production of 2º siRNAs in response to dsRNA is eliminated in animals that lack both MUT-16 and RDE-10 (Figure 2-5C). While the precise mechanisms of amplification are unknown, MUT-16 is thought to nucleate perinuclear foci (74, 104) that recruit many additional components – RDE-2, MUT-7, MUT-14, MUT-15, NYN-1, NYN-2, RDE-8, RDE-3/MUT-2 etc. (80, 104). Of these, the roles of most proteins remain obscure, but RDE-8 (142) and RDE-3/MUT-2 (96) have demonstrated roles in the cleavage and pUGylation of mRNAs, respectively. Yet, the observation of silencing in the absence of MUT-16 that is eliminated upon additional loss of RDE-10 suggests that RDE-10 and associated proteins (e.g., RDE-11, RDE-12) play and independent role in the amplification of 2º siRNAs (102, 103). The subcellular localization of RDE-10 and whether small RNAs that require RDE-10 for production also rely on RDE-8 and RDE-3/MUT-2 as expected for amplification using pUG RNA templates remains to be determined.

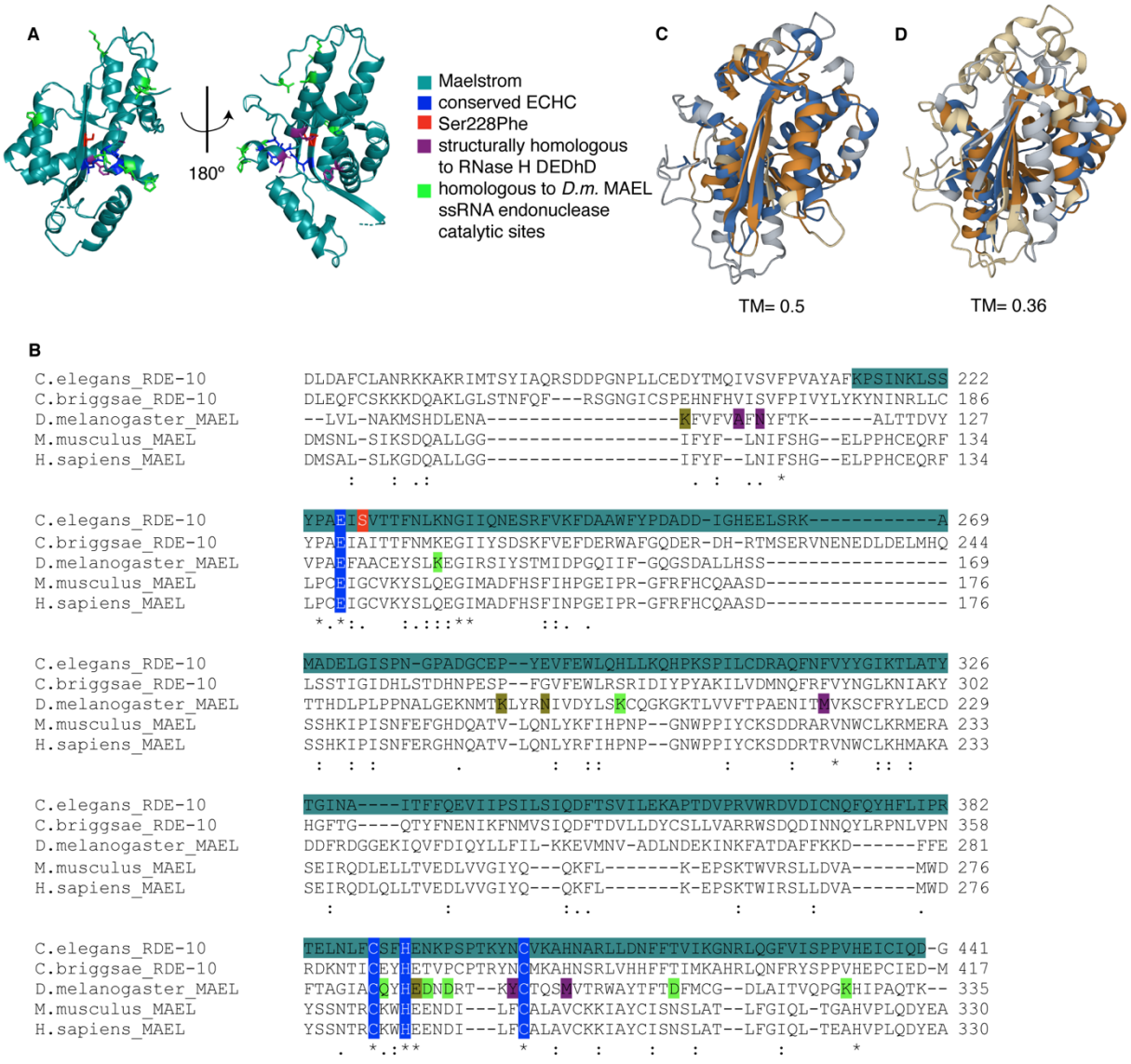


Figure 2-15. The predicted structure of the Maelstrom domain of RDE-10 is similar to that of the 3′-5′ exonuclease ERI-1. (A) Predicted structure of the Maelstrom domain (teal; Pfam: PF13017) of RDE-10. RDE-10 residues were colored based on studies of the *Drosophila* MAEL protein (143). The zinc-binding ECHC motif (dark blue), the Serine residue mutated in *rde-10(jam248)* (red), residues homologous to the catalytic residues of the Lassa virus exonuclease (purple), and residues homologous to those required for single-stranded RNA endonuclease activity (green) are shown. (B) Alignment of maelstrom domain-containing proteins from multiple species. Asterisks indicate conserved residues, colon indicates residues with strongly similar properties and a period indicates residues with weakly similar properties (130). Residues of interest are shaded as in (A). (C) Structural alignments of the Maelstrom domain of RDE-10 with the 3′-5′ exonuclease domains of ERI-1 (*left*) and MUT-7 (*right*). Template modeling scores (TM = 0.5 for ERI-1 and TM = 0.36 for MUT-7) and regions of high homology (blue and orange) are shown.

Loss of RDE-10 reduces the production of 22G RNAs downstream of exogenous dsRNA and downstream of endogenous small RNAs called 26G RNAs that are 26-nt long and have a 5′ G (102, 103). Current models for the production of 26G RNAs (92, 144) propose that the RdRP RRF-3 transcribes long antisense RNA from internal C nucleotides on template mRNA, the phosphatase PIR-1 converts the 5′ triphosphate of the RdRP product into 5′ mono phosphate, the template is then trimmed by the 3′-5′ exonuclease ERI-1 to generate a blunt-ended dsRNA, which is then cleaved by DCR-1 to generate the mature 26G RNAs that are bound by the Argonaute ERGO-1. While a similar preference by RdRPs can explain the 5′G bias of the downstream 22G RNAs, the mechanism(s) for generating RNA that are precisely 22 nucleotides long remain unclear. This precision could be achieved either through the trimming of template mRNAs into 22-nt long pieces or through the trimming of secondary small RNAs made by RdRPs into 22-nt long pieces. The detection of long pUG RNAs with no detectable shorter pUG RNAs upstream of sequences matching the dsRNA (Figure 2-13C) argues against the 3′ trimming of mRNA templates to generate shorter RNAs that then get pUGylated to become stabilized templates for RdRPs and against pUG RNA generation driven by successive rounds of 22G RNA production in somatic cells. Furthermore, potential 5′ trimming or endonucleolytic cleavage of long pUG RNA to generate a 22-nt template for RdRPs cannot explain the 5′ G bias of 22G RNAs. Since Argonautes bind the 5′ end of small RNAs and can associate with RNAs of different lengths (90), we suggest a model whereby RDE-10 and downstream Argonautes together play a role in the maturation of 22-nt siRNAs from longer RdRP products.

RDE-10 has a conserved Maelstrom domain that shares homology with the DnaQ-H 3′–5′ exonuclease family (145) and the mutation we identified as disrupting silencing by dsRNA (Figure 2-1D) alters a residue located near the highly conserved ECHC zinc-binding motif (Figure 2-2C).

Intriguingly, the Maelstrom domain of RDE-10 shares high structural homology with the 3′-5′ exonuclease domain of ERI-1 (Figure 2-15C, *left*) but not the exonuclease domain of MUT-7 (Figure 2-15C, *right*). ERI-1 can trim single-stranded RNA overhangs in vitro (119), and is required for the production of 26G RNAs (146) and for the maturation of rRNAs (147). While no 3′–5′ exonuclease activity of RDE-10 or its orthologs has been demonstrated, Maelstrom domain-containing proteins in insects exhibit single-stranded RNA endonuclease activity in vitro (143). Furthermore, RDE-10 could interact with other parts of the RNA silencing machinery (e.g., the Argonaute ERGO-1 as seen using immunoprecipitation (102, 103)) to recruit nucleases (e.g., NYN family exonucleases such as ERI-9 (142)) that trim pre-22G RNAs to the 22-nt size preferred by Argonaute proteins. In support of such exonucleolytic trimming in conjunction with Argonaute binding, the 3′-5′ exonuclease SND1 has been shown to trim the 3′ ends of miRNAs bound to AGO1 in *Arabidopsis* (148). Furthermore, piRNA maturation in *Drosophila* and mice suggests a model where piwi-type Argonautes bind the 5′ end of the pre-piRNA followed by endonucleolytic cutting and exonucleolytic trimming to generate consistently sized mature piRNAs (149). Finally, human ERI1 can trim Ago2-bound micro RNAs to 19-nt (150).

Therefore, we propose that the production of 22G RNAs in response to the addition of dsRNA occurs as follows: (1) non-processive RdRPs (e.g., RRF-1 (151)) make a heterogenous mixture of short RNAs, (2) 2º Argonautes bind the 5′ end of these pre-secondary siRNA, (3) RDE-10 and/or associated protein(s) remove excess 3′ sequence to generate 22-nt siRNAs that are effectively retained by the mature siRNA-Argonaute complex. Similar mechanisms could be used to generate other 22G RNAs that are independent of RDE-10 (102, 103). Future studies are needed to test each aspect of the model.

2.5.3 Trade-offs in RNA interference. RNAi is now a widely applied tool for gene silencing in plants, insects, and humans. Like *C. elegans*, plants (141) and some insects (152) have RdRPs that could be used to make 2º siRNAs, but many other animals, including humans, do not have RdRPs and thus are unlikely to produce 2º siRNAs. However, silencing can fade despite the production of 2º siRNAs (Figure 2-13A), highlighting the importance of dosage for all systems. Two parameters of importance for the acute efficacy of any dsRNA-based drug are the time to knockdown (t_{kd} in 2-8B) and duration of knockdown (t_{kd} in 2-8B). The various values of t_{kd} that are possible for each t_{kd} (2-8C) cautions against using a rapid onset of silencing (low t_{kd}) as the sole indicator of promise during early stages of drug development when long-term effects of a drug are often not evaluated in the interest of expedience. In short, a drug that takes longer to cause an effect could have a more long-lasting effect. Since a dsRNA drug can be synthesized for any target with equal effort, considerations for the choice of target could be worthwhile because differences in RNA metabolism between two targets of equal importance can influence the efficacy of the dsRNA drug in all systems. If two genes are at steady state, then the gene with higher mRNA turnover will be more difficult to knockdown because of higher rates of mRNA production (2-8F). Similarly, in the absence of a steady state, a gene undergoing upregulation of transcription, splicing, and/or mRNA export during the administration of the drug will be difficult to knockdown (e.g., 2-8E).

In the longer term, a concern for any drug is the development of resistance. When a gene with a high threshold for silencing is targeted, it could rely on multiple regulators that act in parallel to contribute to silencing (e.g., *bli-1* in this study), making resistance through the mutation of any one regulator more likely and necessitating another round of drug development. In contrast, genes with a lower threshold may not require all the regulators for silencing (e.g., *unc-22* in this study),

making them ideal targets that remain silenced despite single mutations in many regulators of RNAi (e.g., RDE-10, MUT-16, or NRDE-3 in this study). These trade-offs inform the choice of therapeutic targets and dosage for sustained use of dsRNA-based drugs in agriculture and in human health. Anticipating mechanisms for the development of resistance before widespread use of an RNAi-based drug or treatment will be crucial for avoiding futile cycles of innovation. The ideal drug would require a minimal dose and use multiple intersecting paths to silence the target gene.

Table 2-1: Strains used in Chapter 2

Strain name	Genotype
N2	wild type
AMJ174	*oxSi487[mex-5p::mCherry::H2B::tbb-2 3'UTR::gpd-2 operon::GFP::H2B::cye-1 3'UTR + unc-119(+)] dpy-2(jam29) II; unc-119(ed3)? III; lin-2(jam30) X*
AMJ183	*rde-4(ne301) III; nrde-3(tm1116) X*
AMJ285	*jamSi1 [mex-5p::rde-4(+)] II; rde-4(ne301) III*
AMJ345	*jamSi2 [mex-5p::rde-1(+)] II; rde-1(ne219) V*
AMJ422	*jamSi6 [nas-9p::rde-4(+)] II; unc-119(ed) III*
AMJ489	*nrde-3(tm1116) X; eri-1(mg366) IV*
AMJ565	*jamSi6 [Pnas-9::rde-4(+)::rde-4 3'UTR] II; unc-119(ed3) III rde-*
AMJ611	*4(ne301) III* *jamSi6 [nas-9p::rde-4(+)::rde-4 3'UTR] II; rde-4(ne301) III; nrde-3(tm1116) X*
AMJ1023	*mut-16(jam138) I; oxSi487 dpy-2(jam29) II; unc-119(ed3)? III; lin-2(jam30) X*
AMJ1025	*mut-16(jam139) rde-10(jam248) I; oxSi487 dpy-2(jam29) II; unc-119(ed3)? III; lin-2(jam30) X*
AMJ1035	*mut-16(jam140) I; oxSi487 dpy-2(jam29) II; unc-119(ed3)? III; lin-2(jam30) X*
AMJ1042	*mut-16(jam141) I; oxSi487 dpy-2(jam29) II; unc-119(ed3)? III; lin-2(jam30) X*
AMJ1091	*mut-16(jam247) I; oxSi487 dpy-2(jam29) II; unc-119(ed3)? III; lin-2(jam30) X*
AMJ1195	*jamSi59 [Pmex-5::gfp::cye-1 3'UTR + unc-119(+)] II; unc-119(ed3) III*
AMJ1397	*mut-16(jam148) I*
AMJ1470	*mut-16(jam148) rde-10(jam196) I*
AMJ1489	*rde-10(jam206) I*
AMJ1510	*nrde-3(jam205) X*
AMJ1545	*mut-16(jam148) I; nrde-3(jam205) X*

AMJ1568	*rde-10(jam206) I; nrde-3(jam205) X*
AMJ1611	*mut-16(jam240) rde-10(jam206) I*
AMJ1614	*rde-10(jam243) I*
AMJ1621	*eri-1(mg366) IV; nrde-3(jam205) X*
AMJ1622	*rde-10(jam206) I; eri-1(mg366) IV*
AMJ1623	*rde-10(jam206) I; eri-1(mg366) IV*
AMJ1624	*rde-10(jam206) I; eri-1(mg366) IV; nrde-3(jam205) X*
AMJ1625	*rde-10(jam206) I; eri-1(mg366) IV; nrde-3(jam205) X*
AMJ1631	*mut-16(jam148) I; eri-1(mg366) IV; nrde-3(jam205) X*
AMJ1632	*mut-16(jam148) I; eri-1(mg366) IV; nrde-3(jam205) X*
AMJ1657	*mut-16(jam240) rde-10(jam206) I; eri-1(jam260) IV*
AMJ1658	*mut-16(jam240) rde-10(jam206) I; eri-1(jam261) IV*
AMJ1659	*mut-16(jam240) rde-10(jam206) I; eri-1(jam262) IV*
AMJ1660	*eri-1(jam263) IV*
AMJ1661	*eri-1(jam264) IV*
AMJ1672	*mut-16(jam265) I; eri-1(jam263) IV*
AMJ1673	*mut-16(jam266) I; eri-1(jam264) IV*
AMJ1674	*mut-16(jam267) I; eri-1(jam264) IV*
AMJ1675	*mut-16(jam268) I*
AMJ1709	*jam297[bli-1p::gfp::cye-1 3'utr + unc-119(+)] II; unc-119(ed3) III*
AMJ1721	*mut-16(jam148) I; jamSi6 [nas-9p::rde-4(+)] II; unc-119(ed)? III*
AMJ1722	*mut-16(jam148) I; jamSi6 II; unc-119(ed)? III; eri-1(jam263) IV*
AMJ1723	*rde-10(jam206) I; jamSi6 II; unc-119(ed)? III*
AMJ1724	*rde-10(jam206) I; jamSi6 II; unc-119(ed)? III; eri-1(mg366) IV*
AMJ1725	*rde-10(jam206) I; jam297[bli-1p::gfp::cye-1 3'utr + unc-119(+)] II; unc-119(ed3)? III*
AMJ1726	*jam297[bli-1p::gfp::cye-1 3'utr + unc-119(+)] II; unc-119(ed3)? III; nrde-3(jam205) X*
AMJ1727	*mut-16(jam148) I; jam297[bli-1p::gfp::cye-1 3'utr + unc-119(+)] II; unc-119(ed3)? III*
AMJ1728	*mut-16(jam148) rde-10(jam196) I; jam297[bli-1p::gfp::cye-1 3'utr + unc-119(+)] II; unc-119(ed3)? III*
AMJ1730	*unc-22(jam300) IV*
AMJ1731	*unc-22(jam301) IV*
AMJ1754	*bli-1(jam307) II*
AMJ1755	*bli-1(jam308) II*
AMJ1757	*unc-22(jam300) IV; nrde-3(jam205) X*
AMJ1758	*bli-1(jam307) II; nrde-3(jam205) X*
AMJ1771	*bli-1(jam308) II; nrde-3(jam205) X*
EG6787	*oxSi487 II; unc-119(ed3) III*
GR1373	*eri-1(mg366) IV*
WM27	*rde-1(ne219) V*
WM49	*rde-4(ne301) III*
WM156	*nrde-3(tm1116) X*

Table 2-2: Oligonucleotides used (5′ to 3′) in Chapter 2

Primer	Sequence
P1	atttaggtgacactatagaaatgctcagagatgctcggttttagagctagaaatagcaag
P2	tcactttcttcgtgcgttcc
P3	ggagaaccactcccagaatg
P4	aatcaatcggctgtccacac
P5	atttaggtgacactatagctggatcacctgggaatccgttttagagctagaaatagcaag
P6	aatcgcaaacgagtgggtac
P7	cgggctagatcataatgagg
P8	ggaccacgtggagttccaggacatccaggttttccaggtgacccaggagagtatggaatt
P9	gaatatttttcgaaaatata
P10	cggcacatgcgaatattttccgaaaatagaaggatattcttcaactcgatccagaaaaac
P11	gctaccataggcaccgcatg
P12	cacttgaacttcaatacggcaagatgagaatgactggaaaccgtaccgcatgcggtgcctatggtagcggag cttcacatggcttcagaccaacagccta
P13	cacaaacgccaggaaaggaag
P14	catttctgcgttgttgtggacc
P15	gttgtaacggatatctctgc
P16	aagattgaatgttgtaacgaatatttcagcaggatacgatgaaagcttattgattgatgg
P17	ccgaaatccagatgagttcc
P18	gcatctggataaaaccaagc
P19	ccgatacaatcagaatgatc
P20	agcaaggccaccgatacaatcagaatgatttaggcagacaaggatattatgacaagatatt
P21	ggcattcgagccaataatgc
P22	cgttgtgctcggcaacttct
P23	acaccacgtacaaatgtttg
P24	tgcgtcatccacaccacgtacaaacgtttagggcactgcaaaaaagccatccagccaaca
P25	gactgtgctgacgctgtttt
P26	ctcccagtggctttcgtttt
P27	tgtggacacggaatcagatc
P28	gaaacagtcgatgctgctccatatttccgataggatcttcaacggctgtacacatggatg
P29	cctatgtccgacctgtcaga
P30	caattccggatttctgaagag
P31	cagacctcacgatatgtggaaa
P32	ggaacatatggggcattcg
P33	caactttgtatagaaaagtt
P34	acaagtttgtacaaaaaagc
P35	gattacgccaagctatcaactttgtatagaaaagttgcctaccaaagtagaaattcc
P36	acaactccagtgaaaagttcttctcctttactcatgatgaggttagatcacacta
P37	tttcgctgtcctgtcacactc
P38	tacgcggtaagacccaaatg
P39	gaacgcgtcgaggtgatagc
P40	ataaggagttccacgcccag
P41	ctagtgagtcgtattataagtg
P42	tgaagacgacgagccacttg

P43	ctagaaacttctcataatag
P44	ggatacgagagaagccaaat
P45	cttttacaggaaccactattatgagaagtttctagtttaatcatcctgccaccaccactt
P46	ccttatcttctgcggttttcccaactctccgcttcttccaaacatttctcagtcaacag
P47	catacagaaggagaaatcgc
P48	gttgtagtacagtgtcgcat
P49	gcgtcccaattcttgaatca
P50	ggtggcaggatgattagaca
P51	aattctcactcaaaatttgc
P52	tgcaaaatatgcggcagctcttctccttgtctaataactaaaaaaaacttctagtctaac
P53	tgtctttcaaattctcactcaaaatttgctggtatcgatttggcttctctcgtatcc
P54	gacgacgacggcatctatgt
P55	gctatggctgttctcatggcggcgtcgccatattctacttcacacacacacacacaca
P56	gctatggctgttctcatggc
P57	gagttctacgatcacattct
P58	tgctccgtggagcaactcgc
P59	gagcacactattctgtgcat
P60	ggcgtcgccatattctactt
P61	cacttgctggaaagacaagg
P62	cgcaagcatgctggtttgta
P63	gcattccatctgcaatgcga
P64	cagtgtgcttgtaaatcggc
P65	tgctcttcggcagttgcttc
P66	gcaaagaatcttgcagcatgg
P67	gaacacacccagactgaaga
P68	gacgagcaaatgctcaacg
P69	tcgtcttcggcagttgcttc

Table 2-3: Statistics for comparisons in Chapter 2

Figure	**Comparison**	**Total n**	**Silenced n**	**p value**	**Strains**	**notes**
2-1B *bli-1*	wild type vs *mut-16(jam138)*	757, 229	391, 0	<0.00001, *	EG6787, AMJ1023	pooled EG6787 from separate experiments
2-1B *bli-1*	wild type vs *mut-16(jam140)*	757, 277	391, 0	<0.00001, *	EG6787, AMJ1035	pooled EG6787 from separate experiments
2-1B *bli-1*	wild type vs mut-16(jam141)	757, 124	391, 0	<0.00001, *	EG6787, AMJ1042	pooled EG6787 from separate experiments

2-1B *bli-1*	wild type vs mut-16(jam247)	757, 446	391, 1	<0.00001, *	EG6787, AMJ1091	pooled EG6787 from separate experiments
2-1B *bli-1*	wild type vs mut-16(jam139) rde-10(jam248)	757, 412	391, 1	<0.00001, *	EG6787, AMJ1025	pooled EG6787 from separate experiments
2-1B *unc-22*	wild type vs mut-16(jam139) rde-10(jam248)	309, 173	282, 0	<0.00001, *	EG6787, AMJ1025	pooled EG6787 from separate experiments
2-1B *unc-22*	mut-16(jam138) vs mut-16(jam139) rde-10(jam248)	180, 173	111, 0	<0.00001, *	AMJ1023, AMJ1025	pooled EG6787 from separate experiments
2-1B *unc-22*	mut-16(jam140) vs mut-16(jam139) rde-10(jam248)	91, 173	50, 0	<0.00001, *	AMJ1035, AMJ1025	pooled EG6787 from separate experiments
2-1B *unc-22*	mut-16(jam141) vs mut-16(jam139) rde-10(jam248)	267, 173	208, 0	<0.00001, *	AMJ1042, AMJ1025	pooled EG6787 from separate experiments
2-1B *unc-22*	mut-16(jam247) vs mut-16(jam139) rde-10(jam248)	100, 173	84, 0	<0.00001, *	AMJ1091, AMJ1025	pooled EG6787 from separate experiments
2-1D *bli-1*	wild type vs mut-16(jam148)	202, 126	159, 0	<0.00001, *	N2, AMJ1397	
2-1D *bli-1*	wild type vs mut-16(jam148) rde-10(jam196)	202, 209	159, 0	<0.00001, *	N2, AMJ1470	
2-1D *bli-1*	wild type vs rde-10(jam206)	202, 209	159, 0	<0.00001, *	N2, AMJ1489	
2-1D *unc-22*	wild type vs mut-16(jam148)	206, 121	204, 119	0.58802, ns	N2, AMJ1397	
2-1D *unc-22*	wild type vs mut-	206, 146	204, 0	<0.00001, *	N2, AMJ1470	

	16(jam148) rde-10(jam196)					
2-1D *unc-22*	wild type vs rde-10(jam206)	206, 190	204, 185	0.21023, ns	N2, AMJ1489	
2-3B *bli-1*	wild type vs nrde-3(jam205)	295, 274	172, 16	<0.00001, *	N2, AMJ1510	
2-3B *bli-1*	wild type vs rde-10(jam206); nrde-3(jam205)	295, 219	172, 0	<0.00001, *	N2, AMJ1568	
2-3B *bli-1*	wild type vs mut-16(jam148); nrde-3(jam205)	295, 121	172, 0	<0.00001, *	N2, AMJ1545	
2-3B *unc-22*	wild type vs nrde-3(jam205)	129, 110	127, 108	0.87221, ns	N2, AMJ1510	
2-3B *unc-22*	wild type vs rde-10(jam206); nrde-3(jam205)	129, 111	127, 0	<0.00001, *	N2, AMJ1568	
2-3B *unc-22*	wild type vs mut-16(jam148); nrde-3(jam205)	129, 101	127, 0	<0.00001, *	N2, AMJ1545	
2-3E	wild type vs mut-16(jam148)	183, 107	179, 5	<0.00001, *	N2, AMJ1397	
2-3E	wild type vs rde-10(jam206)	183, 116	179, 16	<0.00001, *	N2, AMJ1489	
2-3E	wild type vs nrde-3(jam205)	183, 105	179, 72	<0.00001, *	N2, AMJ1510	
2-3E	mut-16(jam148) vs rde-10(jam206)	107, 116	5, 16	0.0190241, *	AMJ1397, AMJ1489	
2-3E	rde-10(jam206) vs nrde-3(jam205)	116, 105	16, 72	<0.00001, *	AMJ1489, AMJ1510	
2-3F *unc-54*	wild type vs mut-16(jam148)	148, 124	142, 2	<0.00001, *	N2, AMJ1397	
2-3F *unc-54*	wild type vs rde-10(jam206)	148, 128	142, 2	<0.00001, *	N2, AMJ1489	
2-3F *unc-54*	wild type vs nrde-3(jam205)	148, 263	142, 49	<0.00001, *	N2, AMJ1510	Fed on a different day with similar N2 silencing 164/171

						animals showing Unc-54
2-3F *unc-54*	wild type vs mut-16(jam148) rde-10(jam196)	148, 159	142, 0	<0.00001, *	N2, AMJ1470	
2-3F *unc-54*	wild type vs mut-16(jam148); nrde-3(jam205)	148, 166	142, 0	<0.00001, *	N2, AMJ1545	Fed on a different day with similar N2 silencing 164/171 animals showing Unc-54
2-3F *unc-54*	wild type vs rde-10(jam206); nrde-3(jam205)	148, 206	142, 0	<0.00001, *	N2, AMJ1568	Fed on a different day with similar N2 silencing 164/171 animals showing Unc-54
2-3F *unc-54*	nrde-3(jam205) vs mut-16(jam148)	263, 124	49, 2	<0.00001, *	AMJ1510, AMJ1397	
2-3F *unc-54*	nrde-3(jam205) vs rde-10(jam206)	263, 128	49, 2	<0.00001, *	AMJ1510, AMJ1489	
2-3F *dpy-7*	wild type vs mut-16(jam148)	322, 130	279, 34	<0.00001, *	N2, AMJ1397	
2-3F *dpy-7*	wild type vs rde-10(jam206)	322, 159	279, 2	<0.00001, *	N2, AMJ1489	
2-3F *dpy-7*	wild type vs nrde-3(jam205)	322, 126	279, 3	<0.00001, *	N2, AMJ1510	
2-3F *dpy-7*	wild type vs mut-16(jam148) rde-10(jam196)	322, 184	279, 0	<0.00001, *	N2, AMJ1470	
2-3F *dpy-7*	wild type vs mut-16(jam148); nrde-3(jam205)	322, 99	279, 0	<0.00001, *	N2, AMJ1545	
2-3F *dpy-7*	wild type vs rde-10(jam206); nrde-3(jam205)	322, 180	279, 0	<0.00001, *	N2, AMJ1568	
2-3F *dpy-7*	mut-16(jam148) vs rde-10(jam206)	130, 159	34, 2	<0.00001, *	AMJ1397, AMJ1489	

2-3F *dpy-7*	mut-16(jam148) vs nrde-3(jam205)	130, 126	34, 6	<0.00001, *	AMJ1397, AMJ1510	
2F	wild type vs mut-16(jam148)	183, 107	179, 5	<0.00001, *	N2, AMJ1397	
2F	wild type vs rde-10(jam206)	183, 116	179, 16	<0.00001, *	N2, AMJ1489	
2F	wild type vs nrde-3(jam205)	183, 105	179, 72	<0.00001, *	N2, AMJ1510	
2F	mut-16(jam148) vs rde-10(jam206)	107, 116	5, 16	0.0190241, *	AMJ1397, AMJ1489	
2F	rde-10(jam206) vs nrde-3(jam205)	116, 105	16, 72	<0.00001, *	AMJ1489, AMJ1510	
3B	wild type vs eri-1(mg366)	200, 200	134, 145	0.231163, ns	N2, GR1373	N2 from a second experiment showed comparable values (219/304), GR1373 from a second experiment showed comparable values (169/213)
3B	nrde-3(jam205) vs eri-1(mg366); nrde-3(tm1116)	143, 200	3, 167	0.000132, *	N2, AMJ489	
3B	mut-16(148/268) vs mut-16(jam265-7); eri-1(jam263)	172, 354	0, 0	>0.5, ns	AMJ1397, AMJ1675, AMJ1672-4	AMJ1397 (0/110) and AMJ1675 (0/123) were pooled; AMJ1672 (0/130), AMJ1673 (0/88), and AMJ1674 (0/111) were pooled
3B	rde-10(jam206) vs rde-10(jam206); eri-1(mg366)	233, 329	0, 0	>0.5, ns	AMJ1489, AMJ1622, AMJ1623	AMJ1622 (0/171) and AMJ1623 (0/183) were pooled
3B	nrde-3(jam205) vs eri-1(mg366); nrde-3(jam205)	143, 169	3, 130	<0.00001, *	AMJ1510, AMJ1621	
3C	mut-16(jam148/240)	149, 191	1, 10	0.01826, *	AMJ1470, AMJ1611,	AMJ1470 (0/32) and AMJ1661

	rde-10(jam196/206) vs. mut-16(jam240) rde-10(jam 206); eri-1(jam260-2)				AMJ1657-9	(1/116) were pooled; AMJ1657 (9/75), AMJ1658 (0/56), and AMJ1659 (1/50) were pooled
3C	rde-10(jam206); nrde-3(jam205) vs rde-10(jam206); eri-1(mg366); nrde-3(jam205)	113, 265	6, 18	0.58837, ns	AMJ1568, AMJ1624, AMJ1625	AMJ1624 (4/135) and AMJ1625 (14/112) were pooled
3C	mut-16(jam148); nrde-3(jam205) vs mut-16(jam148); eri-1(mg366); nrde-3(jam205)	28, 110	4, 1	0.00072, *	AMJ1545, AMJ1631, AMJ1632	AMJ1631 (1/52) and AMJ1632 (0/57) were pooled
3D *bli-1*	wild type vs rde-1(ne219)	50, 37	41, 0	<0.00001, *	N2, WM27	N2 data from *rde-4(-)* experiment; N2 data from *rde-1(-)* experiment (not shown) is comparable with 41/50 silenced
3D *bli-1*	wild type vs rde-4(ne301)	40, 50	40, 0	<0.00001, *	N2, WM49	N2 data from *rde-4(-)* experiment; N2 data from *rde-1(-)* experiment (not shown) is comparable with 41/50 silenced
3D *bli-1*	wild type vs Si[mex-5p::rde-1(+)]/+; rde-1(ne219)	50, 33	41, 0	<0.00001, *	N2, AMJ345	N2 data from *rde-4(-)* experiment; N2 data from *rde-1(-)* experiment (not shown) is comparable with 41/50 silenced
3D *bli-1*	wild type vs Si[mex-5p::rde-4(+)]/+; rde-4(ne301)	40, 41	40, 41	>0.5, ns	N2, AMJ285	N2 data from *rde-4(-)* experiment; N2 data from *rde-1(-)* experiment (not

						shown) is comparable with 41/50 silenced
3D *unc-22*	wild type vs rde-1(ne219)	25, 25	25, 0	<0.00001, *	N2, WM27	
3D *unc-22*	wild type vs rde-4(ne301)	25, 25	25, 0	<0.00001, *	N2, WM49	
3D *unc-22*	wild type vs Si[mex-5p::rde-1(+)]/+; rde-1(ne219)	25, 24	25, 2	<0.00001, *	N2, AMJ345	
3D *unc-22*	wild type vs Si[mex-5p::rde-4(+)]/+; rde-4(ne301)	25, 24	25, 16	0.001600, †	N2, AMJ285	† indicates statistical significance vs. wild type and vs. *rde-4(ne301)* mutant
3D *unc-22*	rde-4(ne301) vs *Si[mex-5p::rde-4(+)]/+; rde-4(ne301)*	25, 24	0, 16	<0.00001, †	WM49, AMJ285	† indicates statistical significance vs. wild type and vs. *rde-4(ne301)* mutant
3E	wild type vs rde-4(ne301); nrde-3(tm1116)	150, 200	142, 0	<0.00001, *	N2, AMJ183	
3E	wild type vs rde-4(ne301); nrde-3(tm1116); Si[nas-9p::rde-4(+)]	150, 150	142, 98	<0.00001, †	N2, AMJ611	† indicates statistical significance vs. wild type and vs. *rde-4(ne301); nrde-3(tm1116)* mutant
3E	rde-4(ne301); nrde-3(tm1116); vs rde-4(ne301); nrde-3(tm1116); Si[nas-9p::rde-4(+)]	200, 150	0, 98	<0.00001, †	AMJ183, AMJ611	† indicates statistical significance vs. wild type and vs. *rde-4(ne301); nrde-3(tm1116)* mutant
3F	wild type vs eri-1(mg366); nrde-3(jam205)	282, 140	85, 69	0.0001199, *	N2, AMJ1621	
3F	wild type vs rde-	282, 279	85, 0	<0.00001, *	N2, AMJ1622	

	10(jam206); eri-1(mg366)					
3F	wild type v Si[nas-9p::rde-4(+)]; rde-10(jam206)	282, 180	85, 6	<0.00001, *	N2, AMJ1723	
3F	wild type v Si[nas-9p::rde-4(+)]; rde-10(jam206); eri-1(mg366)	282, 202	85, 0	<0.00001, *	N2, AMJ1724	
3F	wild type vs mut-16(jam148); eri-1(mg366)	282, 70	85, 0	<0.00001, *	N2, AMJ1672	
3F	wild type v Si[nas-9p::rde-4(+)]; mut-16(jam148)	282, 152	85, 0	<0.00001, *	N2, AMJ1721	
3F	wild type v Si[nas-9p::rde-4(+)]; mut-16(jam148); eri-1(mg366)	282, 187	85, 0	<0.00001, *	N2, AMJ1722	
5B	wild type vs bli-1(jam307)	488, 443	390, 425	<0.00001, *	N2, AMJ1754	
5B	wild type vs bli-1(jam308)	488, 245	390, 185	0.170996, ns	N2, AMJ1755	
5B	wild type vs nrde-3(jam205)	488, 377	390, 111	<0.00001, *	N2, AMJ1510	
5B	bli-1(jam307) vs bli-1(jam307); nrde-3(jam205)	443, 459	425, 313	<0.00001, *	AMJ1754, AMJ1758	
5B	nrde-3(jam205) vs bli-1(jam307); nrde-3(jam205)	377, 459	111, 313	<0.00001, *	AMJ1510, AMJ1758	
5B	bli-1(jam308) vs bli-1(jam308); nrde-3(jam205)	245, 117	185,38	<0.00001, *	AMJ1755, AMJ1771	
5B	wild type vs bli-1(jam307)	488, 443	390, 425	<0.00001, *	N2, AMJ1754	
5D	*bli-1p::gfp vs mut-*	21, 25	21, 6	<0.00001, *	AMJ1709, AMJ1727	

	16(jam148); bli-1p::gfp					
5D	*bli-1p::gfp vs rde-10(jam206); bli-1p::gfp*	21, 25,	21, 9	<0.00001, *	AMJ1709, AMJ1725	
5D	*bli-1p::gfp vs nrde-3(jam205); bli-1p::gfp*	21, 25	21, 23	0.18508, ns	AMJ1709, AMJ1726	
5D	*bli-1p::gfp vs mut-16(jam148)rde-10(jam196); bli-1p::gfp*	21, 20	21, 0	<0.00001, *	AMJ1709, AMJ1728	
6A	1 vs 2 days post RNAi	94, 91	76, 86	0.00489, *	N2	
6A	1 vs 3 days post RNAi	94, 92	76, 89	0.00062, *	N2	
6A	1 vs 4 days post RNAi	94, 93	76, 89	0.001627, *	N2	
6A	5 days post RNAi versus 7 days on RNAi	110, 55	63, 51	<0.00001, *	N2	
6A	6 days post RNAi versus 7 days on RNAi	104, 55	61, 51	<0.00001, *	N2	
6A	7 days post RNAi versus 7 days on RNAi	112, 55	60, 51	<0.00001, *	N2	
6A	8 days post RNAi versus 7 days on RNAi	124, 55	45, 51	<0.00001, *	N2	
S2B	wild type vs rde-10(jam243)	115, 102	115, 100	0.13140071, ns	N2, AMJ1614	
S2B	wild type vs mut-16(jam240) rde-10(jam206)	115, 137	115, 5	<0.00001, *	N2, AMJ1611	
S2C	wild type vs mut-16(jam268)	322, 74	279, 20	<0.00001, *	N2, AMJ1675	From the same feed in Fig. 2E
S6B	wild type unc-22 vs wild type pL4440	138, 116	138, 0	<0.00001, *	N2	

S6B	wild type unc-22 vs nrde-3(jam205) unc-22	138, 110	138, 79	<0.00001, *	N2, AMJ1510	
S6B	unc-22(jam300) unc-22 vs unc-22(jam300) pL4440	101, 113	101, 101	0.00128, *	AMJ1730	
S6B	unc-22(jam301) unc-22 vs unc-22(jam301) pL4440	101, 65	101, 49	<0.00001, *	AMJ1731	
S6B	unc-22(jam300); nrde-3(jam205) unc-22 vs unc-22(jam300); nrde-3(jam205) pL4440	82, 108	70, 83	0.14214, ns	AMJ1757	
S6B	unc-22(jam300); nrde-3(jam205) unc-22 vs unc-22(jam300) unc-22	82, 101	70, 101	<0.00001, *	AMJ1757, AMJ1730	
S6B	unc-22(jam300); nrde-3(jam205) unc-22 vs nrde-3(jam205) unc-22	82,110	70, 79	0.02592, *	AMJ1757, AMJ1510	

Chapter 3: Disruption of small RNA-based regulation results in nuclear morphology defects in the germline

3.1 Preface This work builds upon initial observations of mutants from the genetic screen (as described in Chapter 2) which was performed by Pravrutha Raman and Farida Ettefa, with mutant validation done by Mary Chey. Rotation student Simoné Parn created the strain AMJ1756, and took the images represented in Figure 3-7A. Antony Jose generated the heatmap in Figure 3-5G. The schematics of the *C. elegans* germline are adapted from (133). All other data was generated by Daphne Knudsen-Palmer. For simplicity, the *oxSi487* transgene (*mex-5p::mCherry::h2b::sl2::gfp::h2b II*) will be referred to as *"T"*.

3.2 Introduction

Understanding what controls nuclear size has remained a question in biology for well over 100 years. As Theodor Boveri noted:

> "The constant, which we must accept as something given and not at present further analyzable, is the fixed proportion between nuclear volume and protoplasmic volume, namely the karyoplasmic ratio." (153)

Since the early 1900′s, many studies have been done to understand which processes could maintain this seemingly fixed ratio of cytosolic volume to nuclear volume. In yeast, mutants that affect nucleocytoplasmic transport (154), the LINC complex, or RNA processing (155) can disrupt this ratio. In the ciliate *Tetrahymena thermophila,* a small, transcriptionally inactive micronucleus (MIC) and a large, transcriptionally active macronucleus (MAC) exist within the same volume of cytosol, suggesting that nuclear size could be actively controlled (reviewed in (156)).

The *C. elegans* germline is comprised of two gonad arms and provides an ideal system to be able to study germ cell development (reviewed in (157)) and nuclear morphology. The distal end of each arm is a syncytium, where many mitotic nuclei share the same cytosol. The gene expression throughout the germline must be carefully spatiotemporally controlled, to allow for the proper development of germ cells (e.g. (158)), including the change from mitosis to meiosis. Some of this gene expression is mediated by small RNAs (e.g. (159)), that can accumulate in foci around the nuclear periphery (reviewed in (80)).

Here we define a connection between small RNA-based regulation and control of nuclear size in the *C. elegans* germline. We find that the loss of MUT-16 results in some germline nuclei that are enlarged, and also show an increase of histone signal. Preliminarily, we report defects in the nuclear envelope and in the nucleolus in mutants of 2º siRNA amplification. Finally, we suggest candidates to explain the nuclear defects based on transcriptomic data. Together, these examples of both normal-sized and enlarged nuclei together in a fixed cytosolic volume suggest that control of nuclear size is an active process.

3.3 Methods

3.3.1 Strains and oligonucleotides

All strains (listed in Table 3-1) were cultured on Nematode Growth Medium (NGM) plates seeded with 100 µl of OP50 *E. coli* at 20ºC and strains made through mating were generated using standard methods (122). Oligonucleotides used are in Table 3-2. For PCR of C17F4.7 (Figure 3-6C), primers (P1) and (P2) were used.

3.3.2 Germline dissections and DAPI staining

Animals were staged at the L4 stage and dissected 24±1 hours later in PBS-Tween plus 0.25 mM levamisole. Incisions were made immediately posterior of the pharynx. Dissected germlines were fixed in PBS-Tween plus 2% formaldehyde for 10 minutes at room temperature. After two washes (PBS-Tween), germlines were incubated for 10 minutes in 70% ethanol on ice. DAPI (1 µg/mL) was added and germlines were incubated in the dark for 30 minutes at room temperature. Germlines were then washed and mounted on a coverslip and put on a slide with a 2% agarose pad.

3.3.3 Microscopy

Epifluorescence microscopy: Animals were mounted in 10 µl of 3 mM levamisole on a 2% agar pad and imaged under a coverslip using a Nikon AZ100 microscope and Photometrics Cool SNAP HQ^2 (Figure 3-1B) or Prime BSI Express sCMOS camera (Figure 3-7A). A C-HGFI Intensilight Hg Illuminator was used to excite GFP (filter cube: 450 to 490 nm excitation, 495 dichroic, and 500 to 550 nm emission) or mCherry (filter cube: 530–560 nm excitation, 570 dichroic, and 590–650 nm emission) Representative images for mCherry expression were adjusted to identical levels in Fiji (NIH) for presentation.

Scanning confocal microscopy: (Figures 3-1D, 3-2B): Dissected germlines were imaged using a Leica SP5X confocal microscope with the 63x oil immersion objective. Z stacks were taken with 1µm steps to encompass the entire diameter of the germline. DAPI was excited using a 405 nm UV laser, GFP fluorescence was captured using a 488 nm argon laser, and mCherry fluorescence was captured using a white light laser set to 594 nm. (Figure 3-2C): Dissected germlines were imaged using a Leica Stellaris 8 confocal microscope with the 63x oil immersion

objective. Z stacks were taken with 0.5 µm steps to encompass the entire diameter of the germline. DAPI was excited using a 405 nm UV laser, GFP fluorescence and mCherry fluorescence was captured using a white light laser set to 488nm and 594 nm, respectively.

Transmission electron microscopy: Germlines were dissected as described above (Chapter 3.3.2) and placed in primary fix (2.5% glutaraldehyde and 1% paraformaldehyde in 0.05 M cacodylate buffer with 0.1 M sucrose) overnight at 4ºC. Samples were washed 3x for 10 minutes in 0.2 M cacodylate buffer and then placed in secondary fix (1% osmium tetroxide in 0.1 M cacodylate with 0.5% potassium ferrocyanide) for 60 minutes at room temperature. Samples were then washed 3x for 10 minutes in double distilled water and then placed in 2% aqueous uranyl acetate for 60 minutes at room temperature. Samples where next dehydrated in 35%, 50%, 70%, and 95% ethanol, sequentially, each for 10 minutes and then 3x 10 minutes in 100% ethanol. Samples were then treated 3x for 10 minutes in propylene oxide, then incubated in propylene oxide:Spurr′s Resin at a ratio of 1:1, 1:2, 1:3, and then 100% Spurr′s Resin, sequentially, for at least 60 minutes and up to overnight. Samples were embedded in Spurr′s Resin and incubated at 70ºC before sectioning and imaging. Images were taken using a Hitachi HT7700 Transmission Electron Microscope (Laboratory for Biological Ultrastructure, University of Maryland, with Tim Maugel).

3.3.4 Genome editing

The gonads of adult *C. elegans* were injected with nuclear-localized Cas9 (PNA Bio) preincubated at 37°C for 10 min with a hybridized crRNA/tracrRNA (Integrated DNA Technologies), as well as an oligonucleotide or PCR-amplified homology repair template. Plates with successfully edited F1 animals were identified by screening the Dpy or Rol animals obtained

when using *dpy-10* editing as a co-CRISPR (123, 124) or for Rol animals when using the pRF4 plasmid as a co-injection marker (125).

To introduce a premature stop codon in *mut-16*: Injection of a crRNA with the target sequence (P3) (Integrated DNA Technologies), tracrRNA, Cas9, a *mut-16(-)* homology repair template (P4) mimicking the mutation in *mut-16(jam139),* predicted amino acid change Y294*, and *dpy-10* crRNA (P5) and *dpy-10(-)* homology repair template (P6) into EG6787 and subsequent screening were performed as described above. Genotyping for *mut-16(jam330)* was performed using duplex PCR (P7, P8) followed by restriction digestion with BstBI. The nonsense mutations in different strains (AMJ1780, AMJ1781) were verified by Sanger sequencing. Generation of AMJ1397 was described in Chapter 2.

To make the *mut-16(-) rde-10(-)* double mutants: Injection of a crRNA with the target sequence (P9) (Integrated DNA Technologies), tracrRNA, Cas9, a *rde-10(-)* homology repair template (P10) mimicking the mutation in *rde-10(jam248)*, and *dpy-10* crRNA (P5) and *dpy-10(-)* homology repair template (P6) into AMJ1397 (*mut-16(jam148))* and subsequent screening were performed as described above. Genotyping for *rde-10(-)* was performed using duplex PCR (P11, P12) followed by restriction digestion with DpnII. Strains with mutations in *rde-10* that results in at least one early stop codon were designated as AMJ1682 and AMJ1683. Generation of AMJ1470 and AMJ1611 were described in Chapter 2.

3.3.5 RNA extraction and transcriptomics

Total RNA was extracted using TRIzol (Fisher Scientific) from pellets of mixed-stage animals collected from non-starved but crowded plates in biological triplicate for each strain. The aqueous phase was then washed with an equal amount of chloroform and precipitated overnight at

-20°C with 10 µg glycogen (Invitrogen) and 1 ml of isopropanol. RNA pellets were washed twice with 70% ethanol and resuspended in 25 µl of nuclease free water.

3.3.5.1 For poly-A RNA-seq (Figure 3-4): PolyA+ RNAs were purified and converted to DNA libraries by Omega Bioservices using the Illumina TruSeq Library Preparation Kit. FASTQ files were processed using the command "cutadapt -j 0 -a AGATCGGAAGAGCACACGTCTGAACTCCAGTCA -A AGATCGGAAGAGCGTCGTGTAGGGAAAGAGTGT -m 20 -q 20 -o cutread.gz fasta1.gz" (160). Reads were assigned transcript IDs and counted using the command "salmon quant -i celegans.index -l A -r cutread.gz -p 8 –validateMappings -o quant_file" (161). Transcript IDs were converted to gene IDs using tximport (162) in R and only genes with more than 0.1 counts per million for at least 2 samples were used for subsequent analysis. Samples were normalized using the trimmed mean of M-values method (163). Differential expression analysis was performed using limma(voom) (164) in R. Volcano plots were generated with ggplot2 in R.

3.3.5.2 For total RNA-seq (Figure 3-5): Total RNAs were depleted for ribosomal RNAs and then converted to DNA libraries by the Advanced Genomic Technologies Core (part of the Brain and Behavior Institute, University of Maryland). FASTQ files were processed using the command "cutadapt -j 0 -a CTGTCTCTTATACACATCT -A CTGTCTCTTATACACATCT -m 20 -q 20 -o cutread.gz fasta1.gz" (160). Reads were assigned transcript IDs and counted using the command "salmon quant -i celegans.index -l A -r cutread.gz -p 8 –validateMappings -o quant_file" (161) or mapped to the genome using hisat2 using the command "hisat2 -p 8 -x Ccelegans.index -1 cut_reads_R1.fastq.gz -2 cut_reads _R2.fastq.gz -S sam1" (165). Transcript IDs were converted to gene IDs using tximport (162) in R and only genes with more than 0.1 counts per million for at least 2 samples were used for subsequent analysis. Samples were normalized using the trimmed

mean of M-values method (163). Differential expression analysis was performed using limma(voom) (164) in R. Hisat2 reads were visualized in Integrative Genomics Viewer (IGV, v. 2.11.3). Volcano plots were generated from reads generated by Salmon with ggplot2 in R. The chromosome phenogram (Figure 3-5B) was adapted from an image generated from PhenoGram Plot (166).

3.4 Results

3.4.1 Loss of *Mutator foci* components results in some germline nuclei that are enlarged.

From a genetic screen looking for components involved in long-term epigenetic silencing that was previously described (see Chapter 2, (112)), we isolated 15 fertile mutants, each of which were sent for whole genome sequencing. Briefly, we screened for mutants that showed a reactivation of transgene expression (*mex-5p::mCherry::h2b::sl2::gfp::h2b, "T"*) that had been subjected to long-term silencing. In addition to the five *mut-16(-)* mutants we previously reported (112), we also found mutants of other regulators of small RNA-based regulation, including *Mutator* foci components MUT-2, MUT-7, and MUT-15, and the germline nuclear Argonaute HRDE-1. When examining the germlines of these mutants, we found several mutants that showed some germline nuclei that were both enlarged and appeared to have an increase in mCherry::H2B fluorescence (Figure 3-1B), a defect that has not been previously reported in these mutants. In addition to instances of enlarged nuclei, many of the *Mutator* foci mutants showed instances of germlines that appeared much shorter and had fewer total nuclei (for example, *mut-16(jam247)*). The mutants with instances of enlarged nuclei were all components of *Mutator* foci (*mut-16(jam138), mut-16(jam139) rde-10(jam248), mut-16(jam140), mut-16(jam141), mut-16(jam247), mut-2(jam322), mut-2(jam325), mut-7(jam327), mut-7(jam328), mut-15(jam330)*).

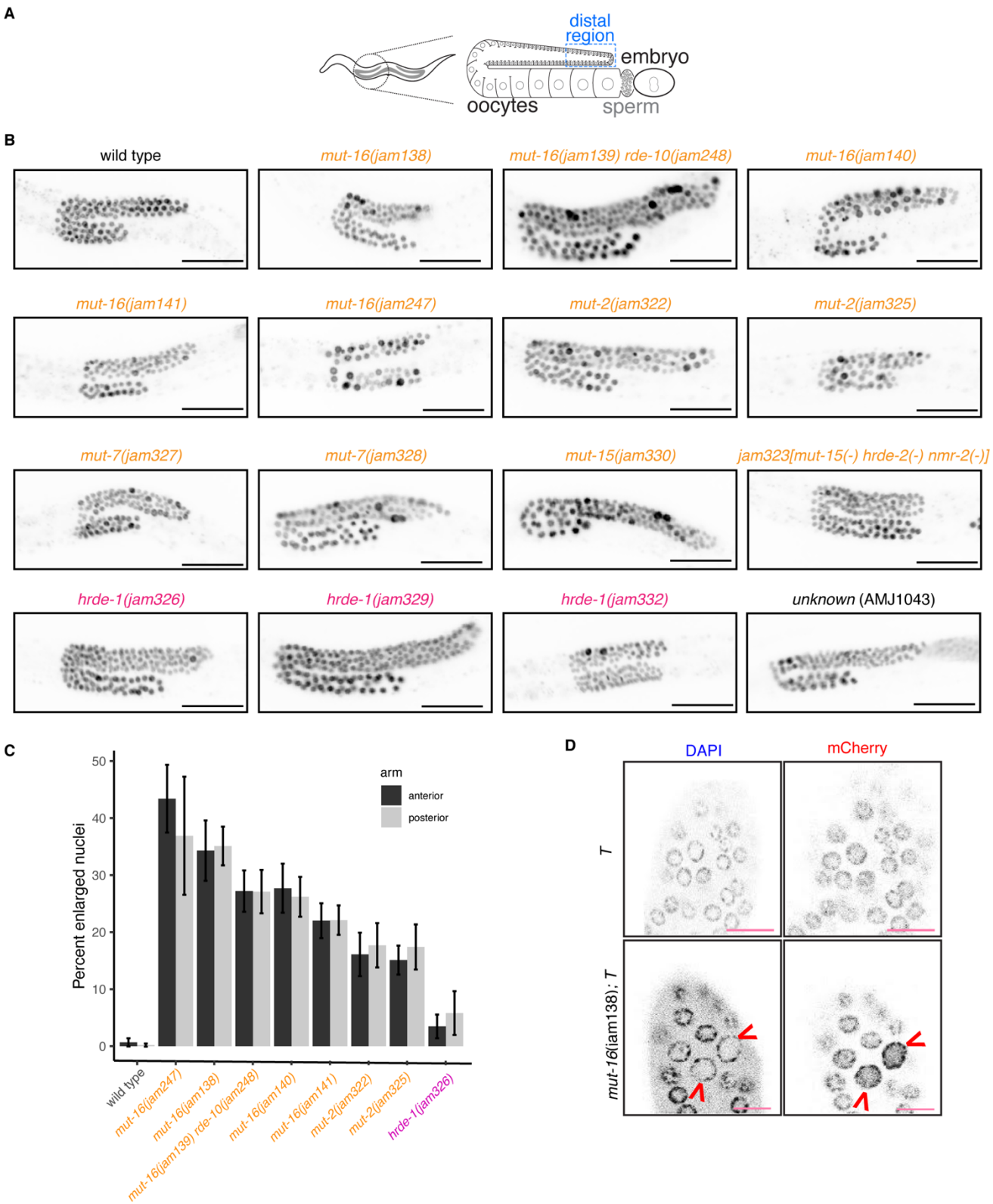

A
distal region
embryo
oocytes
sperm
B
wild type
mut-16(jam138)
mut-16(jam139) rde-10(jam248)
mut-16(jam140)
mut-16(jam141)
mut-16(jam247)
mut-2(jam322)
mut-2(jam325)
mut-7(jam327)
mut-7(jam328)
mut-15(jam330)
jam323[mut-15(-) hrde-2(-) nmr-2(-)]
hrde-1(jam326)
hrde-1(jam329)
hrde-1(jam332)
unknown (AMJ1043)
C
Percent enlarged nuclei
arm
anterior
posterior
wild type
mut-16(jam247)
mut-16(jam138)
mut-16(jam139) rde-10(jam248)
mut-16(jam140)
mut-16(jam141)
mut-2(jam322)
mut-2(jam325)
hrde-1(jam326)
D
DAPI
mCherry
T
mut-16(jam138); T

Figure 3-1. Disruption of small RNA-based regulation results in germline defects. (A) Schematic depicting the adult *C. elegans* germline. The distal mitotic region is highlighted in blue (adapted from (133)). (B) One arm of the germline of L4 animals, where the distal part of the germline is on the top of the image. Mutants that disrupt siRNA amplification are colored in orange; mutants that affect 2º siRNA binding or recognition are shown in pink. Scale bar = 50µm. (C) Quantification of enlarged nuclei in some *Mutator* foci components and one *hrde-1(-)* allele. The number of enlarged nuclei were divided by the total number of nuclei in the distal half of the germline. The anterior (dark gray) and posterior (light gray) arms of the germline were analyzed separated. n=10 animals; error bars indicate 95% CI. (D) Representative cross sections of wild type (*T*) or *mut-16(jam138); T* dissected germlines stained with DAPI and expressing mCherry:H2B, n > 5 germlines. Red arrowheads indicate nuclei that are enlarged and show an increase in mCherry signal. Scale bars = 10µm.

Notably, not all mutants that disrupt small RNA machinery and/or the maintenance of long-term silencing show this defect (e.g. *hrde-1(jam326), hrde-1(jam329)*). One strain, AMJ1043, has no obvious candidates for causative mutations and needs to be explored further, but does not obviously appear to have enlarged nuclei. For some of the strains with the perceived highest penetrance of enlarged nuclei, we plotted the percentage of enlarged nuclei on the distal half of the germline (Figure 3-1C). While there is no observable difference between arms of the gonad, animals that lack MUT-16 show the highest penetrance of enlarged nuclei, showing above 30% nuclei that are enlarged for some alleles, followed by the alleles of *mut-2(-),* with *hrde-1(-)* mutants showing a very modest effect if any. This suggests that not all disruptions of epigenetic silencing can cause defects in nuclear size, and perhaps disruption of *Mutator* foci or specifically amplification of 2º siRNAs is responsible for this defect.

To ask whether these enlarged nuclei had additional copies of the genome, we dissected germlines of *mut-16(-)* mutants and performed a DAPI stain to compare the DNA, GFP::H2B, and mCherry::H2B signals throughout the whole tissue by using confocal microscopy (Figure 3-1D). In animals with a wild-type background and the transgene *T*, each of the nuclei seem to be of uniform size and intensity across all channels. While not all nuclei were affected, some nuclei in *mut-16(-)* mutant germlines were much larger than those surrounding. These nuclei did not appear

to have a brighter DAPI signal; rather the DAPI signal was dimmer, suggesting these nuclei are not endoreduplicated. Consistent with the observations on the epifluorescent microscope, we observed an increase of mCherry::H2B signal in the nuclei that were enlarged.

To ensure the observed enlarged nuclei are being caused by the loss of MUT-16 and not due to any number of potential background mutations from the strains isolated from the screen, nor due to the combination of the lack of MUT-16 in the presence of the transgene, we generated a new *mut-16(jam148)* mutant using CRISPR-Cas9-based editing in a wild type background, which is predicted to result in an early stop codon. We dissected germlines from animals 24 hours post-L4, fixed them, and stained them with DAPI to examine nuclear diameter (Figure 3-2A). We measured the diameter of each nucleus in the most distal 50µm of the dissected germlines by measuring the diameter of each nucleus at its maximum throughout a Z-stack of the germline, and called anything that was 5µm or greater as enlarged (Figure 3-2B). Freshly generated *mut-16(jam148)* mutants in fact do show enlarged nuclei, with a penetrance of 5-10%. Given the potential for *Tc1* transposon hopping in the absence of MUT-16 (101), we outcrossed this new allele to two variants of the transgene *T* (*Tcherry* and *Tcherry-mex*) in an attempt to remove potential background mutations. In each of these cases, germlines that lack MUT-16 show some instances of enlarged nuclei, again with around 10% penetrance.

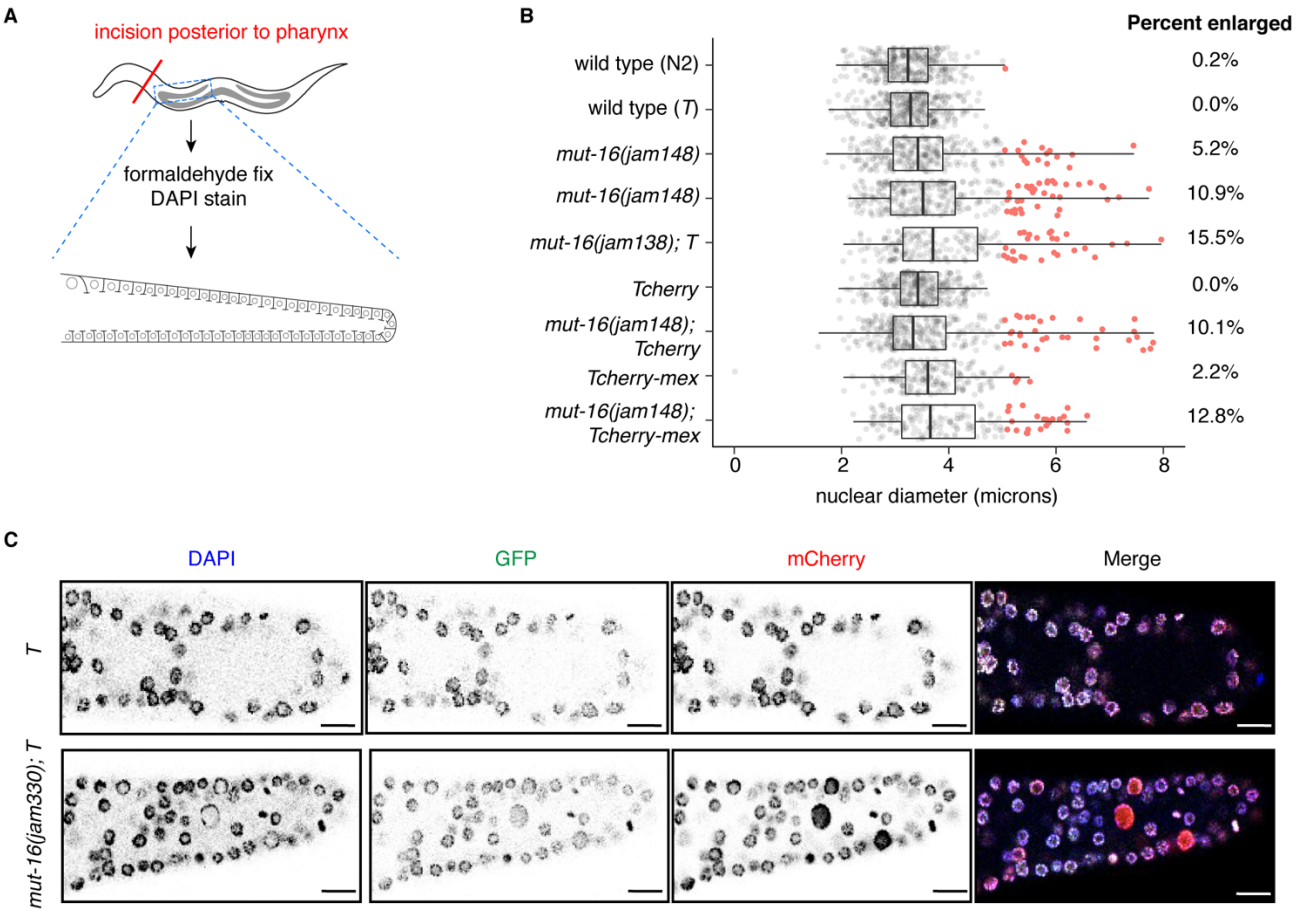


Figure 3-2. Newly generated *mut-16(-)* mutants show some enlarged nuclei. (A) Schematic to describe dissection of *C. elegans* germline. An incision is made below the pharynx (red) which causes the insides of the worm, including the germline, to spill out of the body cavity. Tissues were then fixed in formaldehyde and stained with DAPI (see Methods section 3.3.2). Images were taken from the most distal end of the germline syncytium. (B) Quantification of nuclear diameter from dissected germlines that were stained with DAPI, with box plots showing the lower quartile, median and upper quartile across all points. Wild type animals with or without the transgene (N2, EG6787), two replicates of a newly generated *mut-16(jam148)* mutant, a strain from the screen (*mut-16(jam138;T)*), two variants of the transgene (*Tcherry, Tcherry*-mex), and two out crossed strains of the new mutant (*mut-16(jam148); Tcherry, mut-16(jam148);Tcherry-mex*), are shown. Nuclear diameter is plotted in microns on the x-axis, and any nucleus with a diameter of greater than or equal to 5µm was considered enlarged (red points). The nuclei in the most distal 50µm from the distal tip cell were quantified from n = 5 germlines. The percentage of nuclei above 5µm within the total nuclei within the most distal 50µm is shown for each genotype (right). (C) Representative images of cross sections from dissected germlines. (*top*) Wild type animals with the transgene *T* comparing DAPI, GFP, and mCherry signal with all channels merged on the right. (*bottom*) Same as in (*top*), but for a new mutant of *mut-16(jam330)* created in the EG6787 background. n = 5. Scale bars = 10µm.

To ensure the observed enlarged nuclei are being caused by the loss of MUT-16 alone and not the combination of MUT-16 loss and some background mutation in our lab's wild type N2 strain, we generated a new *mut-16(jam330)* mutation in animals that contain the transgene *T,* a strain which was obtained from a different lab (EG6787). Germlines were dissected and stained with DAPI, and even only four generations after losing MUT-16, we again see instances of enlarged nuclei, again accompanied by diffuse DAPI signal but an increase in mCherry::H2B. While the lack of DAPI signal does not obviously suggest the presence of more DNA, we cannot rule out the possibility that there is more DNA but the DAPI concentration was not high enough to fully saturate the enlarged nuclei. Further experiments are needed to make conclusions about the DNA content in these large nuclei.

Taken together, we conclude that the loss of MUT-16 and associated loss of *Mutator* foci results in disruption of nuclear integrity in the germline.

3.4.2 The loss of MUT-16 and RDE-10 suggests defects in the nuclear envelope and in the nucleolus.

To characterize defects of the enlarged nuclei further, we wanted to look at the ultrastructure using transmission electron microscopy. Cross sections of the distal part of the germline may allow for many nuclei to be compared simultaneously (Figure 3-3A). While we were unable to distinguish normal-sized nuclei from enlarged nuclei (too small of a sample size to say whether differences in diameter were due to the overall size of the nucleus or due to the plane of the cross section hitting or not hitting the true center of the nucleus), we did notice some stark differences between wild-type nuclei and nuclei from *mut-16(jam139) rde-10(jam248)* mutants

(Figure 3-3B). First, the nuclear envelope is clearly visible along the entire periphery of wild-type nuclei.

,

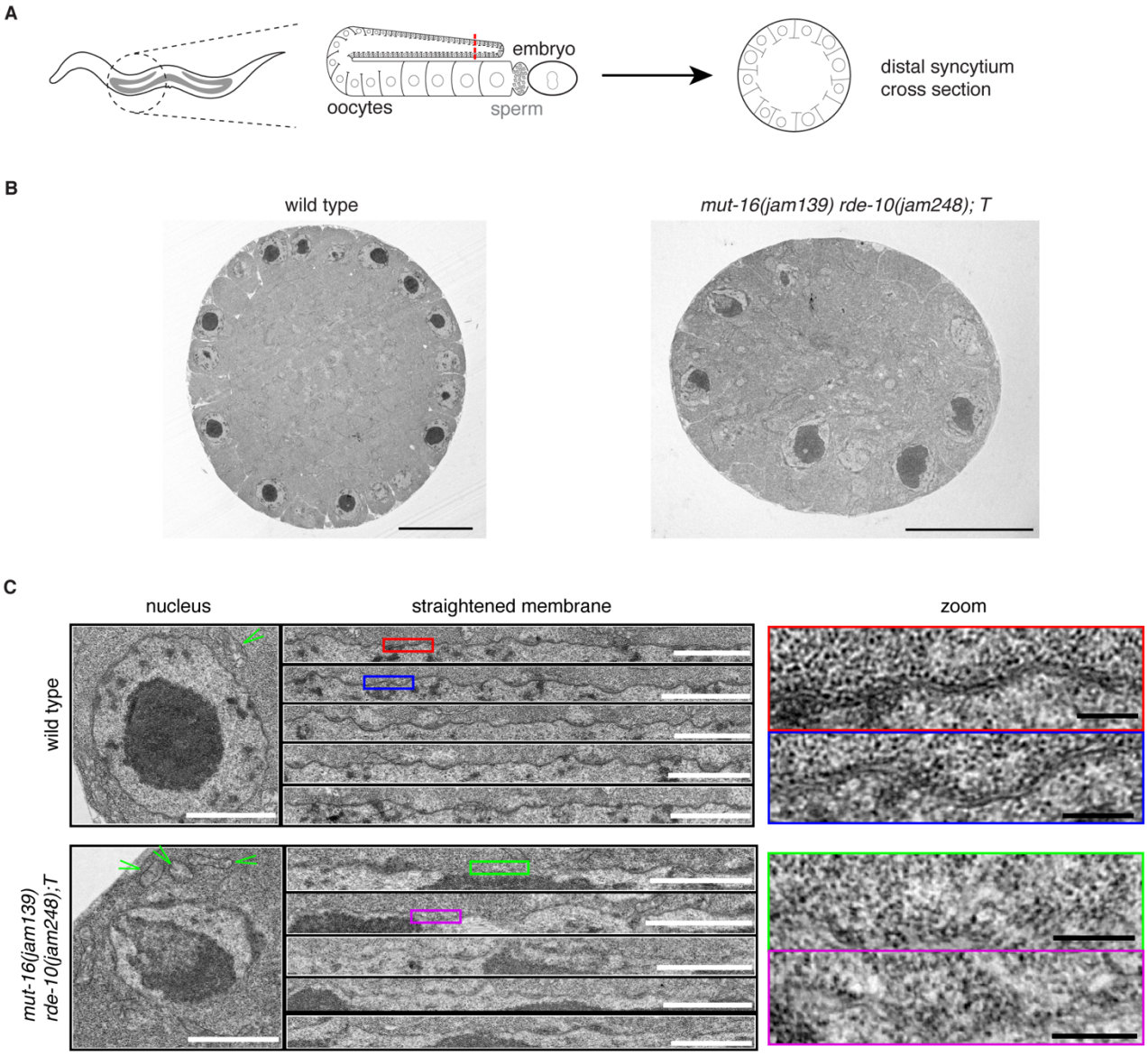


Figure 3-3. Disruption of small RNA amplification in *mut-16(-) rde-10(-)* double mutants shows deformed nuclear envelopes and deformed nucleoli. (A) Schematic depicting the *C. elegans* germline. (*left*) Each gonad arm of the germline contains a syncytium in the distal region, which eventually leads to the development of oocytes, sperm, and embryos in the proximal region. (*right*) Schematic of a cross section of the distal syncytium, where nuclei (in different planes) can

be seen around the periphery of the tissue with a shared cytosol in the center. (B) Representative images of cross sections of germlines dissected from either wild type (*left*) or *mut-16(jam139) rde-10(jam248); T* mutants (*right*). Scale bar = 10µm. (C) (*left*) Representative nuclei from the cross sections in (B). Green arrows indicate mitochondria. (*center*) Images of five nuclei that have been straightened by selecting eight points around the circumference of the nuclei with a 100µm width (Fiji). (*right*) Zoomed in sections of the nuclear envelope in (*center*) with respective colors showing selection. n = 1 germline per genotype. White scale bars = 2.0µm; black scale bars = 0.2µm.

In contrast, in *mut-16(jam139) rde-10(jam248)* mutants, the nuclear envelope can be visible in some parts, but appears to be dissipated or otherwise changed in each nucleus. Second, the nucleolus in wild type animals was consistently both round and well-centered within the nucleus, whereas in the double mutant nuclei the nucleolus seemed misshapen and often resided much closer to the periphery. Note that the total diameter of the double mutant germline seems to be much smaller than that of the wild type germline, which could either be a characteristic of *mut-16(-) rde-10(-)* mutants, or that the section in the wild type sample was taken more proximally within the syncytium.

To illustrate this across more nuclei, we straightened images to show a 100µm border centered around the nuclear envelope by selecting eight points around the circumference of the envelope (Figure 3-3C). For each of the wild type nuclei, the nuclear envelope is traceable throughout the length of the images. The *mut-16(-) rde-10(-)* double mutant in contrast has some places where the nuclear envelope is visible, but often places where it is lacking. The straightened images of the double mutant also have the nucleolus visible, suggesting it is closer to the nuclear periphery than the wild-type nucleoli, which are absent from the straightened images. Two explanations could support these observed differences: 1. the loss of both MUT-16 and RDE-10 could be leading to breakdown of the nuclear envelope or 2. something about the loss of MUT-16 and RDE-10 causes the nuclear envelope to stain more poorly than in wild type. It is also worth

considering the possibility that the double mutant germlines did not get stained as well as the wild type germlines during sample preparation, however the mitochondria surrounding the nuclei look equally well-stained in both genotypes (green arrows).

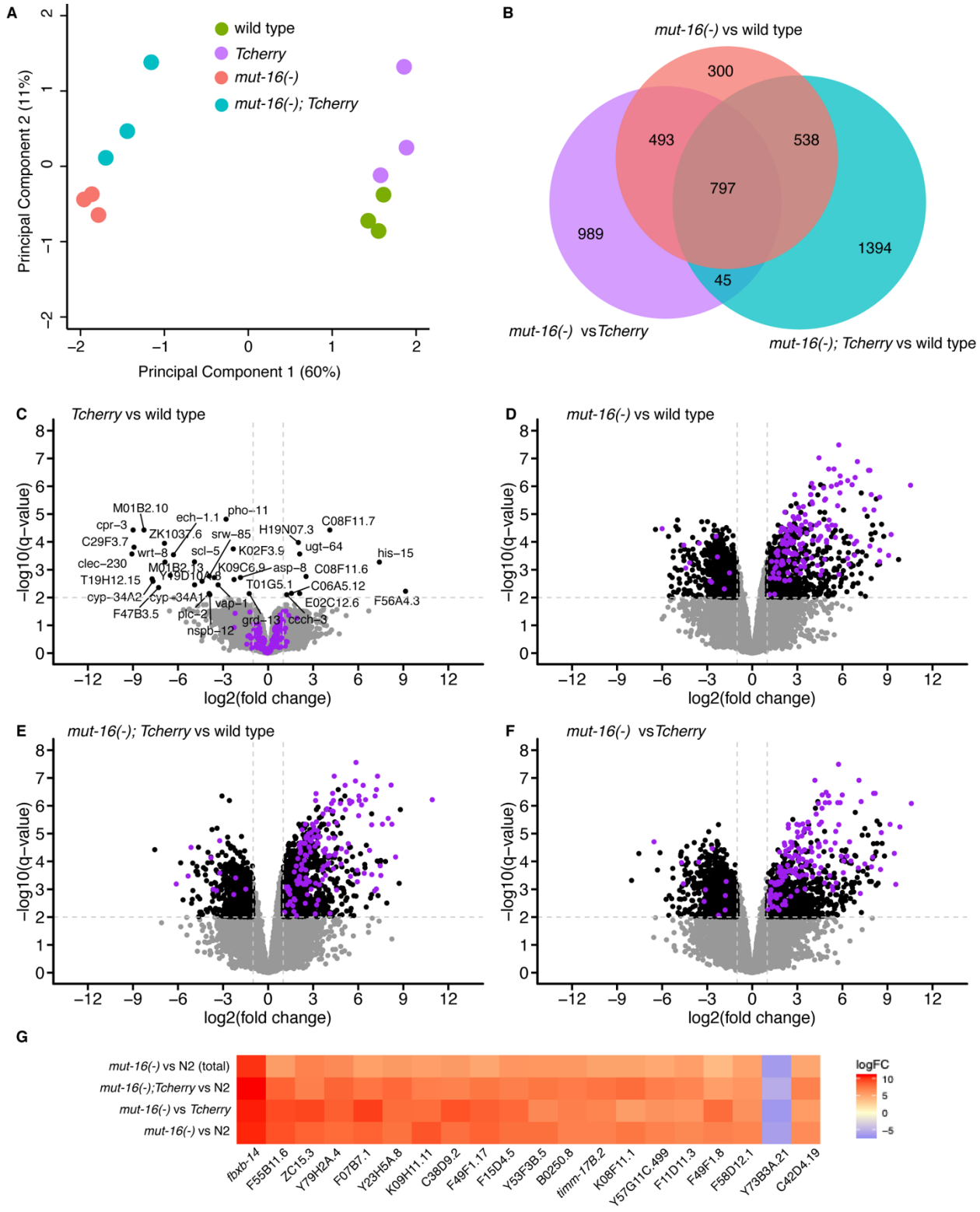


Figure 3-4. The loss of MUT-16 disrupts thousands of genes . (A) Principal component analysis of all replicates. Biological triplicates for each genotype are plotted: wild type (green), *Tcherry* (purple), *mut-16(jam148)* (red), and *mut-16(jam148); Tcherry* (blue). (B) Venn diagram

comparing genes that change more than 2-fold and have an adjusted p-value of less than 0.01 among *mut-16(-)* vs N2 (red), *mut-16(-)* vs *Tcherry* (purple), and *mut-16(-); Tcherry* vs N2 (blue), created using BioVenn (167). (C-F) Volcano plots showing gene expression changes among various comparisons. Genes that change more than 2-fold and have an adjusted p-value of less than 0.01 are colored in black; genes that are significantly regulated by both MUT-16 in each of D-F and in Figure 3-5C are colored in purple; all insignificantly affected genes are colored in gray. (C) Comparison of *Tcherry* RNA-seq data versus wild type. (D) Comparison of *mut-16(-)* RNA-seq data versus wild type. (E) Comparison of *mut-16(-); Tcherry* RNA-seq data versus wild type. (F) Comparison of *mut-16(-)* RNA-seq data versus *Tcherry)*. (G) Heat map showing the top 20 most significantly affected genes found in the following comparisons: 1. *mut-16(-)* vs wild type (N2) from the total RNA-seq experiment in Figure 3-5, 2. *mut-16(-);Tcherry* vs wild type (N2) 3. *mut-16(-)* vs *Tcherry* and 4. *mut-16(-)* vs wildtype (N2). The log fold change is displaced as a gradient from lowest (blue) to highest (red).

The electron microscopy provided an excellent preliminary look at both the nuclear envelope and the nucleolus. Future experiments will investigate the nuclear envelope and the nucleolus via light microscopy. To accomplish this, we can generate a strain that expresses SUN-1::GFP under the *sun-1* (inner nuclear envelope protein) promoter (derived from OCF62, a gift from Orna Cohen-Fix), and expresses a split wrmScarlet, tagging *fib-1* (nucleolar protein) exclusively in the germline (168) . In this background, we can generate new *mut-16(-), rde-10(-),* and *mut-16(-) rde-10(-)* double mutants to ask whether the loss of these regulators disrupts the envelope or nucleolus.

3.4.3 Genes that are redundantly affected by MUT-16 and RDE-10 suggest candidates for explaining defects in nuclear integrity.

The loss of MUT-16 results in hundreds, if not thousands, of misregulated genes (60, 74). Indeed, a poly-A selected RNA sequencing experiment in our hands revealed over 2,000 genes that were misregulated in some comparisons with conservative cutoffs (a log foldchange of greater than 2, with an adjusted p value of less than 0.01), with 797 of those genes being consistent among three comparisons (Figure 3-3B). While it does seem that the enlarged nuclei arise because of the

lack of MUT-16, it is difficult to decide which of the many targets to test in subsequent experiments.

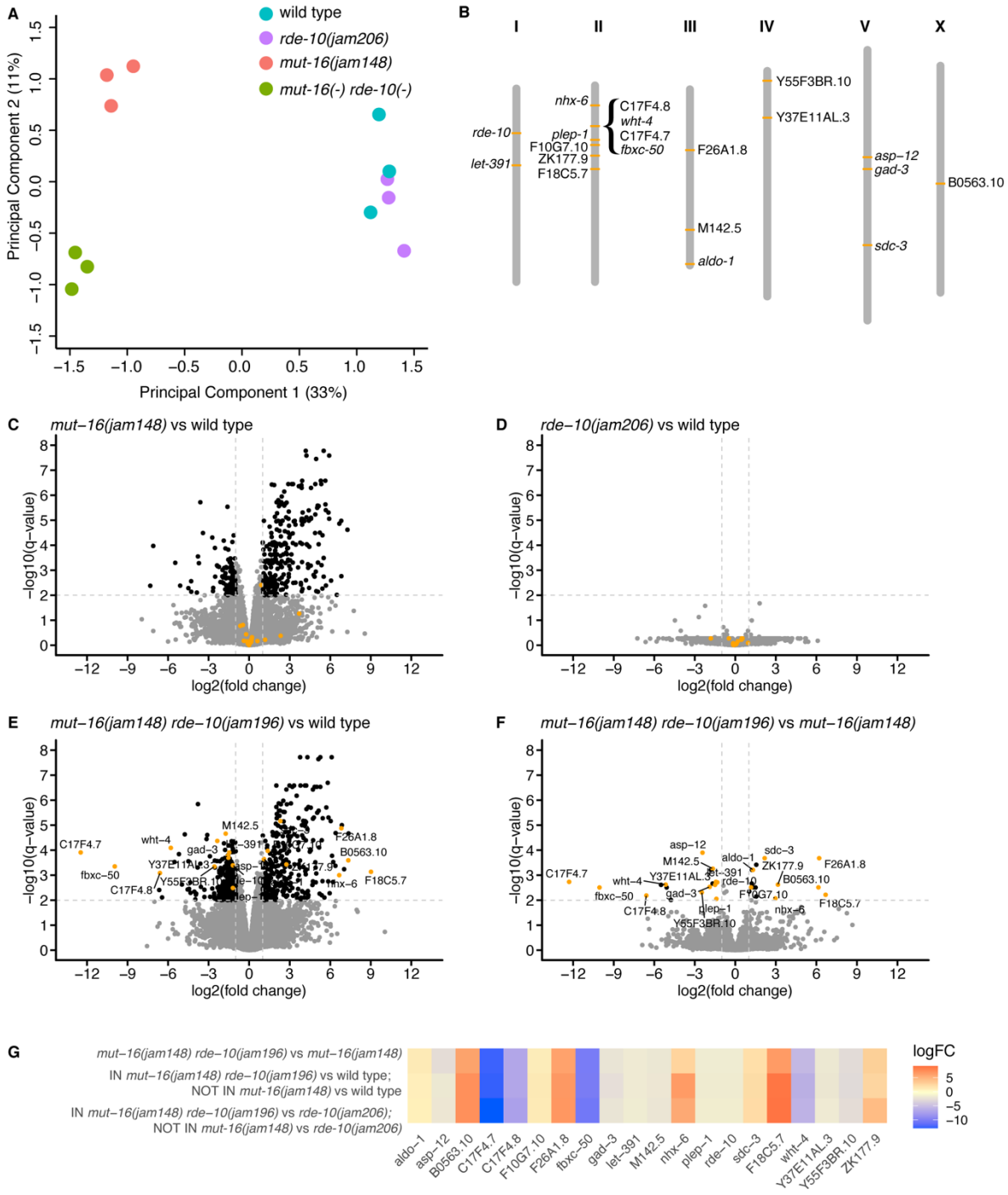


Figure 3-5. Total RNA sequencing reveal genes that are regulated by both MUT-16 and RDE-10. (A) Principal component analysis of all replicates. Biological triplicates for each

genotype are plotted: wild type (blue), *rde-10(jam206)* (purple), *mut-16(jam148)* (red), and *mut-16(jam148) rde-10(jam196)* (green). (B) Schematic of each *C. elegans* chromosome with labels for each of the MUT-16- and RDE-10-depenent genes. (C-F) Volcano plots showing gene expression changes among various comparisons. Genes that change more than 2-fold and have an adjusted p-value of less than 0.01 are colored in black; genes that are significantly regulated by both MUT-16 and RDE-10 together are colored in orange; all insignificantly affected genes are colored in gray. (C) Comparison of *mut-16(jam148)* RNA-seq data versus wild type. (D) Comparison of *rde-10(jam206)* RNA-seq data versus wild type. (E) Comparison of *mut-16(jam148) rde-10(jam196)* RNA-seq data versus wild type. (F) Comparison of *mut-16(jam148) rde-10(jam196)* RNA-seq data versus *mut-16(jam148)*. (G) Heat map showing genes that are significantly affected in groups of comparisons: 1. *mut-16(jam148) rde-10(jam196)* vs *mut-16(jam148),* 2. In *mut-16(jam148) rde-10(jam196)* vs wild type, but not in *mut-16(jam148)* vs wild type, and 3. In *mut-16(jam148) rde-10(jam196)* vs *rde-10(jam206)* but not in *mut-16(jam148)* vs *rde-10(jam206).* The log fold change is displaced as a gradient from lowest (blue) to highest (red).

Given that MUT-16 and RDE-10 have been shown to redundantly regulate targets of exogenous RNAi (Chapter 2, (112)), it seems plausible that there may be endogenous genes that could also be regulated by MUT-16 and RDE-10 together. We performed total RNA-seq with Ribodepletion on wild type, *mut-16(jam148), rde-10(jam206),* and *mut-16(jam148) rde-10(jam196)* mutants in triplicate. While *rde-10(jam206)* mutants did not appear drastically different than wild type, there was variance between *mut-16(jam148)* single mutants and *mut-16(jam148) rde-10(jam196)* double mutants, suggesting there could be a class of targets that is regulated by the two regulators together (Figure 3-5A). When comparing *mut-16(jam148)* mutants to wild type, hundreds of genes were misregulated, as expected (Figure 3-5C). To get a more stringent list of candidate genes, we used conservative cutoffs, where we called genes that changed by a fold-change of greater than two and had an adjusted p-value of less than 0.01 as significant (black). As suggested by the PCA plot (Figure 3-5A), the loss of RDE-10 did not drastically alter endogenous gene expression (Figure 3-5D), which is also consistent with what others have suggested, besides the loss of RDE-10 maybe having a modest effect on 22G RNAs that are downstream of 26G primary siRNAs (102, 103).

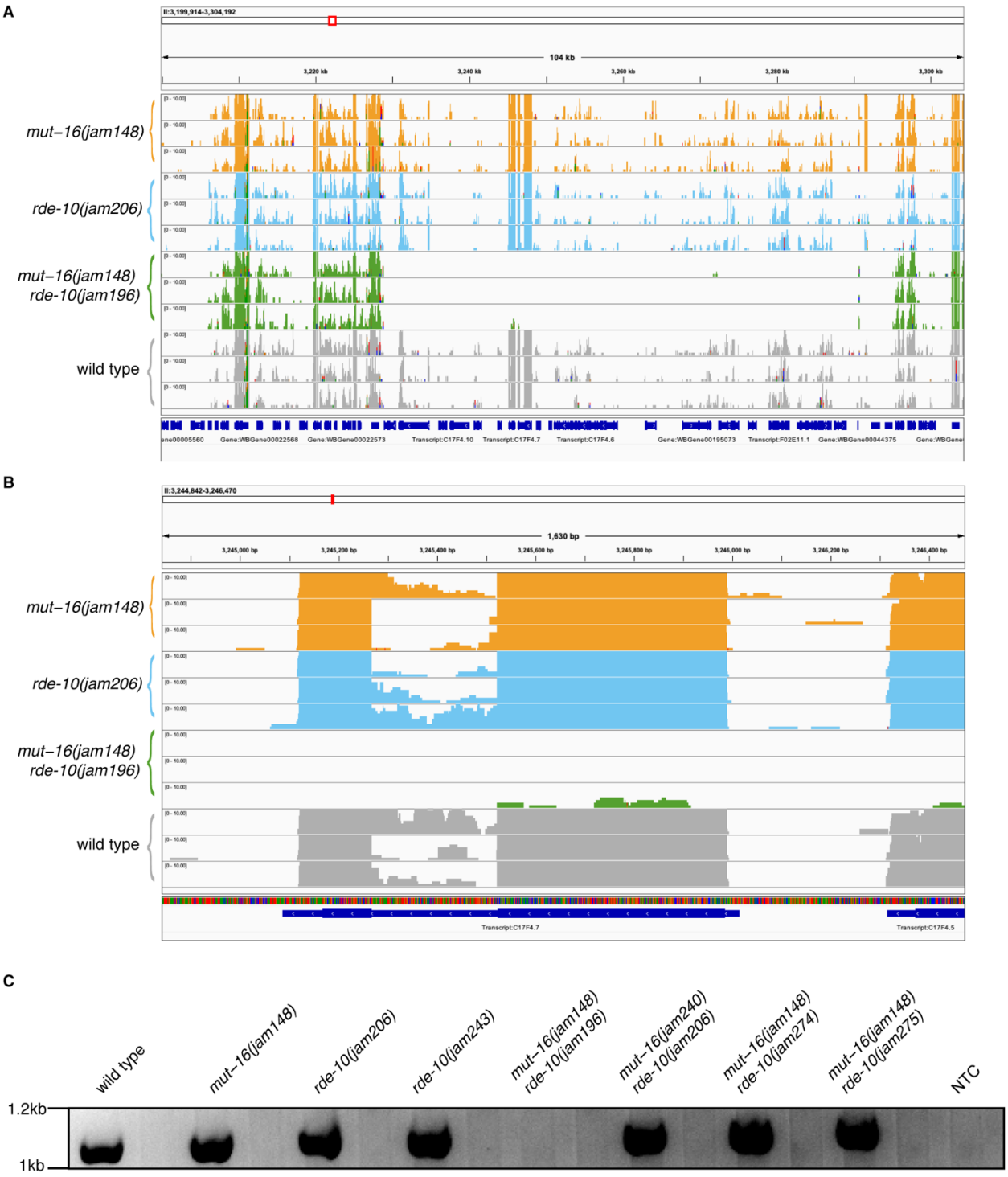


Figure 3-6. A nearly 60kb deletion on Chromosome II is present in *mut-16(jam148) rde-10(jam196)* double mutants. (A-B) Browser shots of RNA-seq reads from experiment in 3-5 but

mapped to the genome using hisat2. Biological triplicate runs are shown for each genotype (*mut-16(jam148),* orange; *rde-10(jam206),* blue; *mut-16(jam148) rde-10(jam196),* green; wild type, gray) and the height of peaks (y-axis) represents abundance (reads per million, rpm). (A) A section of Chromosome II that shows minimal to no reads in the *mut-16(jam148) rde-10(jam196)* mutants is nearly 60kb (kilobases) in length. The y-axis range is 0-2000 rpm. (B) A close look at the reads mapping to C17F4.7. The y-axis range is 0-10 rpm. (C) Polymerase chain reaction (PCR) from pooled worm lysates to amplify ~1kb which includes part of the 5′ *cis*-regulatory region and part of the C17F4.7 gene. The double mutant that was used for total RNA sequencing (*mut-16(jam148) rde-10(jam196)*) was unable to amplify this region, but three other double mutants (*mut-16(jam240) rde-10(jam206), mut-16(jam148) rde-10(jam274), mut-16(jam148) rde-10(jam275)*) could successfully amplify this region. NTC = non-template control.

The double mutant showed many genes that were changed as well (Figure 3-5E), and a comparison to the *mut-16(jam148)* single mutant suggests there are some genes that are uniquely regulated by both MUT-16 and RDE-10 (Figure 3-5F). To get the highest confidence list of candidates, we selected genes that were significantly misregulated in three comparisons: 1. the double mutant versus *mut-16(jam148),* 2. in the double mutant vs wild type, but not in *mut-16(jam148)* versus wild type, and 3. in the double mutant versus *rde-10(jam206)* but not in *mut-16(jam148)* vs *rde-10(jam206)* (Figure 3-5G). This list of twenty genes spans across the genome, but 4 genes that are significantly downregulated (C17F4.7, C17F4.8, *wht-4, fbxc-50*) are clustered together on Chromosome II (Figure 3-5B). This high confidence list of genes did not yield any significant results from a GO-term analysis (data not shown).

Upon further examination of the section of Chromosome II encompassing C17F4.7, C17F4.8, *wht-4,* and *fbxc-50,* it appears there is a nearly 60 kilobase region in the *mut-16(jam148) rde-10(jam196)* double mutant that shows a large depletion of reads (Figure 3-6A). C17F4.7 is a very highly expressed gene, and even when examining potential low levels of expression (0-10 rpm), there appears to be little to no expression in the double mutant (Figure 3-6B). This lack of reads, particularly over such a large region (up to ~60kb) could suggest a genomic deletion. Notably, *mut-16* and *rde-10* are located on Chromosome I, and a BLASTN search of the

crisprRNAs used to make those mutants does not suggest any homology to anywhere else in the worm (data not shown), so this ~60kb region likely was deleted due to unexplained off-target effects of CRISPR-Cas9 editing or *de novo* deletion after generation of the mutant. In *Tetrahymena,* siRNAs are required to target specific genomic deletions (58). A tantalizing possibility is that the drastic reduction of siRNAs due to the lack of MUT-16 and RDE-10 is resulting in a specific genomic deletion.

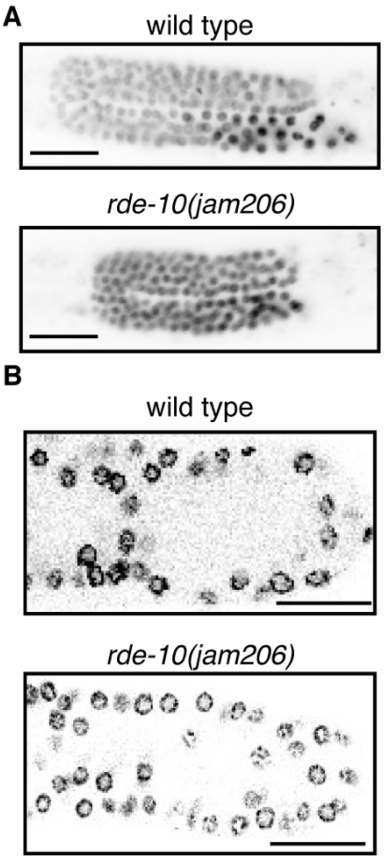


Figure 3-7. The loss of RDE-10 does not result in enlarged nuclei. (A) Representative images of L4 germlines of either wild type *T* or *rde-10(jam206); T* animals. The distal part of the germline is on the top of the image. Scale bars = 25µm. n > 20. (B) Representative cross sections of germlines that were dissected and stained with DAPI 24 hours post L4 in either wild type N2 or *rde-10(jam206)* animals. Scale bar = 10µm. n > 5.

To ask whether this region could have been deleted in the double mutant, we attempted to amplify a region near C17F4.7 using PCR. For comparison, we also looked at single mutants of ether *mut-16* or *rde-10,* as well as three additional *mut-16(-) rde-10(-)* double mutant alleles (Figure 3-6C). Each of the mutants except the double mutant that was prepped for RNA-seq (*mut-16(jam148) rde-10(jam196)*) was able to amplify this region, consistent with a genomic deletion in this particular mutant is possible. Follow-up experiments where we test mRNA levels via qPCR of targets in this region in other double mutants would be required to say whether these genes are actually redundantly regulated by MUT-16 and RDE-10, or if they only appear significant due to the likely genomic deletion on Chromosome II. The possibility that a specific genomic region is targeted for silencing in the *mut-16(-) rde-10(-)* mutant could still exist, perhaps at a low frequency,

which would require testing in individual animals. Future experiments are needed to determine precisely what has been deleted.

3.4.4 The loss of RDE-10 does not appear to affect nuclear size.

Given that RDE-10 and MUT-16 can work together at the level of siRNA amplification (112) and we preliminarily observe nuclear envelope and nucleolar defects in *mut-16(-) rde-10(-)* double mutants (Figure 3-3), we wondered whether the loss of RDE-10 alone is sufficient to cause nuclear defects. We took newly generated missense mutants of *rde-10(jam206*) that have previously been shown to be RNAi defective (112) and crossed them to animals with the *T* transgene. These animals did not appear to have any abnormal nuclei (Figure 3-7A, n > 20). Similarly, in dissected germlines, we saw no incidences of enlarged nuclei (Figrue 3-7B) in contrast to the newly generated *mut-16(jam148)* single mutants which showed 5-10% of nuclei that were enlarged (Figure 3-2B). We conclude that the loss of RDE-10 alone is not sufficient to disrupt nuclear size, and future experiments are needed to ask whether the loss of RDE-10 in a *mut-16(-)* mutant background enhances the penetrance of nuclear defects.

3.5 Discussion

Here we show that the loss of MUT-16 results in some nuclei that are enlarged in the distal part of the germline. These enlarged nuclei show an accumulation of H2B, suggesting defects in either nucleocytoplasmic transport and/or nuclear envelope integrity. Preliminarily, electron microscopy suggests defects in both the nuclear envelope and the nucleolus. Taken together, these observations provide an example to study wild type and defective nuclei side-by-side within a

syncytium and show for the first time that MUT-16 and small RNA-based regulation is required to maintain nuclear integrity in the *C. elegans* germline.

3.5.1 Small RNAs and phase separation

Two hypotheses could explain the defects that are observed when MUT-16 is lost: 1. genes that are regulated by MUT-16 are no longer operating as they do in wild type, leading to the defects or 2. the loss of MUT-16 results in structural changes, both within the nucleus and at the nuclear periphery.

Of the genes that are redundantly regulated by MUT-16 and RDE-10, some genes provide interesting candidates. F10G7.10, while uncharacterized in *C. elegans,* is the homolog of UBR3, an E3 ubiquitin ligase in mammals (169), zebrafish, and in *Drosophila* involved in Hedgehog signaling (170). Although the targets of F10G7.10 are unknown in *C. elegans,* speculatively, perhaps the lack of this putative ubiquitin ligase is causing cell cycle and/or cell differentiation defects in the developing mitotic germ cells. Another interesting candidate is *gad-3* (gastrulation defective), which is a predicted xanthine dehydrogenase (171). WormBase predicts *gad-3* to be involved in the IRE-1-mediated unfolded protein response in mitochondria (172, 173), a process which is closely tied to RNA interference (174). Among some of the comparisons from the poly-A -selected RNA-seq experiment (Figure 3-4), histone H1-like genes *hil-1, hil-7,* and *hil-8* were significantly affected. Another histone-like protein *hil-4* has been shown by others to be affected by MUT-16 (60). Histone-like proteins in prokaryotes can cause topological modifications of the genome (reviewed in (175)), so it is possible that the downregulation of histone-like genes in the absence of small RNA-mediated regulation could result in topological genome defects, potentially

enough to disrupt nuclear size. Future experiments are needed to investigate these and other candidates to determine the cause of the enlarged nuclei we observe in the absence of MUT-16.

P granules have been shown to associate with nuclear pores (69) and require the presence of RNAs in order to form phase-separated granules *in vitro* (76, 77) and while this has not been explicitly tested for *Mutator* foci, the intrinsically disordered regions of MUT-16 are required for phase separation. It is possible that the loss of MUT-16 results in such a drastic reduction of siRNAs that it disrupts the phase-separation of P granules and disrupts nuclear pores, providing one possible hypothesis to explain the nuclear envelope defects. In addition to phase-separation around the nuclear periphery, phase-separation also occurs within the nucleus, forming the nucleolus. Indeed, loss of antiribosomal siRNAs (risiRNAs, (176, 177)) can lead to defects in the nucleolus in *C. elegans* (178), so it is possible that the loss of MUT-16 and associated reduction of siRNAs could also explain the nucleolar defects. Future experiments are needed to examine what happens to other granules (P, Z, SIMR) when *Mutator* foci are absent.

3.5.2 "The Karyoplasmic Ratio"

While nuclear size is almost always proportional to cytosolic volume, there are a few examples were different nuclear sizes can occur within the same cytosol. *Tetrahymena* (and all other ciliates), for example, have one large and transcriptionally active macronucleus and one small, transcriptionally inactive micronucleus, providing an example of two different sized nuclei in one cytosolic volume (reviewed in (156)). The size of both nuclei increase when chimeric proteins of nuclear pore proteins that only localize to one of the nuclei results in mis-localization of those proteins, likely disrupting proper nucleocytoplasmic transport (179). It is possible that the enlarged nuclei in *mut-16(-)* mutants are reflecting improper transport as well, especially given

that these nuclei also show increased mCherry::H2B signal. Perhaps more analogous to the enlarged nuclei in the syncytial germline are examples of differences in nuclear size in *S. pombe* cytokinesis mutants, where larger nuclei are surrounded by larger amounts of cytosol (180). Although the *C. elegans* germline is a syncytium, there are small "pockets" of partially sectioned cytosol surrounding the nuclei (most evident in Figure 3-2B). It is possible that the enlarged nuclei in *mut-16(-)* mutants are also associated with larger subsections of cytoplasm, but further experiments are needed to examine this hypothesis. While the precise causes of the nuclear defects remain to be determined, these *mut-16(-)* mutant germlines provide a prime example for studying control of nuclear size, where wildtype and enlarged nuclei can be compared simultaneously within the same tissue of the same animal.

Table 3-1: Strains used in Chapter 3

Strain name	**Genotype**
N2	wild type
AMJ623	*jfSi1[sun-1p::sun-1::GFP cb-unc-119(+)] II*
AMJ1021	*mut-2(jam322) I; oxSi487 dpy-2(jam29) II; unc-119(ed3)? III; lin-2(jam30) X; rage(-)*
AMJ1023	*mut-16(jam138) I; oxSi487 dpy-2(jam29) II; unc-119(ed3)? III; lin-2(jam30) X; rage(-)*
AMJ1025	*mut-16(jam139) rde-10(jam248) I; oxSi487 dpy-2(jam29) II; unc-119(ed3)? III; lin-2(jam30) X; rage(-)*
AMJ1031	*mut-2(jam325) I; oxSi487 dpy-2(jam29) II; unc-119(ed3)? III; lin-2(jam30) X; rage(-)*
AMJ1032	*oxSi487 dpy-2(jam29) II; unc-119(ed3)? III; jam323[mut-15(-) hrde-2(-) nmr-2(-)] V; lin-2(jam30) X; rage(-)*
AMJ1034	*oxSi487 dpy-2(jam29) II; hrde-1(jam326) unc-119(ed3)? III; lin-2(jam30) X; rage(-)*
AMJ1035	*mut-16(jam140) I; oxSi487 dpy-2(jam29) II; unc-119(ed3)? III; lin-2(jam30) X; rage(-)*
AMJ1036	*oxSi487 dpy-2(jam29) II; mut-7(jam327) unc-119(ed3)? III; lin-2(jam30) X; rage(-)*

AMJ1038	*oxSi487 dpy-2(jam29) II;) hrde-1(jam332) unc-119(ed3)? III; lin-2(jam30) X; rage(-)*
AMJ1042	*mut-16(jam141) I; oxSi487 dpy-2(jam29) II; unc-119(ed3)? III; lin-2(jam30) X; rage(-)*
AMJ1043	*oxSi487 dpy-2(jam29) II; unc-119(ed3)? III; lin-2(jam30) X; rage(-)*
AMJ1091	*mut-16(jam247) I; oxSi487 dpy-2(jam29) II; unc-119(ed3)? III; lin-2(jam30) X rage(-)*
AMJ1094	*oxSi487 dpy-2(jam29) II; mut-7(jam328) unc-119(ed3)? III; lin-2(jam30) X; rage(-)*
AMJ1097	*oxSi487 dpy-2(jam29) II; hrde-1(jam329) unc-119(ed3)? III; lin-2(jam30) X rage(-)*
AMJ1098	*oxSi487 dpy-2(jam29) II; unc-119(ed3)? III; mut-15(jam330) V; lin-2(jam30) X rage(-)*
AMJ1170	*jamSi37 [mex-5p::mCherry::cye-1 3'UTR] II; unc-119(ed3) III*
AMJ1397	*mut-16(jam148) I*
AMJ1415	*jamSi46[unc-119(+) mex-5p::mCherry::mex-5 3'utr] II; hrde-1(+)III*
AMJ1432	*mut-16(jam148) I; jamSi37 [mex-5p::mCherry::cye-1 3'UTR] II; unc-119(ed3)? III*
AMJ1470	*mut-16(jam148) rde-10(jam196) I*
AMJ1489	*rde-10(jam206) I*
AMJ1503	*mut-16(jam148) I; jamSi48[unc-119(+) Pmex-5::mCherry::mex-5 3'utr] II; hrde-1(+) III*
AMJ1611	*mut-16(jam240) rde-10(jam206) I*
AMJ1614	*rde-10(jam243) I*
AMJ1682	*mut-16(jam148) rde-10(jam274) I*
AMJ1683	*mut-16(jam148) rde-10(jam275) I*
AMJ1756	*rde-10(jam206) I; oxSi487 II*
AMJ1780	*mut-16(jam330) I; oxSi487 II*
CF4639	*glh-1(sam140[glh-1::T2A::wrmScarlet(1-10)]) I; fib-1(mu498[wrmScarlet11::fib-1]) V*
EG6787	*oxSi487[mex-5p::mCherry::H2B::tbb-2 3'UTR::gpd-2 operon::GFP::H2B::cye-1 3'UTR + unc-119] II; unc-119(ed3) III*

Table 3-2: Oligonucleotides used (5′ to 3′) in Chapter 3

Primer	**Sequence**
P1	ccggacatctcaggtcttac
P2	ggatttccagttcgtagggc
P3	gaatatttttcgaaaatata
P4	cggcacatgcgaatattttccgaaaatagaaggatattcttcaactcgatccagaaaaac
P5	gctaccataggcaccgcatg

P6	cacttgaacttcaatacggcaagatgagaatgactggaaaccgtaccgcatgcggtgcctatggtagcgg agcttcacatggcttcagaccaacagccta
P7	cacaaacgccaggaaaggaag
P8	catttctgcgttgttgtggacc
P9	ccgatacaatcagaatgatc
P10	agcaaggccaccgatacaatcagaatgatttaggcagacaaggatattatgacaagatatt
P11	ggcattcgagccaataatgc
P12	cgttgtgctcggcaacttct

Chapter 4: General Discussion

4.1 Toward the ideal drug

The perfect drug would be one that required only one dose and induced no off-target affects. The use of dsRNA as a therapeutic provides a very highly specific method for knocking down specific mRNAs (see Chapter 1.3). However, RNAi can cause off-target effects, particularly for genes of high homology (reviewed in (181)), so choosing a target with little homology to other genes is crucial for a therapeutic purpose, although choosing a target with homology to many genes could even be beneficial for a pesticide.

As suggested by our quantitative modeling (Chapter 2, Figures 2-8, 2-9), many factors aside from sequence can affect the efficacy of knockdown, including turnover rates of the target mRNA at steady-state (Figure 2-8G), changes in transcription rate (Figure 2-8F), but not necessarily the abundance of small RNAs (Figure 2-8E) as was previously used as a metric for strong silencing within the field (e.g. in (60)). These considerations, while reasonable *a priori,* are not often explicitly considered, and looking for targets with a low steady-state turnover rate may yield more effective drugs. Additionally, we observe that mRNA levels can recover in response to a pulse of dsRNA despite the presence of amplification mechanisms (Figure 2-13), which is an important consideration for determining dosage of a drug that targets any RNAi system with RNA-dependent RNA polymerases.

Aside from choice of target, one of the biggest challenges facing RNAi-based therapeutics is that of endosomal escape (reviewed in (182)). siRNA therapeutics have only been shown to release up to 0.3% of its cargo outside of the endosome, meaning that over 99% of the drug is ineffective (183). Despite this, inclisiran has been shown to be effective for only one dose per

every six months (184). However, this means the dose that is administered is likely much higher than would be needed if we can solve the issue of endosomal escape, which would likely cut down on the overall cost to produce the drug. Future siRNA therapeutics will improve by both choosing targets that are expected to be easily knocked down and improving the issues involved in endosomal escape.

4.2 Non-infinite amplification of siRNAs

Amplification of secondary siRNAs (2º siRNAs) occurs when an RNA-dependent RNA Polymerase (RdRP) produces antisense RNAs downstream of primary siRNAs. While not found in humans, RdRPs are found in *C. elegans* (98, 185–187)*,* plants (reviewed in (188)), fungi (189), and ciliates (190). While mechanisms of RdRP activity differ between systems, they are often a critical part of RNA interference.

In *C. elegans,* RdRP activity is required for both production of 2º siRNAs, and 3º siRNAs, which can arise in the germline and are the result of 2º siRNA-2º Argonaute recognition of a transcript, and re-initiation of RdRP activity (135, 140). For somatic targets of RNAi, the cleavage of target mRNAs appears to be restricted (Chapter 2, Figure 2-13) which nevertheless would allow for RdRPs to potentially make 2º siRNAs anywhere upstream of the cleavage. As with RNAi of germline targets, the highest abundance of 2º siRNAs accumulate near the trigger, towards the 3′ end of the target (140, 191). Tertiary siRNAs can arise if 2º siRNA-2º Argonaute complexes are capable of initiating cleavage and the addition of poly-UG repeats. Given that RdRP's transcribe in the 5′ to 3′ direction, this means that 3º siRNAs must be antisense to even more upstream sections of the target, and each successive round of cleavage, poly-UG addition, and amplification,

can only occur closer and closer to the 5′ end of the target. Presumably, at some point there would be no template mRNA left to produce more siRNAs, resulting in epigenetic recovery.

Some germline targets of RNA silencing can show inheritance of that silencing in subsequent generations, ranging from a couple to tens of generations (e.g., (120, 133, 192, 193)), but there are rare examples of cases where genes silencing appears to be permanent (133). If we think about a gene that becomes silenced through small RNA-mediated processes seemingly permanently, it is reasonable to assume that 3º siRNAs must be involved.

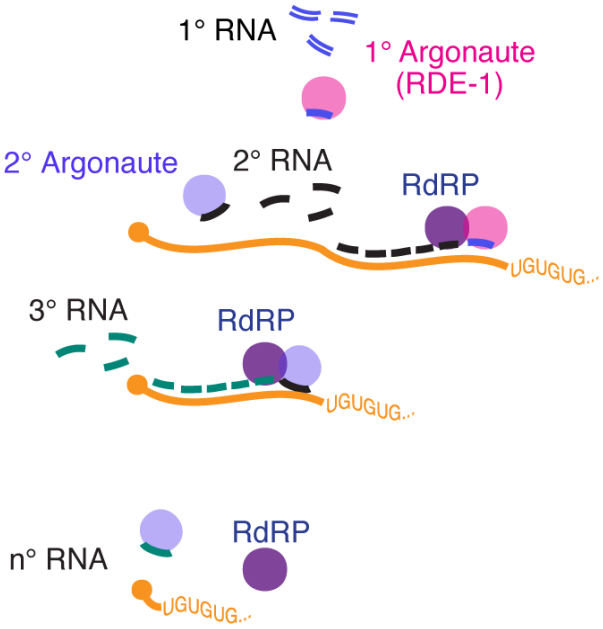


Figure 4-1. Amplification of siRNAs with respect to a target transcript (adapted from Figure 2-13). Target mRNAs (orange) act as a template for amplification by RdRPs (purple). Cleavage of a template is guided by the 1º siRNA-1º Argonaute complex (blue and pink), or by a 2º siRNA-2º Argonaute complex (black and lavender). 3º siRNAs (teal) will be unable to initiate further rounds of amplification if they are too far upstream on the template.

If each new population of siRNAs is produced antisense closer to the 5′ end of the transcript, there could reach a point where the lack of mRNA to act as a template could result in a loss of siRNAs, allowing for recovery. Assuming this is true, a case of seemingly permanent epigenetic silencing (133) would suggest a constant or recurring trigger, in order to have effective silencing in each generation. Therefore, it is important not to associate the production of 3º siRNAs

with permanent silencing, and in cases of permanent epigenetic silencing, it is worth investigating whether there is a constant or reoccurring trigger.

4.3 Is the control of nuclear size an active or a passive process?

A long-standing question among eukaryotes is understanding how nuclear size is controlled. For a given cell type in a given organism, there appears to be a fixed ratio between the nuclear volume and the cytosolic volume, or the karyoplasmic ratio ((153), see also Chapter 3). While many mutants have been observed that can disrupt this ratio, for example mutants that affect nucleocytoplasmic transport (154), the LINC complex, or RNA processing (155), it is unclear whether these processes are actively controlling nuclear size. Nuclear import seems to be highly correlated to nuclear size: disrupting normal import by making chimeric nuclear pore proteins increases the size of nuclei in *Tetrahymena* (179) and reducing nuclear import in pronuclei by removing the nuclear pore protein Ndc1 reduces nuclear size (194). We have observed some instances of enlarged nuclei in *mut-16(-)* mutants that also show an increase of mCherry::H2B (Figures 3-1, 3-2). In trying to understand this relationship of size to histone accumulation, it is impossible to discern whether the there is more histone *because* the nuclei are larger, or if the nuclei are enlarged *because* of the additional histones. Further experiments are needed to parse the cause and effect.

The enlarged nuclei we observed in the germline of animals that lack MUT-16 (Chapter 3) are not the only examples of differences in nuclear size within a syncytium. Cytokinesis mutants in *S. pombe* show differences in nuclear size (180) and mutants of the *gnu* gene in *Drosophila* show some enlarged nuclei within the syncytial blastoderm (195). Some mutants in *C. elegans* can disrupt the size of each nucleus, such as the knockdown of cyclin E homolog *cye-1,* resulting in

enlargement of each nucleus in the distal germline (196). In cases were each nucleus is enlarged, it is once again hard to entangle whether the enlarged nuclei are a by-product of the mutant, or if the mutant gene is normally directly involved in nuclear size control. For the examples where only some nuclei are disrupted, it seems plausible that control of nuclear size is an active process; while some nuclei become enlarged, the disruption is not great enough to inhibit the control of the surrounding nuclei. However, it may be difficult or impossible to distinguish between whether nuclear size is controlled passively by physical processes or whether biological processes must actively restrict nuclear size. Future experiments in the *C. elegans* germline and syncytial tissues in other systems may help shed light on the mechanics involved in controlling nuclear size.

Chapter 5: Future Directions

5.1 Preface

All data generated in this chapter was generated by Daphne Knudsen-Palmer.

5.2 Introduction

While a role for RDE-10 in somatic RNA interference has been further characterized in this work, namely in its contributions to 2º siRNA amplification along with MUT-16 (see Chapter 2 for details), the mechanics of how and if RDE-10 functions in endogenous small RNA-based regulation remains unclear. While other Maelstrom domain containing homologs in mice and *Drosophila* localize to germ granules and have roles in piRNA-based silencing (64, 197), RDE-10 itself has not been tagged and visualized. Additionally, the loss of RDE-10 alone seems to have a modest effect on endogenous RNA expression, if any (Figure 3-5, (102, 103)).

RDE-10 has been shown to associate with RSD-2 (102, 103), which is required for systemic RNAi and in turn associates with Tudor domain-containing protein RSD-6 (198). Vasa homolog and DEAD box helicase RDE-12 can localize to P granules, or to RSD-6-rich foci called R2 bodies (199, 200), so it is possible that RDE-10 localizes to these R2 granules as well. Here we consider the potential roles for RDE-10 in the germline and in regulating endogenous targets.

5.3 Materials and methods

5.3.1 Strains

All strains (listed in Table 5-1) were cultured on Nematode Growth Medium (NGM) plates seeded with 100 µl of OP50 *E. coli* at 20ºC and strains made through mating were generated using standard methods (122).

Table 5-1: Strains used in Chapter 5

Strain name	Genotype
N2	wild type
AMJ1489	*rde-10(jam206) I*
AMJ1614	*rde-10(jam243) I*
AMJ1709	*jam297[bli-1p::gfp::cye-1 3'utr + unc-119(+)] II; unc-119(ed3) III*
AMJ1725	*rde-10(jam206) I; jam297[bli-1p::gfp::cye-1 3'utr + unc-119(+)] II; unc-119(ed3)? III*
AMJ1726	*jam297[bli-1p::gfp::cye-1 3'utr + unc-119(+)] II; unc-119(ed3)? III; nrde-3(jam205) X*
AMJ1727	*mut-16(jam148) I; jam297[bli-1p::gfp::cye-1 3'utr + unc-119(+)] II; unc-119(ed3)? III*
AMJ1728	*mut-16(jam148) rde-10(jam196) I; jam297[bli-1p::gfp::cye-1 3'utr + unc-119(+)] II; unc-119(ed3)? III*
EG6787	*oxSi487 II; unc-119(ed3) III*

5.3.2 Feeding RNAi

Control RNAi by feeding *E. coli* containing the empty dsRNA-expression vector (L4440), which can generate a short dsRNA derived from the multiple cloning site but does not produce dsRNA against any *C. elegans* gene, was done in parallel with all RNAi assays.

P0 and F1 feeding: Bacteria expressing dsRNA was cultured in LB media with 100 µg/µl carbenicillin overnight at 37ºC at 250 rpm. 100 µL of cultured bacteria was then seeded onto RNAi plates [NG agar plate supplemented with 1 mM isopropyl β-D-1-thiogalactopyranoside (IPTG) (Omega) and 25 µg/ml carbenicillin (MP Biochemicals)]. Adult animals were passaged onto seeded RNAi plates and removed after 24hr. Progeny were scored for silencing by bacteria expressing dsRNA targeting *gfp* (defect evident as lack of detectable GFP expression).

F1 only feeding: Gravid adults were placed on RNAi plates that were seeded with 100 µL of bacteria expressing dsRNA (prepped as above), and bleached. Embryos from these bleached adults were scored once animals reached adulthood.

5.3.3 Microscopy

Adult (Figures 5-1A, 5-1B) or L4 (Figure 5-1C) animals were mounted in 10 µl of 3 mM levamisole on a 2% agar pad and imaged under a coverslip using a Nikon AZ100 microscope and Prime BSI Express sCMOS camera (Figures 5-1A, 5-1B) or Photometrics Cool SNAP HQ^2 camera (Figure 5-1C). A C-HGFI Intensilight Hg Illuminator was used to excite GFP (filter cube: 450 to 490 nm excitation, 495 dichroic, and 500 to 550 nm emission) or mCherry (filter cube: 530–560 nm excitation, 570 dichroic, and 590–650 nm emission).

5.4 Results

To ask whether RDE-10 is required for silencing of a germline target, dsRNA targeting *gfp* was fed to animals with a dual promoter transgene (*bli-1p::mex-5p::gfp*). This strain (used also in Figures 2-10, 2-12 to examine hypodermal silencing) expresses GFP both in the hypodermis and in the germline, and here we wanted to look at the requirements for silencing in the germline only. Following a P0 and F1 feed, RDE-10 and NRDE-3 did not appear to be required for silencing, whereas MUT-16 was strictly required (Figure 5-1A). While not many germline RNAi targets have been tested in *rde-10(-)* mutants, RDE-10 does appear to be required to silence *pos-1* (102, 103). In contrast to the P0 and F1 feed, RDE-10 appears to be required for silencing *gfp* when only the F1 generation is exposed to *gfp* dsRNA (Figure 5-1B). Given the association of RDE-10 with

RNAi Spreading Defective proteins RSD-2 and indirectly RSD-6, it is possible that RDE-10 plays a role in "spreading" ingested dsRNA from the soma to the germline.

We have previously shown that some components of RNAi machinery, including MUT-16, MUT-2/RDE-3, and HRDE-1 were required to maintain long-term silencing (133). To ask whether RDE-10 is required to maintain this same long-term silencing, animals with a silenced transgene (*T*) and a Dpy marker were crossed to two *rde-10(-)* mutants, *rde-10(jam206)* which is predicted to cause a missense mutation (see Figure 2-2C), or *rde-10(jam243)* which is predicted to encode a premature stop codon. We found that both alleles of *rde-10* did not result in a reactivation of the transgene, suggesting that the loss of RDE-10 is not sufficient to disrupt long-term silencing.

Given the potential for RDE-10 to be involved in "spreading" RNAi due to its close associations with RSD-2 and RSD-6 (102, 103, 198), it is possible that RDE-10 is required to initiate long-term silencing (mating-induced silencing, as in (133)). Future experiments are needed to test this hypothesis.

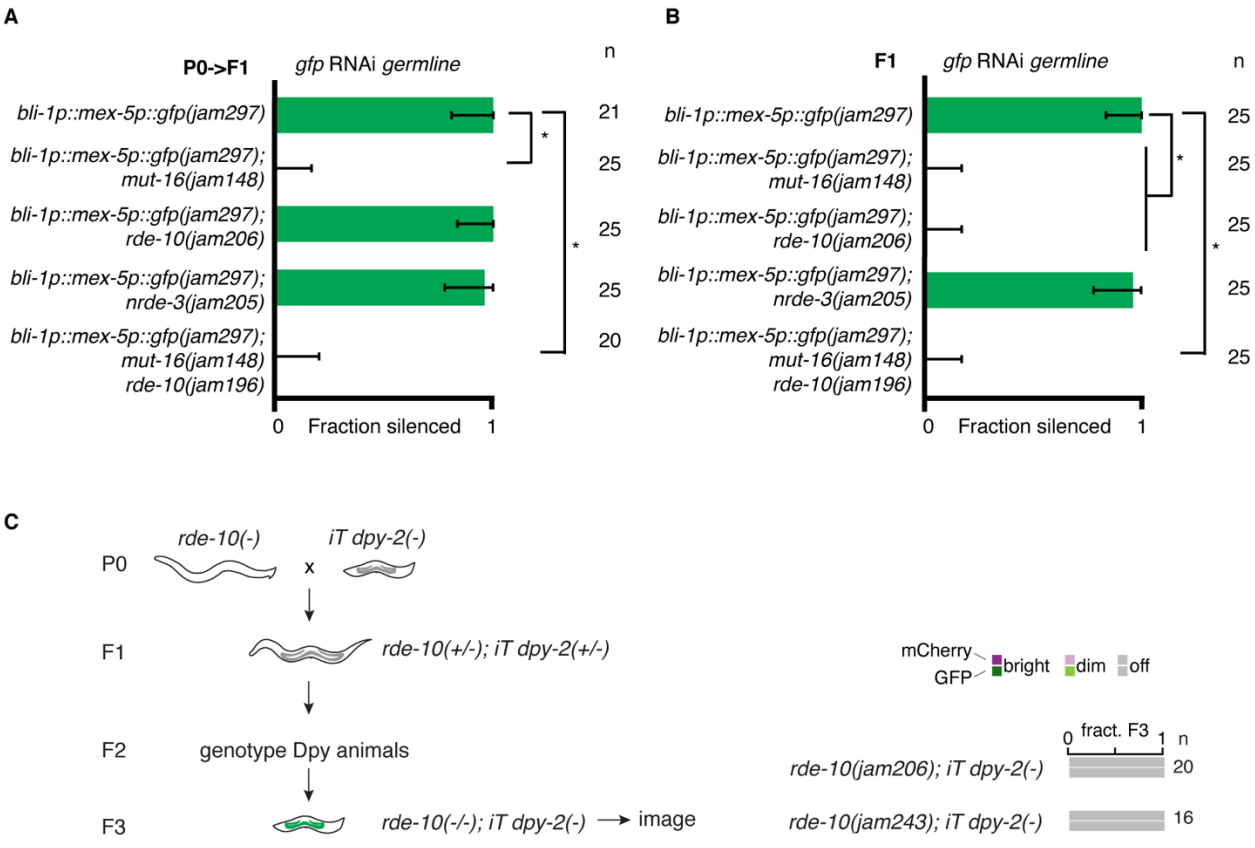


Figure 5-1. Exploring roles for RDE-10 in the germline. (A) P0 and F1 RNAi feed. *rde-10(jam206)* and *nrde-3(jam205)* mutants are comparable to wild type levels of silencing, but *mut-16(jam148)* or *mut-16(jam148) rde-10(jam196)* mutants were completely deficient for silencing *gfp* in the germline. For each mutant, the fraction of animals that showed *gfp* silencing (fraction silenced) and the numbers of animals scored (n) are shown. Asterisks indicate $p < 0.05$ for each comparison (brackets) using Wilson′s estimates with continuity correction and error bars represent 95% confidence interval. (B) F1 only RNAi feed. *nrde-3(jam205)* mutants are comparable to wild type levels of silencing, but *mut-16(jam148), rde-10(jam206),* or *mut-16(jam148) rde-10(jam196)* mutants were completely deficient for silencing *gfp* in the germline. Fractions silenced, numbers scored, comparisons, asterisks, and error bars are as in (A). (C) (*left*) Schematic to test for re-activation of long-term silencing. Males that lack RDE-10 (*rde-10(jam206)* with a predicted amino acid change of Ser228Phe, or *rde-10(jam243)* with a premature stop codon) were mated with hermaphrodites containing a transgene that was silencing via mating-induced silencing with a *dpy-2(-)* mutation as a marker. Heterozygous (non-Dpy) cross progeny were isolated, then F2 progeny were isolated and allowed to lay progeny. F3 progeny from parents that were Dpy (homozygous for the transgene) and homozygous for either *rde-10(jam206)* or *rde-10(jam243)* were imaged. (*right*) Loss of RDE-10 is not sufficient to re-activate long-term silencing of a transgene; 100% of animals show no detectable expression from the transgene.

We have previously discussed the similarity of RDE-10 to other Maelstrom domain-containing proteins (see Chapter 2). In *Drosophila,* Maelstrom has been shown to exhibit ssRNA endonuclease activity (143) and can also inhibit canonical transcription (93). RDE-10 has been shown to form a complex with RDE-11, where *rde-10(-)* mutants appear to have the same deficiencies in RNA silencing as *rde-11(-)* mutants (102, 103). We wondered whether RDE-11 could be playing a similar role to the transcriptional repressive roles of *Drosophila* Maelstrom. We aligned the crystal structure of the MAEL domain from *Drosophila* (PDB: 4YGB) to the predicted structure of the MAEL domain of RDE-10 (UniProt: Q9N3S2) (Figure 5-2A). These structures overlap with a TM score of 0.63, suggesting these structures are the same shape (130). The MAEL domain accounts for about half of the *Drosophila* protein, the other half with a predicted HMG domain (UniProt: L0CQ14). The predicted structure of RDE-11 (UniProt: Q6BET5), while uncharacterized, could potentially have two domains (Figure 5-2B). We used Foldseek to search for structural homology to either half of the protein (201). Among the search results for the high confidence N terminal half of RDE-11 were proteins with predicted kinases domains in *Glycine max* (soybeans, UniProt: K7N228, I1KL68, A0A0R0G6N2, A0A0R0IPF3), L-type lectin-like proteins in *Onchocerca volvulus* (filarial nematode, UniProt: A0A044SFJ3), *Strongyloides stercoralis* (parasitic roundworm, UniProt: A0A0K0E1Q0) and many other species, and vesicular membrane proteins in mice (UniProt: Q9DBH5) and humans (UniProt: Q12907). Among the search results for the low confidence C terminal half of RDE-11 were RING-type E3 ubiquitin proteins in *Danio rerio* (UniProt: F1Q4N1), *Glycine max* (UniProt: I1MXG4) and *Arabidopsis thaliana* (UniProt: Q0WQX9), and Roquin-1 in mice (UniProt: Q4VGL6) and humans (UniProt: Q5TC82), a post-transcriptional repressor of mRNAs. Given that the predicted structure of RDE-11 seems likely to have a function other than DNA-binding, it seems unlikely that RDE-11 could

be suppressing transcription as the *Drosophila* Maelstrom protein does. Future experiments are required to elucidate the biochemical roles of both RDE-10 and RDE-11.

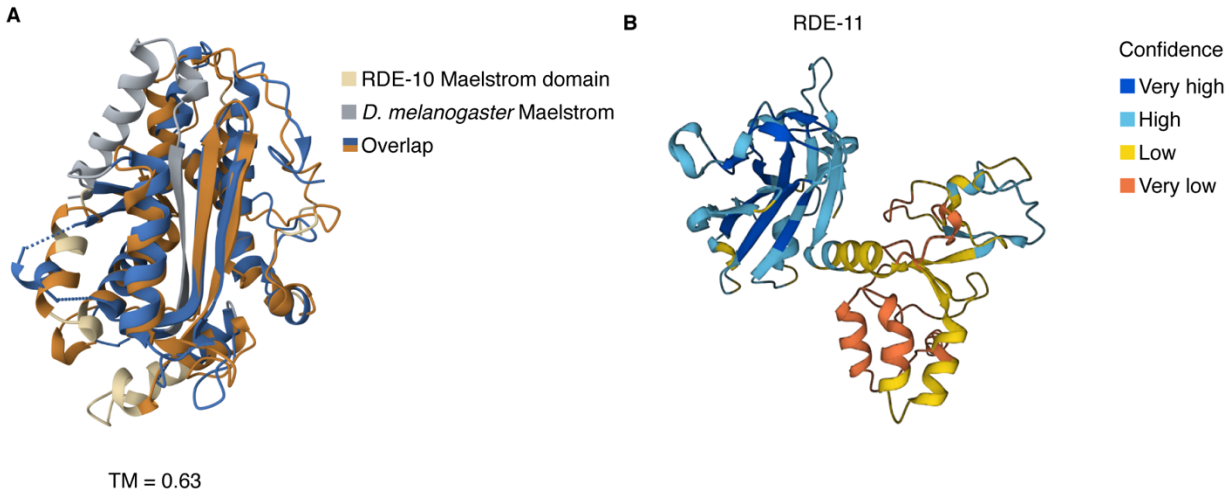


Figure 5-2. Structural speculations for RDE-10 and RDE-11. (A) Structural alignment of the predicted Maelstrom domain of RDE-10 with the crystal structure of the MAEL domain from the *Drosophila* Maelstrom protein (PDB: 4YGB), done using the Pairwise Structure Alignment from Protein Data Bank with rigid parameters (RMSD Cutoff 3; AFP Distance Cutoff: 1600; Fragment length: 8). Template modeling score (TM=0.63) and regions of high similarity (blue and orange) are shown. (B) Predicted structure of RDE-11 from AlphaFold (UniProt: Q6BET5) colored by confidence of the structure: very high (dark blue, pLDDT > 90), high (light blue, 90 > pLDDT > 70), low (yellow, 70 > pLDDT > 50), and very low (orange, pLDDT < 50).

5.5 Discussion

While it is clear that RDE-10 and RDE-11 are required for proper RNA silencing in response to imported dsRNA, the precise roles of these proteins remain unclear. Nuage components in *Drosophila* aside from Maelstrom (64) include Vasa, a DEAD-box helicase (202, 203), Aubergine, an Argonaute (68, 204), and SPN-E, another helicase (205). While homologs for these proteins exist in *C. elegans* (RDE-12 is a DEAD-box helicase (199, 200), RDE-1 is a primary Argonaute(88)), there is not an obvious candidate for a Nuage component that is similar to RDE-11. The RDE-10 homolog Maelstrom does localize to Nuage (64), and the mouse homolog MAEL

localizes to germ granules (67), however, the subcellular localization of RDE-10 has not been explicitly shown. Given the localization in germ granules homologs and the indirect association with RDE-12 through RSD-2 and RSD-6 (102, 103), it seems plausible that RDE-10 may localize to P granules and cytoplasmic R2 bodies, which are distinct from P bodies (199, 200). Taken together, it appears RDE-10 could be playing roles in RNA-based silencing in the germline along with RDE-11, and the details behind the mechanism of action for these two proteins remains to be investigated.

Appendix A: Exploration of an *hrde-1(-) missense mutant.*

A.1 Preface

All data in this appendix was generated by Daphne Knudsen-Palmer. The genetic screen was performed by lab alumni Pravrutha Raman and Farida Ettefa as previously described (Chapter 2). The strain AMJ975 was made by lab alumna Snusha Ravikumar and some primers were designed by lab member Mary Chey.

A.2 Introduction

One of the mutants identified in the genetic screen (as described in Chapter 2) showed a resistance to silence *bli-1* in response to feeding RNAi, but appeared to silence *gfp* and *unc-22* similarly to wild type levels (data not shown). When doing complementation tests with the mutants from this screen, one mutant appeared to be dominant-negative for *bli-1* silencing (data by Mary Chey, not shown). After whole genome sequencing (as described in Chapter 2.3.4), this mutant strain (AMJ1097) was predicted to have a mutation in *hrde-1* that results in a glycine 259 to aspartic acid change. This mutation (which will be referred to as G259D) was confirmed via Sanger sequencing. Through the investigation in this appendix, it seems there was a mix up of the mutant strain names, so AMJ1097 is not likely the strain that was found to be dominant-negative. Nevertheless this appendix highlights some structural aspects of Argonautes that may be relevant across species.

Argonautes are small RNA-binding proteins that can be found in a number of organisms. Argonautes are characterized by three main domains (PAZ, MID, PIWI), which are connected by two linkers (reviewed in (206)). The PIWI domain shares homology to RNase H domains, and the

MID and PAZ domains are responsible for binding the 5′ and 3′ ends of small RNAs, respectively. Mutations that alter the shape of the Argonaute have the potential to affect the binding affinity to small RNAs and thus may reduce downstream efficacy of RNA silencing.

To test whether this particular mutation in HRDE-1 could result in a mutant that is dominant-negative for *bli-1* silencing, a new HRDE-1(G259D) mutant was created (AMJ1582) and tested the capabilities of the mutant in silencing *bli-1*.

A.3 Materials and Methods

A.3.1 Strains and oligonucleotides used

All strains were cultured on Nematode Growth Medium (NGM) plates seeded with 100µl OP50 at 20°C (122). All strains used are listed in Table A-1 and all oligonucleotides used are listed in Table A-2. Heterozygous mutant worm strains were made by standard genetic crosses.

Table A-1. Strains used in Appendix A.

Strain Name	Genotype
N2	wild type
AMJ975	*sur-5(jam79[sur-5::gfp]) X*
AMJ1097	*oxSi487 dpy-2(jam29) II; hrde-1(jam329) unc-119(ed3)? III; lin-2(jam30) X rage(-)*
AMJ1397	*mut-16(jam148) I*
AMJ1564	*hrde-1(jam224) III*
AMJ1582	*hrde-1(jam235) III*

Table A-2. Oligonucleotides used (5′ to3′) in Appendix A.

Oligo	Sequence
P1	GAAUAUUUUUCGAAAAUAUAGUUUUAGAGCUAUGCU
P2	CGGCACATGCGAATATTTTCCGAAAATAGAAGGATATTCTTC AACTCGATCCAGAAAAAC

P3	gctaccataggcaccgcatg
P4	cacttgaacttcaatacggcaagatgagaatgactggaaaccgtaccgcatgcggtgcctatggtagc ggagcttcacatggcttcagaccaacagccta
P5	CACAAACGCCAGGAAAGGAAG
P6	CATTTCTGCGTTGTTGTGGACC
P7	AATGAGGATTACTTACAATT
P8	AAAGCTCAACAATGAGGATTACTTATAATTTGGTAATGCCAC ATTCCCACGTCTTTCTCC
P9	GTGTCGAAGTTGTCTCGCAG
P10	ACGGTATCCACCACGAGAG
P11	GCTATTTCGGAGATCCGCTC
P12	GGAACCTGATGCTATTTCGGAGATCCGCTCCGATTTTGCGAA AGTATCTCGTCTATCGCA

A.3.2 P0 and F1 feeding RNAi

Bacteria expressing dsRNA was cultured in LB media with 100 µg/µL carbenicillin overnight at 37ºC at 250 rpm. 100 µL of cultured bacteria was then seeded onto RNAi plates. Adult animals were passaged onto seeded RNAi plates and removed after 24hr; progeny were scored for silencing by bacteria expressing dsRNA targeting *bli-1* (blisters) or expressing L4440 as an empty vector control.

A.3.3 Making heterozygous mutants for feeding RNAi.

L4 AMJ975 males (*sur-5::gfp*) were placed on a plate with hermaphrodites (of either N2, AMJ1564, or AMJ1582, at a male:hermaphrodite ratio of 9:3) on plates seeded with 10 µL of OP50 and allowed to mate for 24 hr after which all worms were transferred to RNAi plates seeded with *bli-1* RNAi. Once progeny reached adulthood, they were placed in 15 µL of 3mM levamisole on a 2% agar pad and imaged; animals showing *gfp* expression were scored as heterozygous cross-progeny. Imaging was done using a Nikon AZ100 microscope and Photometrics Cool SNAP HQ[2]

camera. A C-HGFI Intensilight Hg Illuminator was used to excite GFP (filter cube: 450 to 490 nm excitation, 495 dichroic, and 500 to 550 nm emission).

A.3.4 CRISPR Cas9-based genome editing

Genome editing was performed by injecting nuclear-localized Cas9 (PNA Bio) preincubated at 37°C for 10 min with a hybridized crRNA/tracrRNA (preincubated at 95°C for 1 min, Integrated DNA Technologies), as well as an oligonucleotide or PCR-amplified homology repair template, into the *C. elegans* distal gonad. Animals were injected 24hr post-L4 stage. Screening for plates with successfully edited F1 animals was performed using either dpy-10 co-CRISPR (123, 124) or the pRF4 plasmid used as a co-injection marker (125).

To make a premature stop codon in *mut-16:* A *mut-16*-targeted crRNA **P1,** tracrRNA, Cas9, a *mut-16(-)* homology repair template **P2**, *dpy-10* crRNA **P3** and *dpy-10(-)* homology repair template **P4** were injected into N2 animals. F1 animals showing the "roller" phenotype (indicative of heterozygous *dpy-10(-/+)*) were isolated and allowed to lay progeny. F2 animals that were non-dumpy and non-rollers were genotyped for *mut-16(-)* using duplex PCR with primers **P5** and **P6** and restriction digestion with enzyme BstBI (New England BioLabs). Once animals appearing homozygous for the mutation via PCR/restriction digest were isolated, the nonsense mutation was verified by Sanger sequencing.

To make a premature stop codon (Q234*) in *hrde-1:* A *hrde-1*-targeted crRNA **P7,** tracrRNA, Cas9, a *hrde-1(null)* homology repair template **P8**, and the pRF4 plasmid were injected into N2 animals. F1 animals showing the "roller" phenotype (indicative of successful injection) were isolated and allowed to lay progeny. Animals were genotyped for *hrde-1(null)* using duplex PCR with primers **P9** and **P10** and restriction digestion with enzyme PsiI-v2 (New England

BioLabs). Once animals appearing homozygous for the mutation via PCR/restriction digest were isolated, a strain with a several premature stop codons was designated as AMJ1564.

To make a missense mutation (G259D) in *hrde-1:* A *hrde-1*-targeted crRNA **P11,** tracrRNA, Cas9, a *hrde-1(mis)* homology repair template **P12**, and the pRF4 plasmid were injected into N2 animals. F1 animals showing the "roller" phenotype (indicative of successful injection) were isolated and allowed to lay progeny. Animals were genotyped for the missense mutation (G259D) and verified via Sanger sequencing and designated as AMJ1582.

A.3.5 Sequence Alignments

The protein sequence for each *C. elegans* protein was obtained from WormBase; all other sequences were obtained from UniProt. The alignment was created using EMBL-EBI Clustal Omega.

A.3.6 Protein domain identification and Pymol

Pymol (v. 2.4.1) was used to modify PDB files. The HRDE-1 (UniProt: Q09249) PDB file is based on predictions from AlphaFold. Ago2 (UniProt: Q9UKV8) was modified from the crystal structure determined by (207) (PDB: 4W5O). Protein domains were colored based on homology to domains as found in the EMBL-EBI Pfam database (MID: PF16487, Argonaute Linker 1: PF08699, Argonaute Linker 2: PF16488, PIWI: PF02171, PAZ: PF02170).

A.4 Results

A.4.1 Sequence alignment of protein-coding Argonautes suggests that a glycine in the L1 domain is highly conserved. We first asked whether the predicted amino acid change in the

hrde-1(-) mutant (glycine at position 259, switched to an aspartic acid) could be in a region that is highly conserved among Argonautes and whether this mutation could disrupt small RNA binding. A protein sequence alignment revealed that a glycine at this position in the Linker 1 (L1) domain is strongly conserved among all 20 of the *C. elegans* protein-coding Argonautes, the four *H. sapiens* Argonautes, *D. melanogaster* Argonautes PIWI, Aubergine, and Ago2, *D. rerio* AGO2, and *A. thaliana* AGO2 (*red,* Figure A-1). While not as highly conserved as the glycine, we also noted a relatively well-conserved phenylalanine also in the L1 domain (*blue,* Figure A-1), suggesting that these sites could be important for the overall function of the Argonaute.

The predicted structure of HRDE-1 (AlphaFold: Q09249) suggests that mutations of the G259 amino acid may cause steric hinderance with other parts of the linker domain (Figure A-2A, G259 *red,* F240 *blue*). Two possible orientations of aspartic acid are shown to mimic what was found in the strain from the screen. Each orientation appears to clash with the F240 residue on another beta sheet.

While Argonautes in *C. elegans* have not yet been crystallized, a crystal structure of the human Ago2 with parts of both small RNA and mRNA has been achieved (PDB: 4W5O, (207)).

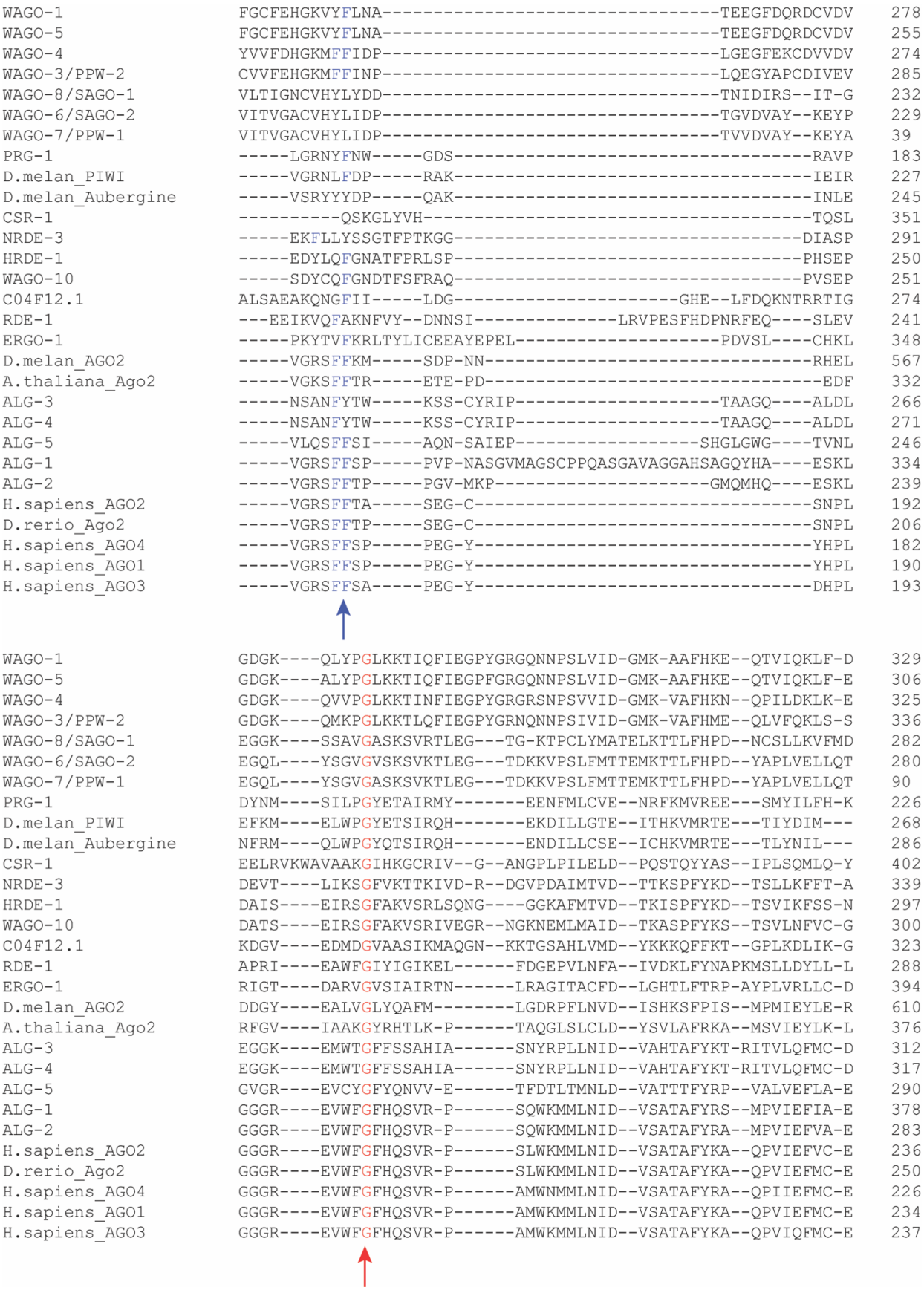

WAGO-1 FGCFEHGKVYFLNA----------TEEGFDQRDCVDV 278
WAGO-5 FGCFEHGKVYFLNA----------TEEGFDQRDCVDV 255
WAGO-4 YVVFDHGKMFFIDP----------LGEGFEKCDVVDV 274
WAGO-3/PPW-2 CVVFEHGKMFFINP----------LQEGYAPCDIVEV 285
WAGO-8/SAGO-1 VLTIGNCVHYLYDD----------TNIDIRS--IT-G 232
WAGO-6/SAGO-2 VITVGACVHYLIDP----------TGVDVAY--KEYP 229
WAGO-7/PPW-1 VITVGACVHYLIDP----------TVVDVAY--KEYA 39
PRG-1 -----LGRNYFNW-----GDS----------RAVP 183
D.melan_PIWI -----VGRNLFDP-----RAK----------IEIR 227
D.melan_Aubergine -----VSRYYYDP-----QAK----------INLE 245
CSR-1 ----------QSKGLYVH----------TQSL 351
NRDE-3 -----EKFLLYSSGTFPTKGG----------DIASP 291
HRDE-1 -----EDYLQFGNATFPRLSP----------PHSEP 250
WAGO-10 -----SDYCQFGNDTFSFRAQ----------PVSEP 251
C04F12.1 ALSAEAKQNGFII-----LDG----------GHE--LFDQKNTRRTIG 274
RDE-1 ---EEIKVQFAKNFVY--DNNSI----------LRVPESFHDPNRFEQ----SLEV 241
ERGO-1 -----PKYTVFKRLTYLICEEAYEPEL----------PDVSL----CHKL 348
D.melan_AGO2 -----VGRSFFKM-----SDP-NN----------RHEL 567
A.thaliana_Ago2 -----VGKSFFTR-----ETE-PD----------EDF 332
ALG-3 -----NSANFYTW-----KSS-CYRIP----------TAAGQ----ALDL 266
ALG-4 -----NSANFYTW-----KSS-CYRIP----------TAAGQ----ALDL 271
ALG-5 -----VLQSFFSI-----AQN-SAIEP----------SHGLGWG----TVNL 246
ALG-1 -----VGRSFFSP-----PVP-NASGVMAGSCPPQASGAVAGGAHSAGQYHA----ESKL 334
ALG-2 -----VGRSFFTP-----PGV-MKP----------GMQMHQ----ESKL 239
H.sapiens_AGO2 -----VGRSFFTA-----SEG-C----------SNPL 192
D.rerio_Ago2 -----VGRSFFTP-----SEG-C----------SNPL 206
H.sapiens_AGO4 -----VGRSFFSP-----PEG-Y----------YHPL 182
H.sapiens_AGO1 -----VGRSFFSP-----PEG-Y----------YHPL 190
H.sapiens_AGO3 -----VGRSFFSA-----PEG-Y----------DHPL 193
WAGO-1 GDGK----QLYPGLKKTIQFIEGPYGRGQNNPSLVID-GMK-AAFHKE--QTVIQKLF-D 329
WAGO-5 GDGK----ALYPGLKKTIQFIEGPFGRGQNNPSLVID-GMK-AAFHKE--QTVIQKLF-E 306
WAGO-4 GDGK----QVVPGLKKTINFIEGPYGRGRSNPSVVID-GMK-VAFHKN--QPILDKLK-E 325
WAGO-3/PPW-2 GDGK----QMKPGLKKTLQFIEGPYGRNQNNPSIVID-GMK-VAFHME--QLVFQKLS-S 336
WAGO-8/SAGO-1 EGGK----SSAVGASKSVRTLEG---TG-KTPCLYMATELKTTLFHPD--NCSLLKVFMD 282
WAGO-6/SAGO-2 EGQL----YSGVGVSKSVKTLEG---TDKKVPSLFMTTEMKTTLFHPD--YAPLVELLQT 280
WAGO-7/PPW-1 EGQL----YSGVGASKSVKTLEG---TDKKVPSLFMTTEMKTTLFHPD--YAPLVELLQT 90
PRG-1 DYNM----SILPGYETAIRMY-------EENFMLCVE--NRFKMVREE---SMYILFH-K 226
D.melan_PIWI EFKM----ELWPGYETSIRQH-------EKDILLGTE--ITHKVMRTE---TIYDIM--- 268
D.melan_Aubergine NFRM----QLWPGYQTSIRQH-------ENDILLCSE--ICHKVMRTE---TLYNIL--- 286
CSR-1 EELRVKWAVAAKGIHKGCRIV--G--ANGPLPILELD--PQSTQYYAS--IPLSQMLQ-Y 402
NRDE-3 DEVT----LIKSGFVKTTKIVD-R--DGVPDAIMTVD--TTKSPFYKD--TSLLKFFT-A 339
HRDE-1 DAIS----EIRSGFAKVSRLSQNG----GGKAFMTVD--TKISPFYKD--TSVIKFSS-N 297
WAGO-10 DATS----EIRSGFAKVSRIVEGR--NGKNEMLMAID--TKASPFYKS--TSVLNFVC-G 300
C04F12.1 KDGV----EDMDGVAASIKMAQGN--KKTGSAHLVMD--YKKKQFFKT--GPLKDLIK-G 323
RDE-1 APRI----EAWFGIYIGIKEL------FDGEPVLNFA--IVDKLFYNAPKMSLLDYLL-L 288
ERGO-1 RIGT----DARVGVSIAIRTN------LRAGITACFD--LGHTLFTRP-AYPLVRLLC-D 394
D.melan_AGO2 DDGY----EALVGLYQAFM--------LGDRPFLNVD--ISHKSFPIS--MPMIEYLE-R 610
A.thaliana_Ago2 RFGV----IAAKGYRHTLK-P------TAQGLSLCLD--YSVLAFRKA--MSVIEYLK-L 376
ALG-3 EGGK----EMWTGFFSSAHIA------SNYRPLLNID--VAHTAFYKT-RITVLQFMC-D 312
ALG-4 EGGK----EMWTGFFSSAHIA------SNYRPLLNID--VAHTAFYKT-RITVLQFMC-D 317
ALG-5 GVGR----EVCYGFYQNVV-E------TFDTLTMNLD--VATTTFYRP--VALVEFLA-E 290
ALG-1 GGGR----EVWFGFHQSVR-P------SQWKMMLNID--VSATAFYRS--MPVIEFIA-E 378
ALG-2 GGGR----EVWFGFHQSVR-P------SQWKMMLNID--VSATAFYRA--MPVIEFVA-E 283
H.sapiens_AGO2 GGGR----EVWFGFHQSVR-P------SLWKMMLNID--VSATAFYKA--QPVIEFVC-E 236
D.rerio_Ago2 GGGR----EVWFGFHQSVR-P------SLWKMMLNID--VSATAFYKA--QPVIEFMC-E 250
H.sapiens_AGO4 GGGR----EVWFGFHQSVR-P------AMWNMMLNID--VSATAFYRA--QPIIEFMC-E 226
H.sapiens_AGO1 GGGR----EVWFGFHQSVR-P------AMWKMMLNID--VSATAFYKA--QPVIEFMC-E 234
H.sapiens_AGO3 GGGR----EVWFGFHQSVR-P------AMWKMMLNID--VSATAFYKA--QPVIQFMC-E 237

Figure A-1. Protein-coding Argonautes share a conserved glycine within the Linker 1 domain. Amino acid sequences of protein-coding Argonautes in various species were aligned and a portion of the L1 domain for each protein is shown. *D. melan, A. thaliana, D. rerio,* and *H. sapiens* represent *Drosophila melanogaster, Arabidopsis thaliana, Danio rerio,* and *Homo sapiens,* respectively. Protein names without species designations are from *Caenorhabditis elegans.* The conserved glycine residue is highlighted in the bottom (red) and the phenylalanine residue that is likely close to the conserved residue in the folded protein is highlighted in the top (blue). The number of the right-most amino acid is noted at the end of each row.

Given this structure, we wondered whether a mutation in the homologous glycine could potentially disrupt the Argonaute′s ability to bind either type of RNA (Figure A-2B). While the G201D mutation looks like it could sterically hinder a phenylalanine within the L1 domain (F182), it does not appear that this residue nor any missense mutation in the L1 domain could drastically affect small RNA or mRNA binding by the Argonaute. However, the likely hinderance in the L1 domain may be sufficient to disrupt function of the Argonaute.

A.4.2 Mutation within a conserved residue does not disrupt *bli-1* silencing capability.

To ask whether the missense mutation found in the strain from the *rage* screen was resulting in an RNAi defect, the mutant was recreated in a wild type background using CRISPR-Cas9 (*hrde-1(jam235)*). For comparison, we also generated a null mutant to ask whether a null mutant of the germline Argonaute would result in somatic RNAi defects (*hrde-1(jam224)*). In response to dsRNA targeting *bli-1,* we found that both the *hrde-1(jam235)* and *hrde-1(jam224)* mutants showed silencing comparable to wild type levels (Figure A-3). Since the complementation tests suggested that the unknown mutant could be acting in a dominant-negative manner, we tested heterozygous animals by crossing in a wildtype copy of HRDE-1 in a strain with a GFP marker (*sur-5::gfp*) to identify cross-progeny. We found that heterozygous *hrde-1(jam235/+)* or *hrde-1(jam224l/+)* also did not show any differences in *bli-1* silencing compared to wild type animals.

Animals that lack MUT-16 (*mut-16(jam148)*) in contrast showed no animals that blistered. Taken together, these data suggest that HRDE-1 does not play a role in the silencing of *bli-1*.

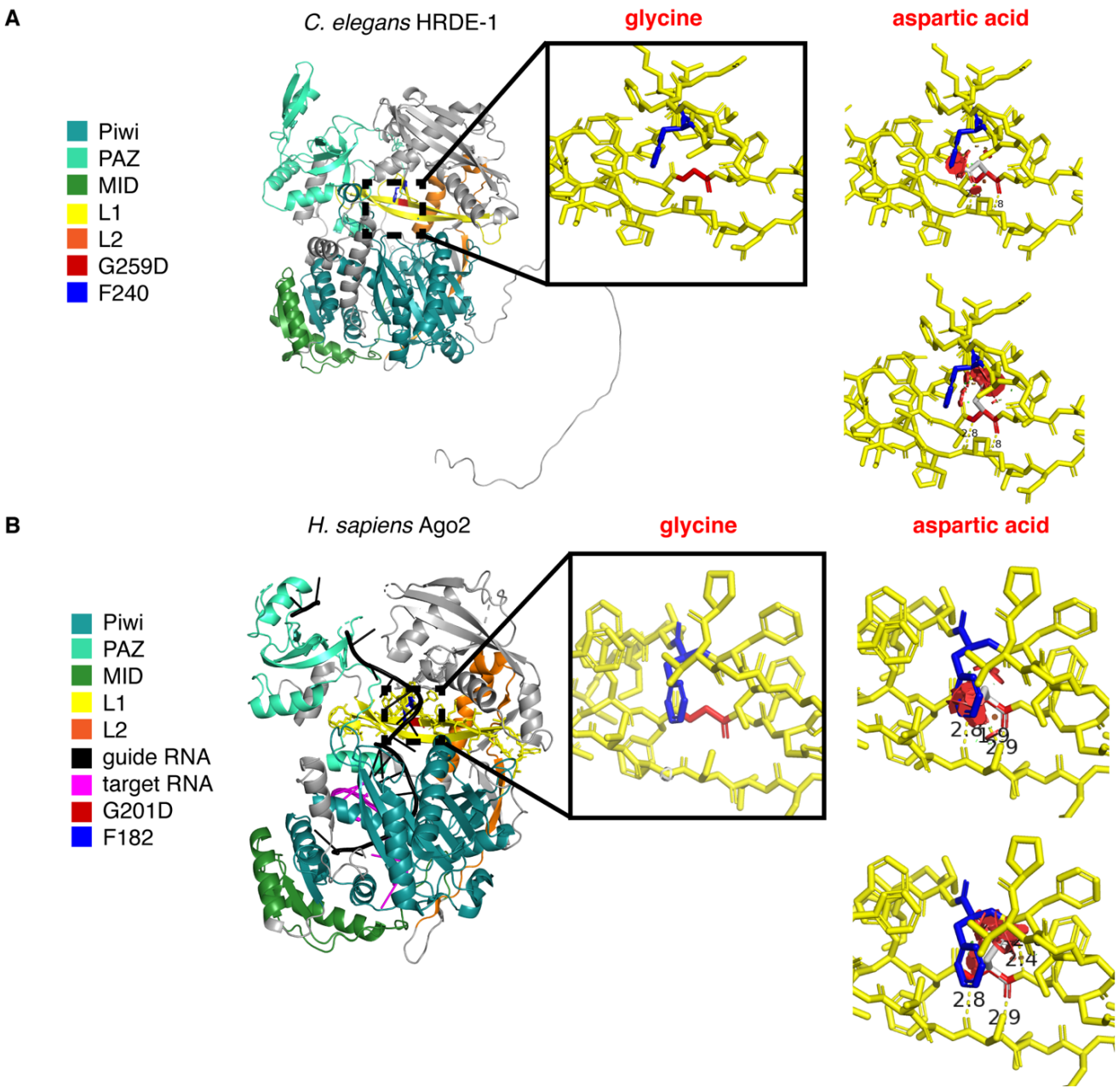


Figure A-2. Disruption of the conserved glycine has the potential to disrupt folding of the L1 domain. (**A-B**) Structures of Argonautes with conserved domains highlighted: Piwi (dark teal), PAZ (light teal), MID (green), L1 (yellow), L2 (orange). (**A**) Predicted structure of HRDE-1. The zoomed and simplified image highlights the wild type glycine (G259, red) and a nearby phenylalanine (F240, blue). The right images show two possible orientations of aspartic acid in

place of the conserved glycine (red). (**B**) Same as in **A** except shown in the crystal structure of *Homo sapiens* AGO2 (G201, red; F182, blue). A few nucleotides of a guide siRNA (black) and the target mRNA (magenta) are shown.

We wondered whether the strain designated as AMJ1097 was in fact the strain with the predicted HRDE-1(G259D) mutation, so we sent a portion of the *hrde-1* gene for Sanger sequencing. we confirmed that the strain AMJ1097 does have the expected missense mutation in *hrde-1* (Figure A-4) but does not have a defect in silencing *bli-1* (data not shown). We conclude that AMJ1097 and newly created missense mutants are not defective for *bli-1* silencing, and the strain that appears to be dominant-negative for silencing *bli-1* must be a different *rage* mutant.

A.5 Discussion

Despite not identifying a mutant that is deficient in RNAi, we have bioinformatically identified a residue that is conserved across Argonautes of many species.

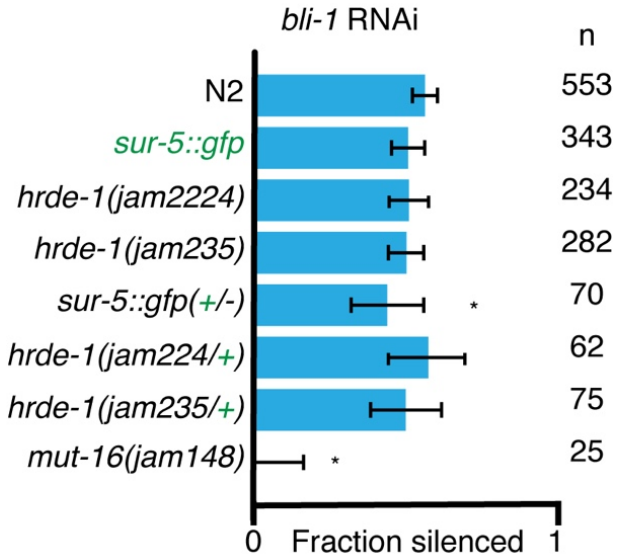


Figure A-3. Animals lacking HRDE-1 do not show a defect in *bli-1* silencing. Fraction of animals that showed observable silencing in response to *bli-1* RNAi. Asterisks indicate $p < 0.05$ when compared to the wild type N2 using Wilson′s estimates with continuity correction and error bars represent 95% confidence interval.

The most likely explanation for these results is that the *rage* mutant that was shown to be dominant-negative for *bli-1* silencing must be a strain other than AMJ1097, and one that likely contains a mutation in a gene other than HRDE-1. While it is enticing that a dominant-negative Argonaute mutant could exist, given the abundance of Argonaute paralogs in *C. elegans* (105), it is more likely that this mutant is one of the other mutants of RNAi machinery, perhaps the *mut-7(jam328),* which is predicted to encode a missense mutation (Glu437Gly). A systematic test for *bli-1* silencing capability would help identify this mutant, although each of the *mut-16(-)* mutants (AMJ1023, AMJ1025, AMJ1035, AMJ1042, AMJ1091) have already been retested (Figure 2-1B) and indeed were resistant to *bli-1* silencing.

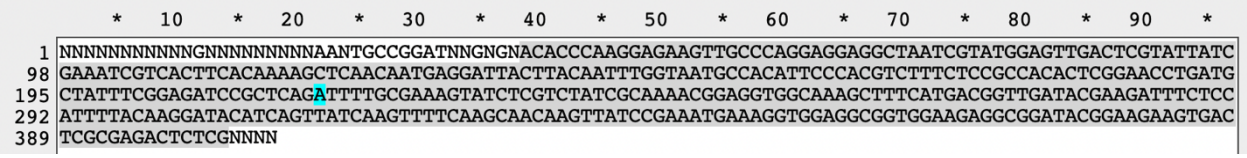


Figure A-4. Sanger sequencing of AMJ1097. A portion of the *hrde-1* gene was amplified and sent for sequencing that includes the mutation predicted to cause a G259D amino acid change. The adenine highlighted in blue reflects a mutation that is different from wild type; gray represents homology to the wildtype gene.

Appendix B: Ectopic expression of a germline gene in the intestine

B.1 Preface

The observations in this appendix were first noted by Farida Ettefa and then repeated by Daphne Knudsen-Palmer.

B.2 Introduction

Different cell types rely on the expression of different genes in order to maintain function and identity. In *C. elegans,* other germline-specific genes such as PGL-1 can be misexpressed in the soma when the retinoblastoma (Rb/*lin*-15b) pathway has been disrupted (208). It has previously been observed in the lab that *hrde-1(-)* mutants can cause misexpression of a germline promoted fluorescent transgene within some nuclei in the intestine. We wanted to further explore this potential misexpression, to ask whether it is observed in other RNAi mutants.

Intestinal cells have been shown to be mosaic, particularly for components of the RNAi pathway including the RNA-dependent RNA polymerases RRF-1 and EGO-1 (82). Since not all intestinal cell show misexpression of the germline transgene in *hrde-1(-)* mutants at high temperatures, it is worth exploring whether these cells have a dependency on RRF-1, EGO-1, or neither.

B.3 Materials and methods

B.3.1 Strains and oligonucleotides

All strains (listed in Table B-1) were cultured on Nematode Growth Medium (NGM) plates seeded with 100 µl of OP50 *E. coli* at 20ºC and strains made through mating were generated using standard methods (122). Oligonucleotides used are in Table B-2.

Table B-1. Strains used in Appendix B.

Strain Name	Genotype
N2	wild type
AMJ977	*rrf-1(ok589) I; qtIs49 III; sur-5(jam79[sur-5::gfp]) IV*
AMJ1025	*mut-16(jam139) rde-10(jam248) I; oxSi487 dpy-2(jam29) II; unc-119(ed3)? III; lin-2(jam30) X; rage(-)*
AMJ1045	*oxSi487 II; unc-119(ed3)? hrde-1(tm1200) III*
AMJ1522	*oxSi487 II; qtIs49 III; sur-5::gfp X*
AMJ1600	*rrf-1(ok589) I; oxSi487 II; qtIs49 III; sur-5::gfp X*
AMJ1601	*rrf-1(ok589) I; oxSi487 II; qtIs49 III; sur-5::gfp X*
AMJ1602	*rrf-1(ok589) I; oxSi487 II; qtIs49 III; sur-5::gfp X*
AMJ1603	*rrf-1(ok589) I; oxSi487 II; sur-5::gfp X*
AMJ1604	*rrf-1(ok589) I; oxSi487 II; sur-5::gfp X*
AMJ1605	*rrf-1(ok589) I; oxSi487 II; sur-5::gfp X*
AMJ1606	*oxSi487 II; sur-5::gfp X*
AMJ1607	*oxSi487 II; sur-5::gfp X*
AMJ1608	*oxSi487 II; sur-5::gfp X*
EG6787	*oxSi487 II*

Table B-2. Oligonucleotides used (5′ to 3′) in Appendix B.

Oligo	Sequence
P1	ataaggagttccacgcccag
P2	ctagtgagtcgtattataagtg
P3	tgaagacgacgagccacttg
P4	tgccatcgcagatagtcc
P5	tggaagcagctaggaacag
P6	ccgtgacaacagacattcaatc
P7	aacaggttcaggcaatgagc
P8	cagccattgtttctaaactcc
P9	gtgtccaagaatgtttccatc

B.3.2 Heat shock

Three L4 animals were passaged on NG plates and placed at 25ºC and kept at 25ºC until the F1 progeny reached L4 stage when they were selected for imaging.

B.3.3 Microscopy

Animals were mounted in 10 µl of 3 mM levamisole on a 2% agar pad and imaged under a coverslip using a Nikon AZ100 microscope and Photometrics Cool SNAP HQ^2 camera. A C-HGFI Intensilight Hg Illuminator was used to excite GFP (filter cube: 450 to 490 nm excitation, 495 dichroic, and 500 to 550 nm emission) or mCherry (filter cube: 530–560 nm excitation, 570 dichroic, and 590–650 nm emission). Representative images for mCherry expression were adjusted to identical levels in Fiji (NIH) for presentation.

B.3.4 Creation of *rrf-1(-);T* strains

EG6787 males were crossed with AMJ977 hermaphrodites. F1 worms were isolated and allowed to lay progeny. The *qtIs49* allele induces a Rol phenotype, so selection for or against this transgene was done by selecting plates 100% with or 100% without the Rol phenotype in the F2 generation. Primers **P1, P2,** and **P3** were used to detect the presence of *oxSi487* (*T*). Primers **P4, P5,** and **P6** were used to distinguish *rrf-1(ok589)* from wild type. Primers **P7, P8,** and **P9** were used to distinguish *sur-5::gfp* from wild type. Genotyping the strains once thawed to check the correct genotype is recommended.

B.4 Results

Previously, *hrde-1(-); T* animals where shown to show expression of *T* in the intestine when the strain was grown at an elevated temperature (Farida Ettefa, data not shown). To ask whether this result was reproducible and to ask whether other mutants in the RNAi pathway could cause this result, animals with the transgene *T* of various genotypes were grown for one generation at 25ºC. Wild type animals show normal expression of the transgene even when grown at 25ºC (Figure B-1). In contrast, animals that lack HRDE-1 show some somatic expression, particularly noticeable in intestinal cells when grown at 25ºC. While the germlines of *mut-16(-) rde-10(-)* double mutants appeared to have defects at both 20ºC and 25ºC, it is unclear whether there is expression in the intestinal cells or in coelomocytes.

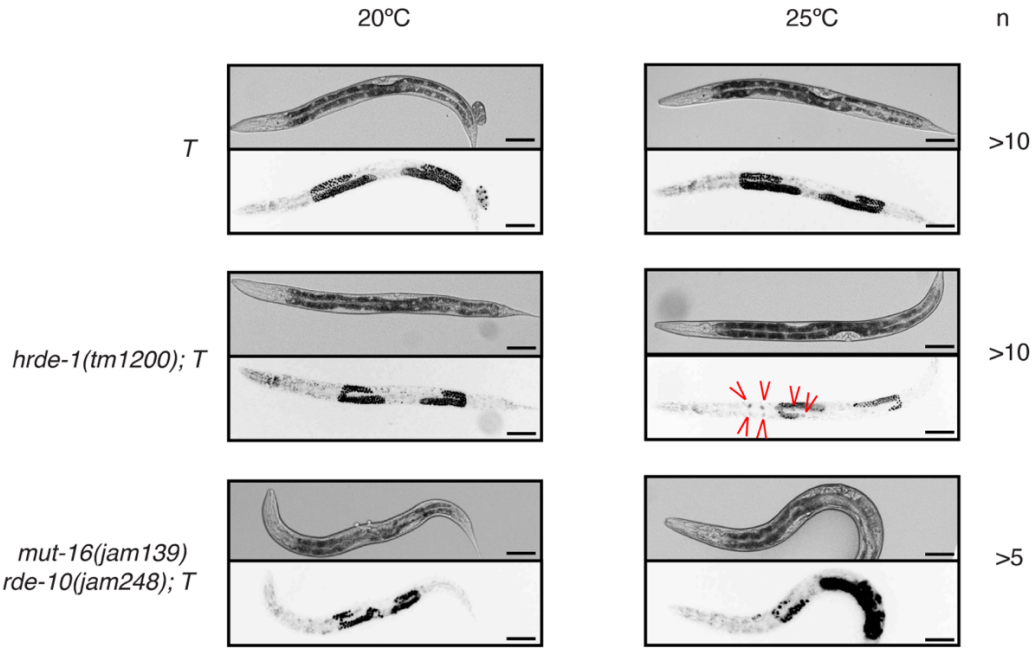


Figure B-1. Loss of HRDE-1 at high temperatures leads to misexpression of a germline gene in the soma. Images of representative L4 worms after one generation of heat shock at 25ºC (*right*) or maintained at 20ºC (*left*) (top, DIC; bottom, mCherry). Scale bars = 100µm. Intestinal misexpression of the transgene is indicated with red arrowheads.

B.5 Discussion

We are able to reproducibly find intestinal expression of the germline transgene *T* in the absence of HRDE-1 at high temperatures. It is possible that in a wild type animal, HRDE-1 is responsible for preventing expression of *T* in the soma, despite being considered a "germline Argonaute." An alternate hypothesis to the germline misexpression is that transcripts of the transgene are being absorbed as part of programmed cytoplasm engulfment by intestinal cells (209).

An immediate future direction for this observation would be to use CRISPR-Cas9 to create an *hrde-1(-)* mutant in strains AMJ1522, AMJ1600, AMJ1603, and AMJ1606 to ask whether the cells that misexpress *T* in the intestine are RRF-1 dependent (see Appendix A for oligos to create an *hrde-1(null)*). Future studies are required to understand the nature of this misexpression and to understand why HRDE-1 loss would cause this effect when loss of 2º siRNA amplification (loss of MUT-16 and RDE-10) would not.

Bibliography

1. Mattick,J.S., Amaral,P.P., Carninci,P., Carpenter,S., Chang,H.Y., Chen,L.-L., Chen,R., Dean,C., Dinger,M.E., Fitzgerald,K.A., *et al.* (2023) Long non-coding RNAs: definitions, functions, challenges and recommendations. *Nat. Rev. Mol. Cell Biol.*, **24**, 430–447.

2. Shang,R., Lee,S., Senavirathne,G. and Lai,E.C. (2023) microRNAs in action: biogenesis, function and regulation. *Nat. Rev. Genet.*, **24**, 816–833.

3. Ozata,D.M., Gainetdinov,I., Zoch,A., O'Carroll,D. and Zamore,P.D. (2019) PIWI-interacting RNAs: small RNAs with big functions. *Nat. Rev. Genet.*, **20**, 89–108.

4. Dana,H., Chalbatani,G.M., Mahmoodzadeh,H., Karimloo,R., Rezaiean,O., Moradzadeh,A., Mehmandoost,N., Moazzen,F., Mazraeh,A., Marmari,V., *et al.* (2017) Molecular Mechanisms and Biological Functions of siRNA. *Int. J. Biomed. Sci. IJBS*, **13**, 48–57.

5. Lakhotia,S.C. and Sharma,A. (1996) The 93D (hsr-omega) locus of Drosophila: non-coding gene with house-keeping functions. *Genetica*, **97**, 339–348.

6. Teramoto,H., Toyama,T., Takeba,G. and Tsuji,H. (1996) Noncoding RNA for CR20, a cytokinin-repressed gene of cucumber. *Plant Mol. Biol.*, **32**, 797–808.

7. Ota,T., Suzuki,Y., Nishikawa,T., Otsuki,T., Sugiyama,T., Irie,R., Wakamatsu,A., Hayashi,K., Sato,H., Nagai,K., *et al.* (2004) Complete sequencing and characterization of 21,243 full-length human cDNAs. *Nat. Genet.*, **36**, 40–45.

8. Kapranov,P., Cheng,J., Dike,S., Nix,D.A., Duttagupta,R., Willingham,A.T., Stadler,P.F., Hertel,J., Hackermüller,J., Hofacker,I.L., *et al.* (2007) RNA Maps Reveal New RNA Classes and a Possible Function for Pervasive Transcription. *Science*, **316**, 1484–1488.

9. Struhl,K. (2007) Transcriptional noise and the fidelity of initiation by RNA polymerase II. *Nat. Struct. Mol. Biol.*, **14**, 103–105.

10. Amaral,P.P. and Mattick,J.S. (2008) Noncoding RNA in development. *Mamm. Genome*, **19**, 454–492.

11. Dinger,M.E., Amaral,P.P., Mercer,T.R., Pang,K.C., Bruce,S.J., Gardiner,B.B., Askarian-Amiri,M.E., Ru,K., Soldà,G., Simons,C., *et al.* (2008) Long noncoding RNAs in mouse embryonic stem cell pluripotency and differentiation. *Genome Res.*, **18**, 1433–1445.

12. Rinn,J.L., Kertesz,M., Wang,J.K., Squazzo,S.L., Xu,X., Brugmann,S.A., Goodnough,L.H., Helms,J.A., Farnham,P.J., Segal,E., *et al.* (2007) Functional Demarcation of Active and Silent Chromatin Domains in Human HOX Loci by Noncoding RNAs. *Cell*, **129**, 1311–1323.

13. Gupta,R.A., Shah,N., Wang,K.C., Kim,J., Horlings,H.M., Wong,D.J., Tsai,M.-C., Hung,T., Argani,P., Rinn,J.L., *et al.* (2010) Long non-coding RNA HOTAIR reprograms chromatin state to promote cancer metastasis. *Nature*, **464**, 1071–1076.

14. Kim,K., Jutooru,I., Chadalapaka,G., Johnson,G., Frank,J., Burghardt,R., Kim,S. and Safe,S. (2013) HOTAIR is a negative prognostic factor and exhibits pro-oncogenic activity in pancreatic cancer. *Oncogene*, **32**, 1616–1625.

15. Li,X., Wu,Z., Mei,Q., Li,X., Guo,M., Fu,X. and Han,W. (2013) Long non-coding RNA HOTAIR, a driver of malignancy, predicts negative prognosis and exhibits oncogenic activity in oesophageal squamous cell carcinoma. *Br. J. Cancer*, **109**, 2266–2278.

16. Ma,M., Li,C., Zhang,Y., Weng,M., Zhang,M., Qin,Y., Gong,W. and Quan,Z. (2014) Long non-coding RNA HOTAIR, a c-Myc activated driver of malignancy, negatively regulates miRNA-130a in gallbladder cancer. *Mol. Cancer*, **13**, 156.

17. Müller,M., Fazi,F. and Ciaudo,C. (2020) Argonaute Proteins: From Structure to Function in Development and Pathological Cell Fate Determination. *Front. Cell Dev. Biol.*, **7**.

18. Lee,R.C., Feinbaum,R.L. and Ambros,V. (1993) The C. elegans heterochronic gene lin-4 encodes small RNAs with antisense complementarity to lin-14. *Cell*, **75**, 843–854.

19. Wightman,B., Ha,I. and Ruvkun,G. (1993) Posttranscriptional regulation of the heterochronic gene lin-14 by lin-4 mediates temporal pattern formation in C. elegans. *Cell*, **75**, 855–862.

20. Grimson,A., Farh,K.K.-H., Johnston,W.K., Garrett-Engele,P., Lim,L.P. and Bartel,D.P. (2007) MicroRNA Targeting Specificity in Mammals: Determinants Beyond Seed Pairing. *Mol. Cell*, **27**, 91–105.

21. Gu,S., Jin,L., Zhang,F., Sarnow,P. and Kay,M.A. (2009) The biological basis for microRNA target restriction to the 3' untranslated region in mammalian mRNAs. *Nat. Struct. Mol. Biol.*, **16**, 144–150.

22. Vagin,V.V., Sigova,A., Li,C., Seitz,H., Gvozdev,V. and Zamore,P.D. (2006) A distinct small RNA pathway silences selfish genetic elements in the germline. *Science*, **313**, 320–324.

23. Houwing,S., Kamminga,L.M., Berezikov,E., Cronembold,D., Girard,A., van den Elst,H., Filippov,D.V., Blaser,H., Raz,E., Moens,C.B., *et al.* (2007) A role for Piwi and piRNAs in germ cell maintenance and transposon silencing in Zebrafish. *Cell*, **129**, 69–82.

24. Brennecke,J., Aravin,A.A., Stark,A., Dus,M., Kellis,M., Sachidanandam,R. and Hannon,G.J. (2007) Discrete small RNA-generating loci as master regulators of transposon activity in Drosophila. *Cell*, **128**, 1089–1103.

25. Aravin,A.A., Sachidanandam,R., Girard,A., Fejes-Toth,K. and Hannon,G.J. (2007) Developmentally regulated piRNA clusters implicate MILI in transposon control. *Science*, **316**, 744–747.

26. Aravin,A.A., Sachidanandam,R., Bourc'his,D., Schaefer,C., Pezic,D., Toth,K.F., Bestor,T. and Hannon,G.J. (2008) A piRNA pathway primed by individual transposons is linked to de novo DNA methylation in mice. *Mol. Cell*, **31**, 785–799.

27. Kuramochi-Miyagawa,S., Watanabe,T., Gotoh,K., Totoki,Y., Toyoda,A., Ikawa,M., Asada,N., Kojima,K., Yamaguchi,Y., Ijiri,T.W., *et al.* (2008) DNA methylation of retrotransposon genes is regulated by Piwi family members MILI and MIWI2 in murine fetal testes. *Genes Dev.*, **22**, 908–917.

28. Fire,A., Xu,S., Montgomery,M.K., Kostas,S.A., Driver,S.E. and Mello,C.C. (1998) Potent and specific genetic interference by double-stranded RNA in. **391**.

29. Obbard,D.J., Gordon,K.H.J., Buck,A.H. and Jiggins,F.M. (2008) The evolution of RNAi as a defence against viruses and transposable elements. *Philos. Trans. R. Soc. B Biol. Sci.*, **364**, 99–115.

30. Drinnenberg,I.A., Weinberg,D.E., Xie,K.T., Mower,J.P., Wolfe,K.H., Fink,G.R. and Bartel,D.P. (2009) RNAi in Budding Yeast. *Science*, **326**, 544–550.

31. Metzlaff,M., O'Dell,M., Cluster,P.D. and Flavell,R.B. (1997) RNA-Mediated RNA Degradation and Chalcone Synthase A Silencing in Petunia. *Cell*, **88**, 845–854.

32. Waterhouse,P.M., Graham,M.W. and Wang,M.-B. (1998) Virus resistance and gene silencing in plants can be induced by simultaneous expression of sense and antisense RNA. *Proc. Natl. Acad. Sci.*, **95**, 13959–13964.

33. Hamilton,A.J. and Baulcombe,D.C. (1999) A Species of Small Antisense RNA in Posttranscriptional Gene Silencing in Plants. *Science*, **286**, 950–952.

34. Mourrain,P., Béclin,C., Elmayan,T., Feuerbach,F., Godon,C., Morel,J.-B., Jouette,D., Lacombe,A.-M., Nikic,S., Picault,N., *et al.* (2000) Arabidopsis SGS2 and SGS3 Genes Are Required for Posttranscriptional Gene Silencing and Natural Virus Resistance. *Cell*, **101**, 533–542.

35. Kennerdell,J.R. and Carthew,R.W. (1998) Use of dsRNA-Mediated Genetic Interference to Demonstrate that frizzled and frizzled 2 Act in the Wingless Pathway. *Cell*, **95**, 1017–1026.

36. Pal-Bhadra,M., Bhadra,U. and Birchler,J.A. (2002) RNAi Related Mechanisms Affect Both Transcriptional and Posttranscriptional Transgene Silencing in Drosophila. *Mol. Cell*, **9**, 315–327.

37. Chiu,Y.-L. and Rana,T.M. (2002) RNAi in Human Cells: Basic Structural and Functional Features of Small Interfering RNA. *Mol. Cell*, **10**, 549–561.

38. Setten,R.L., Rossi,J.J. and Han,S. (2019) The current state and future directions of RNAi-based therapeutics. *Nat. Rev. Drug Discov.*, **18**, 421–446.

39. Hu,B., Zhong,L., Weng,Y., Peng,L., Huang,Y., Zhao,Y. and Liang,X.-J. (2020) Therapeutic siRNA: state of the art. *Signal Transduct. Target. Ther.*, **5**, 1–25.

40. Hernández-Soto,A. and Chacón-Cerdas,R. (2021) RNAi Crop Protection Advances. *Int. J. Mol. Sci.*, **22**, 12148.

41. Adams,D., Gonzalez-Duarte,A., O'Riordan,W.D., Yang,C.-C., Ueda,M., Kristen,A.V., Tournev,I., Schmidt,H.H., Coelho,T., Berk,J.L., *et al.* (2018) Patisiran, an RNAi Therapeutic, for Hereditary Transthyretin Amyloidosis. *N. Engl. J. Med.*, **379**, 11–21.

42. Keam,S.J. (2022) Vutrisiran: First Approval. *Drugs*, **82**, 1419–1425.

43. Scott,L.J. (2020) Givosiran: First Approval. *Drugs*, **80**, 335–339.

44. German,C.A. and Shapiro,M.D. (2020) Small Interfering RNA Therapeutic Inclisiran: A New Approach to Targeting PCSK9. *BioDrugs*, **34**, 1–9.

45. Garrelfs,S.F., Frishberg,Y., Hulton,S.A., Koren,M.J., O'Riordan,W.D., Cochat,P., Deschênes,G., Shasha-Lavsky,H., Saland,J.M., van't Hoff,W.G., *et al.* (2021) Lumasiran, an RNAi Therapeutic for Primary Hyperoxaluria Type 1. *N. Engl. J. Med.*, **384**, 1216–1226.

46. Syed,Y.Y. (2023) Nedosiran: First Approval. *Drugs*, **83**, 1729–1733.

47. World Health Organization. DDT and its derivatives. Environmental Health Criteria. Geneva, Switzerland, 1979; Vol. 9.

48. Casarett & Doull's toxicology. The basic science of poisons, Fifth edition.; Klaassen, C. D., Amdur, M. O., Doull,J., Eds.; McGraw-Hill: New York,1996.

49. Casida, J. E.; Quistad, G. B. Golden age of insecticide research: past, present, or future? Annu. Rev. Entomol.1998, 43, 1-16. http://biomedical.AnnualReviews.org/.

50. Toxicology Profile for 4,4'-DDT, 4,4'-DDE, 4,4'-DDD (Update); U. S. Department of Human Health &Human Services, Agency for Toxic Substances and Disease Registry, 1994.

51. Suspended, canceled, and restricted use pesticides; EPA-20T-1002; U. S. Environmental Protection Agency,Office of Pesticide Programs, U. S. Government Printing Office: Washington, DC, 1990.

52. Head,G.P., Carroll,M.W., Evans,S.P., Rule,D.M., Willse,A.R., Clark,T.L., Storer,N.P., Flannagan,R.D., Samuel,L.W. and Meinke,L.J. (2017) Evaluation of SmartStax and SmartStax PRO maize against western corn rootworm and northern corn rootworm: efficacy and resistance management. *Pest Manag. Sci.*, **73**, 1883–1899.

53. Bolognesi,R., Ramaseshadri,P., Anderson,J., Bachman,P., Clinton,W., Flannagan,R., Ilagan,O., Lawrence,C., Levine,S., Moar,W., *et al.* (2012) Characterizing the Mechanism

of Action of Double-Stranded RNA Activity against Western Corn Rootworm (Diabrotica virgifera virgifera LeConte). *PLOS ONE*, **7**, e47534.

54. Koči,J., Ramaseshadri,P., Bolognesi,R., Segers,G., Flannagan,R. and Park,Y. (2014) Ultrastructural Changes Caused by Snf7 RNAi in Larval Enterocytes of Western Corn Rootworm (Diabrotica virgifera virgifera Le Conte). *PLOS ONE*, **9**, e83985.

55. Worrall,E.A., Bravo-Cazar,A., Nilon,A.T., Fletcher,S.J., Robinson,K.E., Carr,J.P. and Mitter,N. (2019) Exogenous Application of RNAi-Inducing Double-Stranded RNA Inhibits Aphid-Mediated Transmission of a Plant Virus. *Front. Plant Sci.*, **10**.

56. Law,J.A. and Jacobsen,S.E. (2010) Establishing, maintaining and modifying DNA methylation patterns in plants and animals. *Nat. Rev. Genet.*, **11**, 204–220.

57. Erdmann,R.M. and Picard,C.L. (2020) RNA-directed DNA Methylation. *PLoS Genet.*, **16**, e1009034.

58. Mochizuki,K., Fine,N.A., Fujisawa,T. and Gorovsky,M.A. (2002) Analysis of a piwi-Related Gene Implicates Small RNAs in Genome Rearrangement in Tetrahymena. *Cell*, **110**, 689–699.

59. Fields,B.D. and Kennedy,S. (2019) Chromatin Compaction by Small RNAs and the Nuclear RNAi Machinery in C. elegans. *Sci. Rep.*, **9**, 9030.

60. Reed,K.J., Svendsen,J.M., Brown,K.C., Montgomery,B.E., Marks,T.N., Vijayasarathy,T., Parker,D.M., Nishimura,E.O., Updike,D.L. and Montgomery,T.A. (2020) Widespread roles for piRNAs and WAGO-class siRNAs in shaping the germline transcriptome of Caenorhabditis elegans. *Nucleic Acids Res.*, **48**, 1811–1827.

61. Brangwynne,C.P., Eckmann,C.R., Courson,D.S., Rybarska,A., Hoege,C., Gharakhani,J., Jülicher,F. and Hyman,A.A. (2009) Germline P Granules Are Liquid Droplets That Localize by Controlled Dissolution/Condensation. *Science*, **324**, 1729–1732.

62. Brangwynne,C.P., Mitchison,T.J. and Hyman,A.A. (2011) Active liquid-like behavior of nucleoli determines their size and shape in Xenopus laevis oocytes. *Proc. Natl. Acad. Sci.*, **108**, 4334–4339.

63. Li,P., Banjade,S., Cheng,H.-C., Kim,S., Chen,B., Guo,L., Llaguno,M., Hollingsworth,J.V., King,D.S., Banani,S.F., *et al.* (2012) Phase transitions in the assembly of multivalent signalling proteins. *Nature*, **483**, 336–340.

64. Findley,S.D., Tamanaha,M., Clegg,N.J. and Ruohola-Baker,H. (2003) Maelstrom, a Drosophila spindle-class gene, encodes a protein that colocalizes with Vasa and RDE1/AGO1 homolog, Aubergine, in nuage. *Development*, **130**, 859–871.

65. Kotaja,N., Bhattacharyya,S.N., Jaskiewicz,L., Kimmins,S., Parvinen,M., Filipowicz,W. and Sassone-Corsi,P. (2006) The chromatoid body of male germ cells: similarity with

processing bodies and presence of Dicer and microRNA pathway components. *Proc. Natl. Acad. Sci. U. S. A.*, **103**, 2647–2652.

66. Kotaja,N. and Sassone-Corsi,P. (2007) The chromatoid body: a germ-cell-specific RNA-processing centre. *Nat. Rev. Mol. Cell Biol.*, **8**, 85–90.

67. Soper,S.F.C., van der Heijden,G.W., Hardiman,T.C., Goodheart,M., Martin,S.L., de Boer,P. and Bortvin,A. (2008) Mouse maelstrom, a component of nuage, is essential for spermatogenesis and transposon repression in meiosis. *Dev. Cell*, **15**, 285–297.

68. Snee,M.J. and Macdonald,P.M. (2004) Live imaging of nuage and polar granules: evidence against a precursor-product relationship and a novel role for Oskar in stabilization of polar granule components. *J. Cell Sci.*, **117**, 2109–2120.

69. Pitt,J.N., Schisa,J.A. and Priess,J.R. (2000) P Granules in the Germ Cells of *Caenorhabditis elegans* Adults Are Associated with Clusters of Nuclear Pores and Contain RNA. *Dev. Biol.*, **219**, 315–333.

70. Kawasaki,I., Shim,Y.-H., Kirchner,J., Kaminker,J., Wood,W.B. and Strome,S. (1998) PGL-1, a Predicted RNA-Binding Component of Germ Granules, Is Essential for Fertility in C. elegans. *Cell*, **94**, 635–645.

71. Spatiotemporal regulation of liquid-like condensates in epigenetic inheritance | Nature.

72. Wan,G., Bajaj,L., Fields,B., Dodson,A.E., Pagano,D., Fei,Y. and Kennedy,S. (2021) ZSP-1 is a Z granule surface protein required for Z granule fluidity and germline immortality in Caenorhabditis elegans. *EMBO J.*, **40**, e105612.

73. Manage,K.I., Rogers,A.K., Wallis,D.C., Uebel,C.J., Anderson,D.C., Nguyen,D.A.H., Arca,K., Brown,K.C., Cordeiro Rodrigues,R.J., De Albuquerque,B.F., *et al.* (2020) A tudor domain protein, SIMR-1, promotes siRNA production at piRNA-targeted mRNAs in C. elegans. *eLife*, **9**, e56731.

74. Phillips,C.M., Montgomery,T.A., Breen,P.C. and Ruvkun,G. (2012) MUT-16 promotes formation of perinuclear Mutator foci required for RNA silencing in the C. elegans germline. *Genes Dev.*, **26**, 1433–1444.

75. Uebel,C.J., Agbede,D., Wallis,D.C. and Phillips,C.M. (2020) Mutator foci are regulated by developmental stage, RNA, and the germline cell cycle in Caenorhabditis elegans Genetics.

76. Smith,J., Calidas,D., Schmidt,H., Lu,T., Rasoloson,D. and Seydoux,G. (2016) Spatial patterning of P granules by RNA-induced phase separation of the intrinsically-disordered protein MEG-3. *eLife*, **5**, e21337.

77. Saha,S., Weber,C.A., Nousch,M., Adame-Arana,O., Hoege,C., Hein,M.Y., Osborne-Nishimura,E., Mahamid,J., Jahnel,M., Jawerth,L., *et al.* (2016) Polar Positioning of

Phase-Separated Liquid Compartments in Cells Regulated by an mRNA Competition Mechanism. *Cell*, **166**, 1572-1584.e16.

78. Chen,X., Wang,K., Feng,X., Mufti,F. ud din, Xu,D., Zhu,C., Huang,X., Zeng,C., Jin,Q., Huang,X., *et al.* (2023) Germ granule compartments coordinate specialized small RNA production. 10.1101/2023.12.04.570003.

79. Seroussi,U., Li,C., Sundby,A.E., Lee,T.L., Claycomb,J.M. and Saltzman,A.L. (2022) Mechanisms of epigenetic regulation by C. elegans nuclear RNA interference pathways. *Semin. Cell Dev. Biol.*, **127**, 142–154.

80. Phillips,C.M. and Updike,D.L. (2022) Germ granules and gene regulation in the Caenorhabditis elegans germline. *Genetics*, **220**, iyab195.

81. Timmons,L. and Fire,A. (1998) Specific interference by ingested dsRNA. *Nature*, **395**, 854–854.

82. Ravikumar,S., Devanapally,S. and Jose,A.M. (2019) Gene silencing by double-stranded RNA from C. elegans neurons reveals functional mosaicism of RNA interference. *Nucleic Acids Res.*, **47**, 10059–10071.

83. Devanapally,S., Ravikumar,S. and Jose,A.M. (2015) Double-stranded RNA made in C. elegans neurons can enter the germline and cause transgenerational gene silencing. *Proc. Natl. Acad. Sci.*, **112**, 2133–2138.

84. Winston,W.M., Molodowitch,C. and Hunter,C.P. (2002) Systemic RNAi in *C. elegans* Requires the Putative Transmembrane Protein SID-1. *Science*, **295**, 2456–2459.

85. Feinberg,E.H. and Hunter,C.P. (2003) Transport of dsRNA into Cells by the Transmembrane Protein SID-1. *Science*, **301**, 1545–1547.

86. Tabara,H., Yigit,E., Siomi,H. and Mello,C.C. (2002) The dsRNA Binding Protein RDE-4 Interacts with RDE-1, DCR-1, and a DExH-Box Helicase to Direct RNAi in C. elegans. *Cell*, **109**, 861–871.

87. Parrish,S. and Fire,A. (2001) Distinct roles for RDE-1 and RDE-4 during RNA interference in Caenorhabditis elegans. *RNA*, **7**, 13970402.

88. Tabara,H., Sarkissian,M., Kelly,W.G., Fleenor,J., Grishok,A., Timmons,L., Fire,A. and Mello,C.C. (1999) The rde-1 Gene, RNA Interference, and Transposon Silencing in C. elegans. *Cell*, **99**, 123–132.

89. Shugarts,N., Sathya,A., Yi,A.L., Chan,W.M., Marré,J.A. and Jose,A.M. (2021) SID-1 regulates a retrotransposon-encoded gene to tune heritable RNA silencing Genetics.

90. Ruby,J.G., Jan,C., Player,C., Axtell,M.J., Lee,W., Nusbaum,C., Ge,H. and Bartel,D.P. (2006) Large-Scale Sequencing Reveals 21U-RNAs and Additional MicroRNAs and Endogenous siRNAs in C. elegans. *Cell*, **127**, 1193–1207.

91. Han,T., Manoharan,A.P., Harkins,T.T., Bouffard,P., Fitzpatrick,C., Chu,D.S., Thierry-Mieg,D., Thierry-Mieg,J. and Kim,J.K. (2009) 26G endo-siRNAs regulate spermatogenic and zygotic gene expression in Caenorhabditis elegans. *Proc. Natl. Acad. Sci.*, **106**, 18674–18679.

92. Blumenfeld,A.L. and Jose,A.M. (2015) Reproducible features of small RNAs in C. elegans reveal NU RNAs and provide insights into 22G RNAs and 26G RNAs. *RNA*, 10.1261/rna.054551.115.

93. Chang,T.H., Mattei,E., Gainetdinov,I., Colpan,C., Weng,Z. and Zamore,P.D. (2019) Maelstrom Represses Canonical Polymerase II Transcription within Bi-directional piRNA Clusters in Drosophila melanogaster. *Mol. Cell*, **73**, 291-303.e6.

94. Chen,C.-C.G., Simard,M.J., Tabara,H., Brownell,D.R., McCollough,J.A. and Mello,C.C. (2005) A Member of the Polymerase Beta Nucleotidyltransferase Superfamily Is Required for RNA Interference in C. elegans. *Curr. Biol.*

95. Preston,M.A., Porter,D.F., Chen,F., Buter,N., Lapointe,C.P., Keles,S., Kimble,J. and Wickens,M. (2019) Unbiased screen of RNA tailing activities reveals a poly(UG) polymerase. *Nat. Methods*, **16**, 437–445.

96. Shukla,A., Yan,J., Pagano,D.J., Dodson,A.E., Fei,Y., Gorham,J., Seidman,J.G., Wickens,M. and Kennedy,S. (2020) poly(UG)-tailed RNAs in genome protection and epigenetic inheritance. *Nature*, **582**, 283–288.

97. Escobar,C.A., Petersen,R.J., Tonelli,M., Fan,L., Henzler-Wildman,K.A. and Butcher,S.E. (2023) Solution Structure of Poly(UG) RNA. *J. Mol. Biol.*, **435**, 168340.

98. Smardon,A., Spoerke,J.M., Stacey,S.C., Klein,M.E., Mackin,N. and Maine,E.M. (2000) EGO-1 is related to RNA-directed RNA polymerase and functions in germ-line development and RNA interference in C. elegans. *Curr. Biol. CB*, **10**, 169–178.

99. Sijen,T., Fleenor,J., Simmer,F., Thijssen,K.L., Parrish,S., Timmons,L., Plasterk,R.H.A. and Fire,A. (2001) On the Role of RNA Amplification in dsRNA-Triggered Gene Silencing. *Cell*, **107**, 465–476.

100. Pak,J. and Fire,A. (2007) Distinct Populations of Primary and Secondary Effectors During RNAi in *C. elegans*. *Science*, **315**, 241–244.

101. Zhang,C., Montgomery,T.A., Gabel,H.W., Fischer,S.E.J., Phillips,C.M., Fahlgren,N., Sullivan,C.M., Carrington,J.C. and Ruvkun,G. (2011) mut-16 and other mutator class genes modulate 22G and 26G siRNA pathways in Caenorhabditis elegans. *Proc. Natl. Acad. Sci.*, **108**, 1201–1208.

102. Yang,H., Zhang,Y., Vallandingham,J., Li,H., Florens,L. and Mak,H.Y. (2012) The RDE-10/RDE-11 complex triggers RNAi-induced mRNA degradation by association with target mRNA in *C. elegans*. *Genes Dev.*, **26**, 846–856.

103. Zhang,C., Montgomery,T.A., Fischer,S.E.J., Garcia,S.M.D.A., Riedel,C.G., Fahlgren,N., Sullivan,C.M., Carrington,J.C. and Ruvkun,G. (2012) The Caenorhabditis elegans RDE-10/RDE-11 Complex Regulates RNAi by Promoting Secondary siRNA Amplification. *Curr. Biol.*, **22**, 881–890.

104. Uebel,C.J., Anderson,D.C., Mandarino,L.M., Manage,K.I., Aynaszyan,S. and Phillips,C.M. (2018) Distinct regions of the intrinsically disordered protein MUT-16 mediate assembly of a small RNA amplification complex and promote phase separation of Mutator foci. *PLOS Genet.*, **14**, e1007542.

105. Yigit,E., Batista,P.J., Bei,Y., Pang,K.M., Chen,C.-C.G., Tolia,N.H., Joshua-Tor,L., Mitani,S., Simard,M.J. and Mello,C.C. (2006) Analysis of the C. elegans Argonaute Family Reveals that Distinct Argonautes Act Sequentially during RNAi. *Cell*, **127**, 747–757.

106. Guang,S., Bochner,A.F., Pavelec,D.M., Burkhart,K.B., Harding,S., Lachowiec,J. and Kennedy,S. (2008) An Argonaute Transports siRNAs from the Cytoplasm to the Nucleus. *Science*, **321**, 537–541.

107. Seroussi,U., Lugowski,A., Wadi,L., Lao,R.X., Willis,A.R., Zhao,W., Sundby,A.E., Charlesworth,A.G., Reinke,A.W. and Claycomb,J.M. (2023) A comprehensive survey of C. elegans argonaute proteins reveals organism-wide gene regulatory networks and functions. *eLife*, **12**, e83853.

108. Buckley,B.A., Burkhart,K.B., Gu,S.G., Spracklin,G., Kershner,A., Fritz,H., Kimble,J., Fire,A. and Kennedy,S. (2012) A nuclear Argonaute promotes multigenerational epigenetic inheritance and germline immortality. *Nature*, **489**, 447–451.

109. Sasaki,T., Shiohama,A., Minoshima,S. and Shimizu,N. (2003) Identification of eight members of the Argonaute family in the human genome. *Genomics*, **82**, 323–330.

110. Williams,R.W. and Rubin,G.M. (2002) ARGONAUTE1 is required for efficient RNA interference in Drosophila embryos. *Proc. Natl. Acad. Sci. U. S. A.*, **99**, 6889–6894.

111. Gu,W., Shirayama,M., Conte,D., Vasale,J., Batista,P.J., Claycomb,J.M., Moresco,J.J., Youngman,E.M., Keys,J., Stoltz,M.J., *et al.* (2009) Distinct Argonaute-Mediated 22G-RNA Pathways Direct Genome Surveillance in the C. elegans Germline. *Mol. Cell*, **36**, 231–244.

112. Knudsen-Palmer,D.R., Raman,P., Ettefa,F., De Ravin,L. and Jose,A.M. (2023) Target-specific requirements for RNA interference can be explained by a single regulatory network Genetics.

113. Das,P.R. and Sherif,S.M. (2020) Application of Exogenous dsRNAs-induced RNAi in Agriculture: Challenges and Triumphs. *Front. Plant Sci.*, **11**, 946.

114. Vogel,E., Santos,D., Mingels,L., Verdonckt,T.-W. and Broeck,J.V. (2019) RNA Interference in Insects: Protecting Beneficials and Controlling Pests. *Front. Physiol.*, **9**, 1912.

115. Zhu,Y., Zhu,L., Wang,X. and Jin,H. (2022) RNA-based therapeutics: an overview and prospectus. *Cell Death Dis.*, **13**, 644.

116. Knight,S.W. and Bass,B.L. (2001) A Role for the RNase III Enzyme DCR-1 in RNA Interference and Germ Line Development in Caenorhabditis elegans. *Science*, **293**, 2269–2271.

117. Parker,G.S., Eckert,D.M. and Bass,B.L. (2006) RDE-4 preferentially binds long dsRNA and its dimerization is necessary for cleavage of dsRNA to siRNA. *RNA*, **12**, 807–818.

118. Steiner,F.A., Okihara,K.L., Hoogstrate,S.W., Sijen,T. and Ketting,R.F. (2009) RDE-1 slicer activity is required only for passenger-strand cleavage during RNAi in Caenorhabditis elegans. *Nat. Struct. Mol. Biol.*, **16**, 207–211.

119. Kennedy,S., Wang,D. and Ruvkun,G. (2004) A conserved siRNA-degrading RNase negatively regulates RNA interference in C. elegans. *Nature*, **427**, 645–649.

120. Raman,P., Zaghab,S.M., Traver,E.C. and Jose,A.M. (2017) The double-stranded RNA binding protein RDE-4 can act cell autonomously during feeding RNAi in C. elegans. *Nucleic Acids Res.*, **45**, 8463–8473.

121. Zhuang,J.J. and Hunter,C.P. (2011) Tissue Specificity of *Caenorhabditis elegans* Enhanced RNA Interference Mutants. *Genetics*, **188**, 235–237.

122. Brenner,S. (1974) THE GENETICS OF CAENORHABDITIS ELEGANS. *Genetics*, **77**, 71–94.

123. Arribere,J.A., Bell,R.T., Fu,B.X.H., Artiles,K.L., Hartman,P.S. and Fire,A.Z. (2014) Efficient Marker-Free Recovery of Custom Genetic Modifications with CRISPR/Cas9 in *Caenorhabditis elegans*. *Genetics*, **198**, 837–846.

124. Paix,A., Folkmann,A., Rasoloson,D. and Seydoux,G. (2015) High Efficiency, Homology-Directed Genome Editing in *Caenorhabditis elegans* Using CRISPR-Cas9 Ribonucleoprotein Complexes. *Genetics*, **201**, 47–54.

125. Dokshin,G.A., Ghanta,K.S., Piscopo,K.M. and Mello,C.C. (2018) Robust Genome Editing with Short Single-Stranded and Long, Partially Single-Stranded DNA Donors in *Caenorhabditis elegans*. *Genetics*, **210**, 781–787.

126. Kamath,R.S., Fraser,A.G., Dong,Y., Poulin,G., Durbin,R., Gotta,M., Kanapin,A., Le Bot,N., Moreno,S., Sohrmann,M., *et al.* (2003) Systematic functional analysis of the Caenorhabditis elegans genome using RNAi. *Nature*, **421**, 231–237.

127. Sievers,F., Wilm,A., Dineen,D., Gibson,T.J., Karplus,K., Li,W., Lopez,R., McWilliam,H., Remmert,M., Söding,J., *et al.* (2011) Fast, scalable generation of high-quality protein multiple sequence alignments using Clustal Omega. *Mol. Syst. Biol.*, **7**, 539.

128. Jumper,J., Evans,R., Pritzel,A., Green,T., Figurnov,M., Ronneberger,O., Tunyasuvunakool,K., Bates,R., Žídek,A., Potapenko,A., *et al.* (2021) Highly accurate protein structure prediction with AlphaFold. *Nature*, **596**, 583–589.

129. Varadi,M., Anyango,S., Deshpande,M., Nair,S., Natassia,C., Yordanova,G., Yuan,D., Stroe,O., Wood,G., Laydon,A., *et al.* (2022) AlphaFold Protein Structure Database: massively expanding the structural coverage of protein-sequence space with high-accuracy models. *Nucleic Acids Res.*, **50**, D439–D444.

130. Zhang,Y. (2005) TM-align: a protein structure alignment algorithm based on the TM-score. *Nucleic Acids Res.*, **33**, 2302–2309.

131. Frøkjær-Jensen,C., Davis,M.W., Ailion,M. and Jorgensen,E.M. (2012) Improved Mos1-mediated transgenesis in C. elegans. *Nat. Methods*, **9**, 117–118.

132. Marré,J., Traver,E.C. and Jose,A.M. (2016) Extracellular RNA is transported from one generation to the next in Caenorhabditis elegans. *Proc. Natl. Acad. Sci.*, **113**, 12496–12501.

133. Devanapally,S., Raman,P., Chey,M., Allgood,S., Ettefa,F., Diop,M., Lin,Y., Cho,Y.E. and Jose,A.M. (2021) Mating can initiate stable RNA silencing that overcomes epigenetic recovery. *Nat. Commun.*, **12**, 4239.

134. Ferguson,E.L. and Horvitz,H.R. (1985) IDENTIFICATION AND CHARACTERIZATION OF 22 GENES THAT AFFECT THE VULVAL CELL LINEAGES OF THE NEMATODE *CAENORHABDITIS ELEGANS*. *Genetics*, **110**, 17–72.

135. Pak,J., Maniar,J.M., Mello,C.C. and Fire,A. (2012) Protection from Feed-Forward Amplification in an Amplified RNAi Mechanism. *Cell*, **151**, 885–899.

136. Jobson,M.A., Jordan,J.M., Sandrof,M.A., Hibshman,J.D., Lennox,A.L. and Baugh,L.R. (2015) Transgenerational Effects of Early Life Starvation on Growth, Reproduction, and Stress Resistance in Caenorhabditis elegans. *Genetics*, **201**, 201–212.

137. Lee,R.C., Hammell,C.M. and Ambros,V. (2006) Interacting endogenous and exogenous RNAi pathways in Caenorhabditis elegans. *RNA*, **12**, 589–597.

138. Bergstrom,C.T., McKittrick,E. and Antia,R. (2003) Mathematical models of RNA silencing: Unidirectional amplification limits accidental self-directed reactions. *Proc. Natl. Acad. Sci.*, **100**, 11511–11516.

139. Sandy,P., Ventura,A. and Jacks,T. (2005) Mammalian RNAi: a practical guide. *BioTechniques*, **39**, 215–224.

140. Sapetschnig,A., Sarkies,P., Lehrbach,N.J. and Miska,E.A. (2015) Tertiary siRNAs Mediate Paramutation in C. elegans. *PLOS Genet.*, **11**, e1005078.

141. Sanan-Mishra,N., Abdul Kader Jailani,A., Mandal,B. and Mukherjee,S.K. (2021) Secondary siRNAs in Plants: Biosynthesis, Various Functions, and Applications in Virology. *Front. Plant Sci.*, **12**.

142. Tsai,H.-Y., Chen,C.-C.G., Conte,D., Moresco,J.J., Chaves,D.A., Mitani,S., Yates,J.R., Tsai,M.-D. and Mello,C.C. (2015) A Ribonuclease Coordinates siRNA Amplification and mRNA Cleavage during RNAi. *Cell*, **160**, 407–419.

143. Matsumoto,N., Sato,K., Nishimasu,H., Namba,Y., Miyakubi,K., Dohmae,N., Ishitani,R., Siomi,H., Siomi,M.C. and Nureki,O. (2015) Crystal Structure and Activity of the Endoribonuclease Domain of the piRNA Pathway Factor Maelstrom. *Cell Rep.*, **11**, 366–375.

144. Chaves,D.A., Dai,H., Li,L., Moresco,J.J., Oh,M.E., Conte,D., Yates,J.R., Mello,C.C. and Gu,W. (2021) The RNA phosphatase PIR-1 regulates endogenous small RNA pathways in C. elegans. *Mol. Cell*, **81**, 546-557.e5.

145. Zhang,D., Xiong,H., Shan,J., Xia,X. and Trudeau,V.L. (2008) Functional insight into Maelstrom in the germline piRNA pathway: a unique domain homologous to the DnaQ-H 3'–5' exonuclease, its lineage-specific expansion/loss and evolutionarily active site switch. *Biol. Direct*, **3**, 48.

146. Duchaine,T.F., Wohlschlegel,J.A., Kennedy,S., Bei,Y., Conte,D., Pang,K., Brownell,D.R., Harding,S., Mitani,S., Ruvkun,G., *et al.* (2006) Functional Proteomics Reveals the Biochemical Niche of C. elegans DCR-1 in Multiple Small-RNA-Mediated Pathways. *Cell*, **124**, 343–354.

147. Gabel,H.W. and Ruvkun,G. (2008) The exonuclease ERI-1 has a conserved dual role in 5.8S rRNA processing and RNAi. *Nat. Struct. Mol. Biol.*, **15**, 531–533.

148. Chen,J., Liu,L., You,C., Gu,J., Ruan,W., Zhang,L., Gan,J., Cao,C., Huang,Y., Chen,X., *et al.* (2018) Structural and biochemical insights into small RNA 3′ end trimming by Arabidopsis SDN1. *Nat. Commun.*, **9**, 3585.

149. Stoyko,D., Genzor,P. and Haase,A.D. (2022) Hierarchical length and sequence preferences establish a single major piRNA 3′-end. *iScience*, **25**.

150. Sim,G., Kehling,A.C., Park,M.S., Secor,J., Divoky,C., Zhang,H., Malhotra,N., Bhagdikar,D., Abd El-Wahab,E.W. and Nakanishi,K. (2022) Manganese-dependent microRNA trimming by 3′→5′ exonucleases generates 14-nucleotide or shorter tiny RNAs. *Proc. Natl. Acad. Sci.*, **119**, e2214335119.

151. Aoki,K., Moriguchi,H., Yoshioka,T., Okawa,K. and Tabara,H. (2007) In vitro analyses of the production and activity of secondary small interfering RNAs in C. elegans. *EMBO J.*, **26**, 5007–5019.

152. Pinzón,N., Bertrand,S., Subirana,L., Busseau,I., Escrivá,H. and Seitz,H. (2019) Functional lability of RNA-dependent RNA polymerases in animals. *PLOS Genet.*, **15**, e1007915.

153. Theodor Boveri (1905) Zellenstudien V. Über die Abhängigkeit der Kerngrösse und Zellenzahl bei Seeigellarven von der Chromosomenzahl der Ausganszellen. *Jenaische Z. Für Naturwissenschaft*, **39**, 445–524.

154. Kume,K., Cantwell,H., Neumann,F.R., Jones,A.W., Snijders,A.P. and Nurse,P. (2017) A systematic genomic screen implicates nucleocytoplasmic transport and membrane growth in nuclear size control. *PLOS Genet.*, **13**, e1006767.

155. Cantwell,H. and Nurse,P. (2019) A systematic genetic screen identifies essential factors involved in nuclear size control. *PLOS Genet.*, **15**, e1007929.

156. Ruehle,M.D., Orias,E. and Pearson,C.G. (2016) Tetrahymena as a Unicellular Model Eukaryote: Genetic and Genomic Tools. *Genetics*, **203**, 649–665.

157. Pazdernik,N. and Schedl,T. (2013) Introduction to Germ Cell Development in Caenorhabditis elegans. In Schedl,T. (ed), *Germ Cell Development in C. elegans*, Advances in Experimental Medicine and Biology. Springer, New York, NY, pp. 1–16.

158. Diag,A., Schilling,M., Klironomos,F., Ayoub,S. and Rajewsky,N. (2018) Spatiotemporal m(i)RNA Architecture and 3′ UTR Regulation in the C. elegans Germline. *Dev. Cell*, **47**, 785-800.e8.

159. Price,I.F., Wagner,J.A., Pastore,B., Hertz,H.L. and Tang,W. (2023) C. elegans germ granules sculpt both germline and somatic RNAome. *Nat. Commun.*, **14**, 5965.

160. Martin,M. (2011) Cutadapt removes adapter sequences from high-throughput sequencing reads. *EMBnet.journal*, **17**, 10–12.

161. Patro,R., Duggal,G., Love,M.I., Irizarry,R.A. and Kingsford,C. (2017) Salmon provides fast and bias-aware quantification of transcript expression. *Nat. Methods*, **14**, 417–419.

162. Soneson,C., Love,M.I. and Robinson,M.D. (2015) Differential analyses for RNA-seq: transcript-level estimates improve gene-level inferences. *F1000Research*, **4**, 1521.

163. Robinson,M.D. and Oshlack,A. (2010) A scaling normalization method for differential expression analysis of RNA-seq data. *Genome Biol.*, **11**, R25.

164. Law,C.W., Chen,Y., Shi,W. and Smyth,G.K. (2014) voom: precision weights unlock linear model analysis tools for RNA-seq read counts. *Genome Biol.*, **15**, 1–17.

165. Kim,D., Paggi,J.M., Park,C., Bennett,C. and Salzberg,S.L. (2019) Graph-based genome alignment and genotyping with HISAT2 and HISAT-genotype. *Nat. Biotechnol.*, **37**, 907–915.

166. Marylyn Ritchie PhenoGram PLot.

167. Hulsen,T., de Vlieg,J. and Alkema,W. (2008) BioVenn – a web application for the comparison and visualization of biological lists using area-proportional Venn diagrams. *BMC Genomics*, **9**, 488.

168. Goudeau,J., Sharp,C.S., Paw,J., Savy,L., Leonetti,M.D., York,A.G., Updike,D.L., Kenyon,C. and Ingaramo,M. (2021) Split-wrmScarlet and split-sfGFP: tools for faster, easier fluorescent labeling of endogenous proteins in Caenorhabditis elegans. *Genetics*, **217**, iyab014.

169. Tasaki,T., Sohr,R., Xia,Z., Hellweg,R., Hörtnagl,H., Varshavsky,A. and Kwon,Y.T. (2007) Biochemical and Genetic Studies of UBR3, a Ubiquitin Ligase with a Function in Olfactory and Other Sensory Systems *. *J. Biol. Chem.*, **282**, 18510–18520.

170. Li,T., Fan,J., Blanco-Sánchez,B., Giagtzoglou,N., Lin,G., Yamamoto,S., Jaiswal,M., Chen,K., Zhang,J., Wei,W., *et al.* (2016) Ubr3, a Novel Modulator of Hh Signaling Affects the Degradation of Costal-2 and Kif7 through Poly-ubiquitination. *PLOS Genet.*, **12**, e1006054.

171. Sawyer,J.M., Glass,S., Li,T., Shemer,G., White,N.D., Starostina,N.G., Kipreos,E.T., Jones,C.D. and Goldstein,B. (2011) Overcoming Redundancy: An RNAi Enhancer Screen for Morphogenesis Genes in Caenorhabditis elegans. *Genetics*, **188**, 549–564.

172. Kishore,R., Arnaboldi,V., Van Slyke,C.E., Chan,J., Nash,R.S., Urbano,J.M., Dolan,M.E., Engel,S.R., Shimoyama,M., Sternberg,P.W., *et al.* (2020) Automated generation of gene summaries at the Alliance of Genome Resources. *Database*, **2020**, baaa037.

173. Harris,T.W., Arnaboldi,V., Cain,S., Chan,J., Chen,W.J., Cho,J., Davis,P., Gao,S., Grove,C.A., Kishore,R., *et al.* (2020) WormBase: a modern Model Organism Information Resource. *Nucleic Acids Res.*, **48**, D762–D767.

174. Mao,K., Breen,P. and Ruvkun,G. (2020) Mitochondrial dysfunction induces RNA interference in C. elegans through a pathway homologous to the mammalian RIG-I antiviral response. *PLoS Biol.*, **18**, e3000996.

175. Anuchin,A.M., Goncharenko,A.V., Demidenok,O.I. and Kaprelyants,A.S. (2011) Histone-like proteins of bacteria (review). *Appl. Biochem. Microbiol.*, **47**, 580–585.

176. Zhou,X., Feng,X., Mao,H., Li,M., Xu,F., Hu,K. and Guang,S. (2017) RdRP-synthesized antisense ribosomal siRNAs silence pre-rRNA via the nuclear RNAi pathway. *Nat. Struct. Mol. Biol.*, **24**, 258–269.

177. Ustianenko,D., Pasulka,J., Feketova,Z., Bednarik,L., Zigackova,D., Fortova,A., Zavolan,M. and Vanacova,S. (2016) TUT-DIS3L2 is a mammalian surveillance pathway for aberrant structured non-coding RNAs. *EMBO J.*, **35**, 2179–2191.

178. Xu,D., Chen,X., Kuang,Y., Hong,M., Xu,T., Wang,K., Fu,C., Ruan,K., Zhu,C., Feng,X., *et al.* (2023) rRNA intermediates coordinate the multilayered nucleolar phase transition in C. elegans. 10.1101/2023.01.23.525268.

179. Iwamoto,M., Mori,C., Kojidani,T., Bunai,F., Hori,T., Fukagawa,T., Hiraoka,Y. and Haraguchi,T. (2009) Two Distinct Repeat Sequences of Nup98 Nucleoporins Characterize Dual Nuclei in the Binucleated Ciliate *Tetrahymena*. *Curr. Biol.*, **19**, 843–847.

180. Neumann,F.R. and Nurse,P. (2007) Nuclear size control in fission yeast. *J. Cell Biol.*, **179**, 593–600.

181. Jackson,A.L. and Linsley,P.S. (2010) Recognizing and avoiding siRNA off-target effects for target identification and therapeutic application. *Nat. Rev. Drug Discov.*, **9**, 57–67.

182. Dowdy,S.F. (2023) Endosomal escape of RNA therapeutics: How do we solve this rate-limiting problem? *RNA*, **29**, 396–401.

183. Brown,C.R., Gupta,S., Qin,J., Racie,T., He,G., Lentini,S., Malone,R., Yu,M., Matsuda,S., Shulga-Morskaya,S., *et al.* (2020) Investigating the pharmacodynamic durability of GalNAc-siRNA conjugates. *Nucleic Acids Res.*, **48**, 11827–11844.

184. Fitzgerald,K., White,S., Borodovsky,A., Bettencourt,B.R., Strahs,A., Clausen,V., Wijngaard,P., Horton,J.D., Taubel,J., Brooks,A., *et al.* (2017) A Highly Durable RNAi Therapeutic Inhibitor of PCSK9. *N. Engl. J. Med.*, **376**, 41–51.

185. Gent,J.I., Schvarzstein,M., Villeneuve,A.M., Gu,S.G., Jantsch,V., Fire,A.Z. and Baudrimont,A. (2009) A Caenorhabditis elegans RNA-directed RNA polymerase in sperm development and endogenous RNA interference. *Genetics*, **183**, 1297–1314.

186. Gent,J.I., Lamm,A.T., Pavelec,D.M., Maniar,J.M., Parameswaran,P., Tao,L., Kennedy,S. and Fire,A.Z. (2010) Distinct phases of siRNA synthesis in an endogenous RNAi pathway in C. elegans soma. *Mol. Cell*, **37**, 679–689.

187. Maniar,J.M. and Fire,A.Z. (2011) EGO-1, a C. elegans RdRP, Modulates Gene Expression via Production of mRNA-Templated Short Antisense RNAs. *Curr. Biol.*, **21**, 449–459.

188. Willmann,M.R., Endres,M.W., Cook,R.T. and Gregory,B.D. (2011) The Functions of RNA-Dependent RNA Polymerases in Arabidopsis. *Arab. Book*, **2011**.

189. Makeyev,E.V. and Bamford,D.H. (2002) Cellular RNA-Dependent RNA Polymerase Involved in Posttranscriptional Gene Silencing Has Two Distinct Activity Modes. *Mol. Cell*, **10**, 1417–1427.

190. Marker,S., Le Mouël,A., Meyer,E. and Simon,M. (2010) Distinct RNA-dependent RNA polymerases are required for RNAi triggered by double-stranded RNA versus truncated transgenes in Paramecium tetraurelia. *Nucleic Acids Res.*, **38**, 4092–4107.

191. Ouyang,J.P.T., Zhang,W.L. and Seydoux,G. (2022) The conserved helicase ZNFX-1 memorializes silenced RNAs in perinuclear condensates. *Nat. Cell Biol.*, **24**, 1129–1140.

192. Dickinson,D.J., Ward,J.D., Reiner,D.J. and Goldstein,B. (2013) Engineering the Caenorhabditis elegans genome using Cas9-triggered homologous recombination. *Nat. Methods*, **10**, 1028–1034.

193. Frøkjær-Jensen,C., Jain,N., Hansen,L., Davis,M.W., Li,Y., Zhao,D., Rebora,K., Millet,J.R.M., Liu,X., Kim,S.K., *et al.* (2016) An Abundant Class of Non-coding DNA Can Prevent Stochastic Gene Silencing in the C. elegans Germline. *Cell*, **166**, 343–357.

194. Mauro,M.S., Celma,G., Zimyanin,V., Magaj,M.M., Gibson,K.H., Redemann,S. and Bahmanyar,S. (2022) Ndc1 drives nuclear pore complex assembly independent of membrane biogenesis to promote nuclear formation and growth. *eLife*, **11**, e75513.

195. Freeman,M. and Glover,D.M. (1987) The gnu mutation of Drosophila causes inappropriate DNA synthesis in unfertilized and fertilized eggs. *Genes Dev.*, **1**, 924–930.

196. Jeong,J., Verheyden,J.M. and Kimble,J. (2011) Cyclin E and Cdk2 control GLD-1, the mitosis/meiosis decision, and germline stem cells in Caenorhabditis elegans. *PLoS Genet.*, **7**, e1001348.

197. Aravin,A.A., Heijden,G.W. van der, Castañeda,J., Vagin,V.V., Hannon,G.J. and Bortvin,A. (2009) Cytoplasmic Compartmentalization of the Fetal piRNA Pathway in Mice. *PLOS Genet.*, **5**, e1000764.

198. Tijsterman,M., May,R.C., Simmer,F., Okihara,K.L. and Plasterk,R.H.A. (2004) Genes Required for Systemic RNA Interference in Caenorhabditis elegans. *Curr. Biol.*, **14**, 111–116.

199. Shirayama,M., Stanney,W., Gu,W., Seth,M. and Mello,C.C. (2014) The Vasa Homolog RDE-12 Engages Target mRNA and Multiple Argonaute Proteins to Promote RNAi in C. elegans. *Curr. Biol.*, **24**, 845–851.

200. Yang,H., Vallandingham,J., Shiu,P., Li,H., Hunter,C.P. and Mak,H.Y. (2014) The DEAD Box Helicase RDE-12 Promotes Amplification of RNAi in Cytoplasmic Foci in C. elegans. *Curr. Biol.*, **24**, 832–838.

201. van Kempen,M., Kim,S.S., Tumescheit,C., Mirdita,M., Lee,J., Gilchrist,C.L.M., Söding,J. and Steinegger,M. (2024) Fast and accurate protein structure search with Foldseek. *Nat. Biotechnol.*, **42**, 243–246.

202. Hay,B., Jan,L.Y. and Jan,Y.N. (1988) A protein component of Drosophila polar granules is encoded by vasa and has extensive sequence similarity to ATP-dependent helicases. *Cell*, **55**, 577–587.

203. Lasko,P.F. and Ashburner,M. (1990) Posterior localization of vasa protein correlates with, but is not sufficient for, pole cell development. *Genes Dev.*, **4**, 905–921.

204. Harris,A.N. and Macdonald,P.M. (2001) Aubergine encodes a Drosophila polar granule component required for pole cell formation and related to eIF2C. *Dev. Camb. Engl.*, **128**, 2823–2832.

205. Kennerdell,J.R., Yamaguchi,S. and Carthew,R.W. (2002) RNAi is activated during Drosophila oocyte maturation in a manner dependent on aubergine and spindle-E. *Genes Dev.*, **16**, 1884–1889.

206. Höck,J. and Meister,G. (2008) The Argonaute protein family. *Genome Biol.*, **9**, 210.

207. Schirle,N.T., Sheu-Gruttadauria,J. and MacRae,I.J. (2014) Structural basis for microRNA targeting. *Science*, **346**, 608–613.

208. Wang,D., Kennedy,S., Conte,D., Kim,J.K., Gabel,H.W., Kamath,R.S., Mello,C.C. and Ruvkun,G. (2005) Somatic misexpression of germline P granules and enhanced RNA interference in retinoblastoma pathway mutants. *Nature*, **436**, 593–597.

209. Abdu,Y., Maniscalco,C., Heddleston,J.M., Chew,T.-L. and Nance,J. (2016) Developmentally programmed germ cell remodelling by endodermal cell cannibalism. *Nat. Cell Biol.*, **18**, 1302–1310.